PROTEIN SEPARATION IN ION-EXCHANGE MEMBRANE PARTITIONED FREE-FLOW ISOELECTRIC FOCUSING (IEM-FFIEF) SYSTEM

CHENG JIUHUA

Bachelor Degree of Technology (Hons)

National University of Singapore

A Thesis Submitted for the Degree of Doctor of Philosophy
Department of Chemical & Biomolecular Engineering
National University of Singapore
2010.04.

Acknowledgements

I am first of all deeply obliged to my supervisor, Professor N. T.-S. Chung. His insightful outlook has guided me into a broad scope of membrane science, and over the course of my studies he has taught me the academic research from the very basics. He has also helped me in my further development through his endless enthusiasm in educating me, and has given me every possible resource and facilities to develop the IEM-FFIEF technology. His trust has encouraged me to endure the most arduous times in my research career here. His everlasting mentorship supports me from the beginning to the end: time never stops, but yet his teaching quality never decreases. Moreover, his dedication to science has spurred me to pursue the truth as a real scientist.

I would like to express my appreciation to Prof. S. B. Chen and Prof. B. Liu due to their constructive suggestions on my Ph.D proposal. As an expert in the field of electrophoresis, Prof. Chen has provided a few critical and necessary questions for me to understand the electrophoresis phenomenon, which has been very helpful throughout my Ph.D candidature in NUS.

I would also express my thanks to all the team members in Prof. Chung's research group. Especially thanks are especially conveyed to Dr. Y. C. Xiao and Dr. Y. Li for their guidance in the early stages of my research. Special thanks are also conveyed to Ms. B. T. Low and Dr.

M. M. Teoh, for their noble deeds and patience in helping me through academic life. The advice that I have obtained from Dr. Q. Yang and Dr. K. Y. Wang are all also very valuable. The countless suggestions and help from all my colleagues in Prof. Chung's group made my research life in NUS full of tears and smiles. These colleagues are: Dr. Y. C. Xiao, Ms. B. T. Low, Dr. M. M. Teoh, Ms. W. Natalia, Y. Wang, N. Peng and Z. Z. Zhou.

My thanks also go out to A-star and the National University of Singapore (NUS) for funding this research with the grant numbers of R-279-000-164-305 and R-279-000-249-646.

Last but not least, I am deeply indebted to my husband, Xuehua Liu, for his steadfast support, self-sacrificial attitude as well as his love shown to our family. Special thanks also go to my two daughters, for their toughness and endurance in life, for their growing together with my research. They are Hong Zhan Liu (12 years old), Hong Zhi Liu (4 years old).

Jiu-Hua Cheng

Table of Contents

Summary

Ion Exchange Membrane Partitioned Free-Flow Isoelectric Focusing (IEM-FFIEF) is an emerging separation process combining both membrane technologies and electrophoresis technologies in a series of separated chambers. Driven by electric field, IEM-FFIEF allows charged species freely migrate in bulk solutions, selectively cross the membranes and predeterminedly be concentrated in a certain chamber. Hence, IEM-FFIEF is practically effective and economically feasible for the separation of protein mixtures as well as other bio-products from plasma or fermentation broth. The purpose of this work is to explore the feasibility of IEM-FFIEF, to fabricate high performance protein separation ion exchange membranes, and to investigate the effects of various factors on separation performance. Emphases are placed on the understanding of mass transfer across the separation membrane under an environment of isoelectric focusing.

This study firstly investigated the feasibility of a combination of membrane technology and the Free-Flow Isoelectric Focusing (FFIEF) technology for a high-performance protein separation, in which ion exchange membranes are used as the separation media. A FFIEF device has been designed and extensive experiments have been conducted to prove its efficacy in enhancing the protein separation performance. Three types of membranes were employed in this work to replace conventional immobiline membranes. They were commercial microfiltration (MF) ion exchange membranes, commercial neutral ultrafiltration (UF) cellulose membranes, and home-made ultrafiltration sulfonated polysulfone (UF SPSf) ion exchange membranes. The protein separation results show that the home-made UF SPSf

membranes have the superior selectivity and flux to other membranes. This is due to the fact that a stable pH gradient across the membranes as well as the interaction between the protein molecules and membrane surface play an important role in the high-performance protein separation. By applying a semi-batch separation process and optimizing various experimental conditions, a high-purity (> 90 %) and concentrated target protein is obtained at the permeation side of the home-made UF SPSf membranes with a high flux. This work clearly demonstrates the great potential of FFIEF for industrial applications. Moreover, experimental results in the consecutive semi-batch operations suggests that the membrane fouling phenomenon is not severe, and high reproducibility in separation fluxes can be realized in our designed IEM-FFIEF system.

Secondly, this study was then extended to the investigation of protein mass transfer in IEM-FFIEF system. A series polysulfone based cation-exchange membranes with strong mechanical strength have been developed and applied in free-flow isoelectric focusing (IEM-FFIEF). A fundamental understanding of protein mass transfer in the IEM-FFIEF process has been revealed experimentally, with the aid of boundary effect model contributed by Ennis, Zhang, Steven, Perera and Carnie. We have proven experimentally the existence of a pH gradient across the membrane cross-section when the IEM-FFIEF system is in operation. The boundary effects on particle velocities are calculated based on the IEF assumption and various characterizations, and are compared with the experimental results. In the IEM-FFIEF experiments, a protein mixture (bovine serum albumin (BSA) and myoglobin (Mb)) and sulfonated polysulfone membranes with different ion-exchange capacities (IEC) are applied. Experimental results show that the real velocity and real mobility (of Mb in this study) are

comparable with the mathematic model developed by Ennis et al. These results suggest that the equation proposed by Ennis et al. is sufficient to capture the mass transfer through membrane in the IEM-FFIEF system after considering the effects of pore size distribution and effects of disturbed electric field. The charge properties of the membrane surface play a dominant role on the separation performance of the membranes. Replacing gel-like immobilines, the newly developed porous ion-exchange membranes may effectively perform the selective function for protein separation.

Thirdly, a very unique phenomenon - self-sharpening arisen by ion-exchange membranes is studied in this research work. In order to reduce the overlapping components in a single chamber, aminated poly(2, 6-dimethyl-1, 4-phenylene oxide) (APPO) based anion-exchange membranes are applied in free-flow isoelectric focusing (FFIEF) instead of conventional immobiline membranes as the selective mass transfer media. The APPO polymers with different amination rates are blended with polysulfone and cast on non-woven fabric by the phase inversion technology. Characterizations of XPS scanning, streaming potential and ion-exchange capacity (IEC) demonstrate that the self-prepared membranes posses different extent of amination and IEC values. The performances of the three prepared APPO membranes with different IEC values are compared. Instead of pH imbedded gel-like immobiline membranes, nine pieces of identical porous APPO membranes are employed in FFIEF. The protein mixture comprising bovine serum albumin (BSA), myoglobin (Mb) and lysozyme (Lys) is used as feed solution. Experimental results show that membranes with a higher charge density not only can affect a higher mass transfer rate, but also strengthens the "self-sharpening" function greatly. Therefore, highly charged porous membranes are

favorable in reducing the amount of overlapping components in individual chambers for multi-component protein separations.

Fourthly, by means of amination with diamine and methylation with methyl iodide, we have modified P84 microporous polyimide membranes with characteristics of highly charged anion-exchange membranes. FTIR and XPS scans confirm the amination and methylation reactions on membrane surface. The intrinsic properties of the newly developed anion-exchange membranes have been fully characterized in terms of ζ-potentials, electrical resistances, PWP (pure water permeation) and pore size distributions. By using the newly developed membranes, a free-flow isoelectric focusing (IEM-FFIEF) has been set up for the separation of myoglobin (Mb) and lysozyme (Lys) mixtures. Experimental data show that (1) the Mb flux via the highly charged P84 anion-exchange membrane can be 10 times higher than that of the original P84 membrane and (2) the high surface charge is the predominant factor for the enhanced Mb flux. HPLC results show that not only the Mb flux was high, but its purity in the permeate side is also extremely high. It is therefore concluded that the diamine and methyl iodide modifications can effectively modulate P84 nano-porous membranes with anion-exchange characteristics, which is suitable for the IEM-FFIEF application.

Nomenclatures:

a	Radius of protein solute, in nm.
A	Effective cross-section area of membrane, in m^2.
b	Radius of pore, in nm.
C_{bi}	Concentration of ions dissociated from buffer solution, in $mole.L^{-1}$.
C_i^f	Concentration of ionic species i in feed chamber, in $mole.L^{-1}$.
C_{im}	Concentration of ionic species i in membrane, in $mole.L^{-1}$.
C_{im}^f	Concentration of ionic species i at the feed side of membrane, in $mole.L^{-1}$.
C_{i0}^f	The original concentration of ionic species *i* in feed chamber, in $mole.L^{-1}$.
C_0	Concentration of ionic species i at $z_i = 0$ (x=0) inside membrane, in $mole.L^{-1}$.
D_{im}	The diffusivity of ionic species i in membrane, in $m^2.S^{-1}$.
d_p	Nominal pore diameter of membrane, in nm.
E	Electric field strength $E = \imath/(\kappa_0 A)$, in $V.m^{-1}$.
E_∞	Undisturbed electric field density, in $V.m^{-1}$.
E_∞'	Disturbed electric field density, in $V.m^{-1}$.
e_z	Unit vector in electric field direction.
F	Faraday constant, $F = N_A * e = 96485\ C.mole^{-1}$.
F_p	The percentage of pores above minimal effective pore size d_p=7.8nm.
I	Ionic strength, in $mole.L^{-1}$.
I_o	The zero order term of the first kind of modified Bessel functions.
I_1	The first order term of the first kind of modified Bessel functions.

IEC	Ion exchange capacity, in $meq.m^{-2}$.
$_i$	Ionic species i of protein molecules, i = 1, 2.
L	Effective thickness of membrane, in μm.
l	Total length between two electrodes, in cm.
m_1	Mass of membrane before drying up for porosity measurement, in gram.
m_2	Mass of membrane after drying up for porosity measurement, in gram.
N_i	Total number of amino acid units in a protein molecule.
n_i^z	Charge number on one protein molecule.
ΔP	Pressure drop tested by surface analyzer, in kPa.
p	An electrophoresis constant defined by Svensson, $\mu_{im} = - px$.
q_s	Surface charge quantity, in Coulomb.
R	Ideal gas constant, 8.314 $J.mol^{-1}.K^{-1}$.
R_e	Minimal effective pore radius, in nm.
R_T	The retention also is referred as rejection rate.
T	Temperature in Kelvin.
V	Constant voltage applied on electrophoresis, in volt.
V_f	Volume of feed chamber, in m^3.
ι	Current of electrophoresis, in A.
μ	Mobility, in $m^2.V^{-1}.s^{-1}$.
μ_{im}	Mobility of ionic species i in membrane, in $m^2.V^{-1}.s^{-1}$.
μ_s	Mobility of solute particles in $m^2.V^{-1}.s^{-1}$
z_{bi}	Valence of ion *i* dissociated from the buffer solutes, here z_{bi}=1.
z_i	Effective valence for species i.

z_p	Valence of every charge site for protein molecules, here $z_p = 1$.
x	Coordinate along the direction of membrane thickness. x = 0 at pH=6.8 side.
ζ_s	ζ-potential of protein molecule surface, in mV.
ζ_w^f	ζ-potential of membrane pore surface at feed side, in mV.
ζ_s^f	ζ-potential of protein molecule surface at feed side, in mV.
ζ_t	Interaction potential between membrane and protein molecules, in mV.
γ	$\gamma = \zeta_w/\zeta_s$, the ratio between the ζ-potential of pore wall and the ζ-potential of solute particle.
κ^{-1}	Debye's length, in nm.
κa	The dimensionless size of protein molecules.
κb	The dimensionless size of pore.
κ_0	The conductivity of buffer solution in the feed chamber, in $mS.m^{-1}$.
κ_w	The overall conductivity given by $\kappa_w = \iota / Vl$.
λ	The ratio between protein molecule size and pore size. $\lambda = a / b < 1$ is the ratio of particle size and pore size
ε	Dielectric constant.
ε_p	Membrane porosity.
ε_r	The relative permittivity.
ε_0	The dielectric permittivity of a vacuum. $\varepsilon_0 = 8.85 \times 10^{-12}\ C^2.\ J^{-1}.m^{-1}$.
η	Viscosity of solution, in mPa.sec
ρ_w	Density of water, in $g.cm^{-3}$.

ρ_p	Density of polymer, in g.cm^{-3}.
υ	Translation velocity, in m.sec^{-1}.
υ_{real}	The real velocity measured by experiment, in m.sec^{-1}.
AHA	Dense anion-exchange membrane.
APPO	Aminated poly(2,6-dimethyl-1,4-phenylene oxide).
BPPO	Brominated poly(2,6-dimethyl-1,4-phenylene oxide).
BSA	Bovine serum albumin.
ACN	Acetonitrile.
CEM	Dense cation-exchange membrane.
FESEM	Field emission scanning electron microscopy.
FFE	Free-flow electrophoresis, (Becton-Dickinson Inc., USA).
FFIEF	Free-flow isoelectric focusing.
FTIR-ATR	Fourier transform infrared- attenuated total reflectance.
GR	Guaranteed reagent.
HPLC	High performance liquid chromatography.
IEC	Ion-exchange capacity.
IPA	Isopropanol.
Lys	Lysozyme.
Mb	Myoglobin.
NMP	*N*-methyl-2-pyrrolidone.
pI	Isoelectric points.

PEO	Polyethylene oxide
PEG	Polyethylene glycol
PPO	Poly(2,6-dimethyl-1,4-phenylene oxide) polymer.
PSf	Polysulfone polymer.
PVP	Polyvinylpyrrolidone
PWP	Pure water permeation.
TEA	Triethylamine.
THF	Tetrahydrofurane.
XPS	X-ray photoelectron spectroscopy.

List of Tables

List of Figures

CHAPTER 1 INTRODUCTION

Proteins are the basic, essential and vast distributed material of all form of life on earth; they are vital for organisms and are involve in almost every cellular process. Proteins are the most complicated natural resources which have been recognized as a food commodity since the early days of humans on this planet, and it has only been determined recently that different proteins possess specific biological functions within living organisms. The understanding of protein functions can thus aid scientists in the determination of disease mechanisms; hence leading drug development to aim for reductions in side-effects [1]. Therefore, drug proteins have gained great attention in the market nowadays. Statistics show that drug companies sold nearly $ 33 billion in protein drugs in 2002; rising at an average annual growth rate (AAGR) of 12.2 %, this market was supposed to reach $ 71 billion in 2008 [2]. Among all these protein products, monoclonal antibodies were recognized as having the most potential in the development of therapeutic protein products. Since the first monoclonal antibody was licensed for sale in 1986, 21 antibody products have been licensed and put on the market, causing the antibody market worth to expand to $ 21.9 bn in 2008 [3,4]. Besides protein drugs, there is a great demand for many other types of protein products for various applications like that of bioengineering tissue and organ engineering, as well as for new R & D initiatives. In addition, peptides and their derivatives are also considered as other important sources of therapeutic drugs. Hence, it is believed that the real market (except for food) for purified protein products is much larger than the above statistics of protein drugs.

1.1 Membrane based protein separation and its history

Before the understood as an issue of modern science, membrane technology has been applied in a commodity fashion for thousands years, e.g. the dewatering of milk to make cheese. Early nomads knew how to dewater whey protein through membrane technology: they first put milk in a leather bag and sealed it, then dipped the bag into a river or sand and finally increased the pressure by placing a stone on the bag to remove the water from the milk, finally obtaining cheese as a concentrated whey product.

At the beginning of the last century, membrane technology was recognized as an effective purification process [5]. The earliest membrane applications were limited at laboratory scale for analytical purpose preparations and purifications. Gradually, membrane technology was accepted widely by industry and has since been broadly applied in various filtration processes, including bioseparation processes. Biotechnology is commonly divided into ‘‘upstream’’ and ‘‘downstream’’, which refer to bioreaction and bioseparations respectively. Bioseparations is regarding as the bottle–neck in industry, because of the high intensity in its demand for labor, capital and technology. Most of the time, no single technology can work independently in the purification of biomolecular products; several devices or purification methods such as precipitation, centrifugation and filtration have to be combined in order to achieve a final high level of product purity. In common pharmaceutical practices, most target proteins are expressed within a bacterial cell as a complex mixture, usually within a recombinant bacterial fermentation broth. A requisite separation of the entire biomass from the broth is necessary to obtain a high yield harvest of the desired expressed protein.! However, the application of membrane filtration for biomass concentration in the early stages of purification is not a good choice because of the severe fouling problems encountered.

The most economical method of separating the biomass is to apply a preparative centrifuge followed by repeated cell washing and filtration. Hence, cell lysis or other chemical pretreatments and homogenization are performed to break the cell wall. The cell lysate can then be clarified by centrifugation followed by membrane-based ultrafiltration. Finally, the target protein can be purified through chromatography and extracted through precipitation.

In spite of its various difficulties and inconveniences in bio-applications, membrane processes encompass characteristics of compact plant size, high efficiency and low equipment cost, thus rapidly become a major interest in the separation and purification fields [6]. Seeking a more economical option for protein separation, it was inevitably that scientists' eyes were once again transfixed on membranes as a possible solution. Over the last 40 years, the development of membrane separation technology has accelerated due to the discovery of asymmetric membranes by S. Sourirajan [7]. Huge amounts of attention and tremendous endeavor has been focused on the development of membrane-based protein separations, leading to a rapid growth in publication numbers and accumulation of fundamental knowledge. Gradually but slowly, the mechanisms and methodologies behind asymmetric membranes reached maturation, leading to their adoption in large scale bioseparation processes.

Membrane applications in protein separation processes have been intensively studied over two decades in the areas of ultrafiltration (UF), dia-ultrafiltration [8, 9, 10], membrane chromatography [11, 12], membrane based electrophoretic contactors [13] and membrane partitioned multi-compartment electrophoresis [14, 15, 16]. In practice, the major applications of membranes in protein separation include whey splitting, egg component

splitting, plasma component isolation, monoclonal antibody purifications as well as the purification of synthetic peptides and their derivatives, etc. Nevertheless, the complicacy of the broth solution and the obstacles of membrane technology drastically restrain the performance of membrane based bioseparations, with the problematic phenomena of fouling, low selectivity, low flux and flux reducing with operation time. The complicacy of the broth environment arises from the fact that multi-components with similar molecular weights and similar surface charging characteristics co-exist in the mixture and might interact with each other, while the obstacles of membrane technology come from the ceiling capacity of the currently used filtration process and limited fabrication measures. For example, an acceptable selectivity of ultrafiltration processes appears only when there is a tenfold difference in the molecular weights between the two components to be separated.

With the identification of fundamental principles and novel membranes for protein separation, the lineament of membrane technology to solve the aforementioned issues involving bioseparations has become clearer through literature review. The clue for further exploration includes the understanding of phenomena like i) factors influencing selectivity and flux, ii) surface interactions between protein molecules and porous membranes, iii) effects of hydrodynamic driving forces, iv) effects of applied electric fields as well as iv) disturbed electric fields. Following the development of novel membranes in protein separation applications, these understandings were slowly revealed and consolidated by a few scientific milestones.

1.1.1 Scientific Milestones

A membrane is a semi-permeable barrier that allows the preferential transport of one protein component that composing the feed mixture, hence enabling a separation to occur. In most membrane separation processes, membrane permits preferring species to pass via hindering the gross mass movement between the two phases [17]. The preferential passage of a certain component through the membrane results in its enrichment at the permeate side of the membrane, while a depletion of this component occurs on the feed side. This transport of protein molecules can be driven by a chemical potential gradient, pressure difference or an electrical gradient. However, the strong interaction between protein molecules and pore surface of a membrane results in a decreased efficacy of the chemical potential gradient for directing an effective mass transfer through a membrane thickness of 100 μm; the mass transfer of protein driven by chemical gradient or pH gradient is effective only at a membrane thickness of a few microns. Thus, in this dissertation we will not consider protein mass transfer solely driven by a chemical gradient. Pressure driven processes based on ultrafiltration membranes were widely studied and gained great attention in the separation of singular desired components The theoretical work of pressure driven UF separation hence provided a good start point for this dissertation.

1.1.1.1 Pressure driven ultrafiltration

UF for protein purification have been applied previously in protein separation processes, but its performance still remains a critical issue. The high performance separation (with high selectivity and high fluxes) emerged only after the use of porous ion-exchange membranes. Instead of neutral polymers, charged polymers were developed for the fabrication of porous membranes in contemporary protein separation technologies. The

electrostatic energy of interaction between a charged cylindrical pore surface and a charged spherical solute has been theoretically modeled by Smith and Deen [18], two outstanding scientists in the field of transport phenomena. In their work, a concept of colloid mass transfer through charged membrane was postulated and formulated, thus the further understanding of the surface interaction between solute particles and membrane pores became possible. The equilibrium partition coefficient ø in their work was defined as C_p / C_f, which represents the ratio of the concentration just inside the membrane at z = 0 and the concentration at the immediate external of feed side, as shown in eqn.(1-1):

$$\phi = \frac{C_{p,z=0}}{C_f} = 2\int_0^{1-\lambda} \exp\left[-\frac{\psi_E(\beta)}{k_B T}\right]\beta d\beta \qquad (1\text{-}1)$$

where λ is the radio of solute radius to pore radius, λ = a / b; β = 1 – λ stands for the steric exclusion of the solute when one particle present in the pore; k_B is the Boltzmann constant; ψ_E / k_BT is the dimensionless interaction energy. The final expression of the interaction energy due to constant surface charges is simplified as the followed eqn.(1-2) [19, 20]:

$$\frac{\psi_E}{k_b T} = \left(A_s\sigma_s^2 + A_p\sigma_p^2 + A_{sp}\sigma_s\sigma_p\right)/A_{den} \qquad (1\text{-}2)$$

where coefficients A_s, A_p, A_{sp} and A_{den} are all positive, which depend on the feed ionic strength, the pore size, the solute size, and the solute location in the pore. σ_s represents the dimensionless surface charge density of solute and σ_p represents the dimensionless surface charge density of pore surface, as have been explained elsewhere [19, 20]. Some important relationships in the membrane-based colloid separation process can be established via a simplified eqn.(1-2): 1) the interaction energy depends on both the charge of solute molecules and the charge on the membrane pore surface; 2) the interaction energy is a second order charge-dependent function, which include both the

pore surface charge and solute surface charge; and 3) the interaction energy may be manipulated through varying the surface charges, ionic strength and relative pore size.

Many protein separations have been conducted through unmodified membranes and charged membranes according to a fundamental understanding of Eqns. (1-1) and (1-2). Unmodified membranes usually will possess a slight negative charge, which prevents cations from permeating through the membrane under a given hydraulic pressure driving force. Therefore, based on the electrostatic interaction of the solution ions with the membrane pore surface, the co-ions carrying like charges are rejected while the counter-ions are absorbed on the pore surface. On the other hand, the net charge of protein molecules is the summation of ampholytic amino acids and do possess a unique character of changing surface charge according to its surrounding pH. Therefore, a protein's surface charge can be easily manipulated via pH control. When the ambient pH of an environment equals a protein's pI value, the protein experiences a net neutral surface charge; hence the protein carries zero charge on its surface, such that eqn. (1-2) correspondingly takes purely σ_p^2 into account only. When a pH greater than that of the pI (pH > pI), the protein will carry a net negative charge. On the contrary, when the buffer pH < pI, the protein A will carry positive charge. These relationships are displayed in Eqns. (1-3) and (1-4):

When pH < pI
$$\begin{aligned} R-NH_2 + H^+ &\rightarrow R-NH_3^+ \\ R-COO^- + H^+ &\rightarrow R-COOH \end{aligned} \qquad (1\text{-}3)$$

When pH > pI
$$\begin{aligned} R-NH_3^+ + OH^- &\rightarrow R-NH_2 + H_2O \\ R-COOH + OH^- &\rightarrow R-COO^- + H_2O \end{aligned} \qquad (1\text{-}4)$$

Applying the relationship revealed by eqns. (1-1), (1-2), (1-3) and (1-4), different types of electrostatic interactions can be observed, and the optimal operation conditions can be determined. For a membrane-based filtration process, the best operation conditions were

as highlighted by Zydney in [19, 21]. From Eqns. (1-1) and (1-2), it can be determined mathematically that the smallest interaction energy is satisfied by either of the two conditions: 1) $\sigma_s = 0$ or 2) $\sigma_p = 0$. From the viewpoint of operation ease, the most optimal operating condition is to maintain $\sigma_s = 0$ (i.e. pH = pI). Therefore, UF is practically convenient for the separation of two proteins with different pI values, where the pH of buffer solution can be manipulated to one component's pI or the other, and this idea can be repeated for the removal of all other undesired impurities. Zydney *et al.* could therefore utilize this idea to separate bovine serum albumin (BSA) and haemoglobin (Hb) at separation factors exceeding 70 even though the molecular weights of the two given proteins were almost equal to each other [19].

1.1.1.2 Electric field driven electrophoresis

Membrane-based electrophoretic protein separation has encountered many difficulties in component separations, due to the inability of research workers in separating large molecular substances without changing the nature of those molecules in the course of the conducted experiments [22]. The applications of membranes in the separation of biomolecules or proteins are closely related to the Nobel prize-winning work of Tiselius [23]. The first preparative electrodecantation system (electrodialysis) was engineered by Pauli circa 1922-1924 and set up in Vienna, 13 years prior to Tiselius's electrophoresis work [24, 25]. In the 1930s, the largest electrophoretic equipment yet constructed was built in Malaysia [26]. This was a modification of Pauli's electrodecantation with a large number of parallel units assembled with impermeable membranes, in which mass transfer was driven by direct current electric field [25]. Several workers have adapted this approach for the separation of organic or inorganic colloids.

The earliest idea of applying membrane for protein separation emerged in the early 1940s. Kirkwood proposed an apparatus in 1941 by redesigning Pauli's setup for the first membrane-based protein separation device [27, 28]. In the apparatus diagram setup as shown in Fig.1-1, a top chamber and a bottom chamber can be seen to be spaced out by two membranes, the thin space in between the two membranes served as the electrophoretic channel. The protein mixture was fed into the top chamber; the protein that managed to migrate through the electric field was collected and concentrated in the bottom chamber; while the uncharged protein (whose pI equaled the buffer pH) was desensitized to charge differentials and hence was retained at the top.

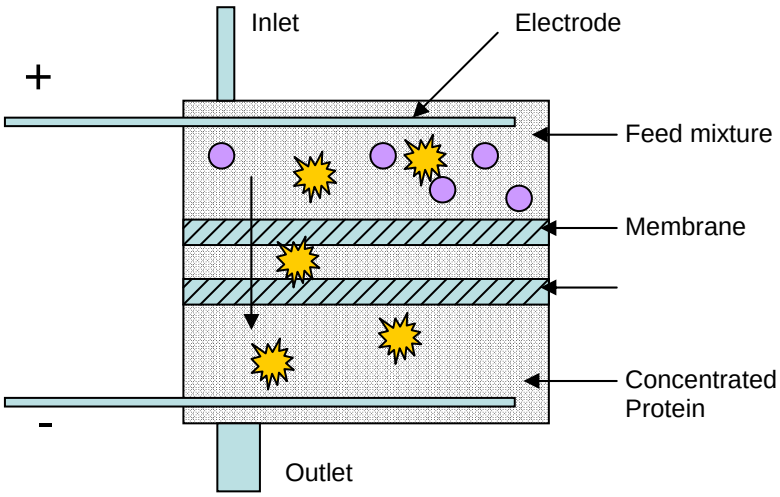

Fig. 1-1 The membrane-based protein separation apparatus suggested by Kirkwood (1941) [27]

At the same time, Tiselius (the Nobel Prize winner of year 1948) employed the principle of isoelectric focusing in the separation of protein mixture. This was a 12-chamber Perspex device with cotton flannel as an intermediate, leather as an anodic and parchment paper as a cathodic membrane. Separation for the mixture of egg albumin and hemoglobin was studied through a 0.005 N sodium sulfate solution and 24 hrs operation.

The analysis results of each individual chamber are detailed in Table 1, indicating a complete separation was achievable. With the electrophoresis method contributed by Tiselius, it thus became possible to study colloids and substances with macro-molecules [22], and the analysis and characterization of protein based on electrophoresis has become a standardized job in the laboratory.

Table 1-1 Separation of egg albumin and hemoglobin by electrical transport [28]

Compartment	Protein conc.,mg.N/ml	
	Egg albumin	Hemoglobin
Anode	0	0
1	0.64	0
2	0.67	0
3	0.82	0
4	0.47	0
5	0.06	0.18
6	0	0.42
7	0	0.52
8	0	0.52
9	0	0.50
10	0	0.43
cathode	0	0

However, the significance of membrane-based electrophoresis is not useful for analytical purposes and laboratory scale preparations, but also in the large scale protein separation processes as required by the industries. Polson reported a series-modified electrodecantation apparatus in 1953 comprising chilling sections, reduced distances between membranes and continuous flow pattern for the separation of complex mixtures [29]; schematic diagrams are shown in Figs. 1-2 and 1-3. The real consideration for large scale applications came in the prevention of protein denaturization due to convective heat transfer generated by high-current. In this modification, multiple chambers were

connected by tubing and cooled by using alternated cooling chambers, improving electrophoretical resolutions dramatically.

However, the mechanism relating the influence of membrane structure and surface charge on protein mass transfer was not analyzed during that period when the apparatus was first developed, as it could be observed that the insertion of an uncharged UF membrane into the above apparatus caused a great reduction in the separation flux [28]. Some scientists pointed out that the finer partitions such as membrane or even gels imposed their own characteristics on the separation process [25]. As a result, monofilament screens of 5-10 μm pore size appeared to be the best choice for the chamber partitioning, because it could offer some resistance to flow but impose the fewest constraints on the transport of protein molecules. This concept has been applied by Bio-Rad in their commercial apparatus Rotofor, which has found great success in laboratory-scale protein fractionation. Based on the same reasoning, Bier, another outstanding contributor within the electrophoresis field, accomplished a successful protein fractionation in their RF3 (Recycling Free-Flow Focusing) apparatus. This apparatus shows that proteins can be sharply separated into three zones within a thin chamber of thickness 0.75 mm without the aid of any intermediary membranes as shown in Fig. 1-4.

In any case, the concept of membrane-based protein separations still maintains a great degree of interest within the scientific world today; as can be represented by the pH-imbedded gel-like membrane “Immobiline” developed by Righetti *et al.* as they

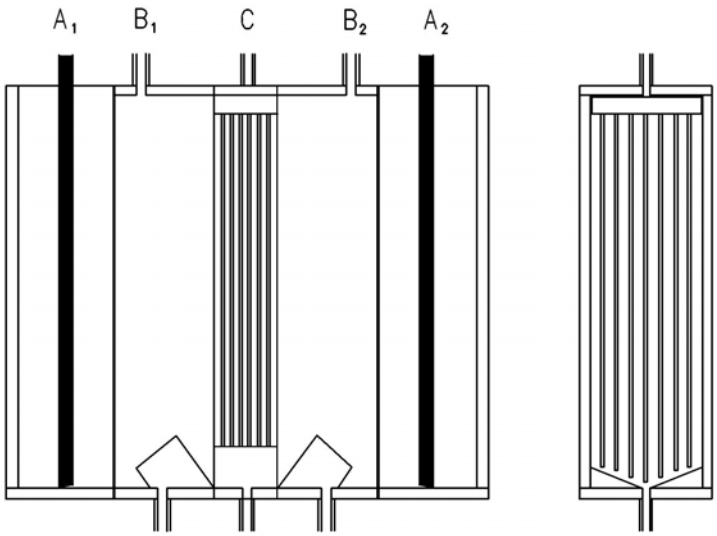

Fig.1-2 The simplest multi-membrane electrodecantation apparatus of Polson, 1953 [29].

A1 and A2 are electrode compartments, B1 and B2, are compartments through which cooled buffer is circulated and C is the separation cell packed with "cellophane" membranes and "perspex" frames.

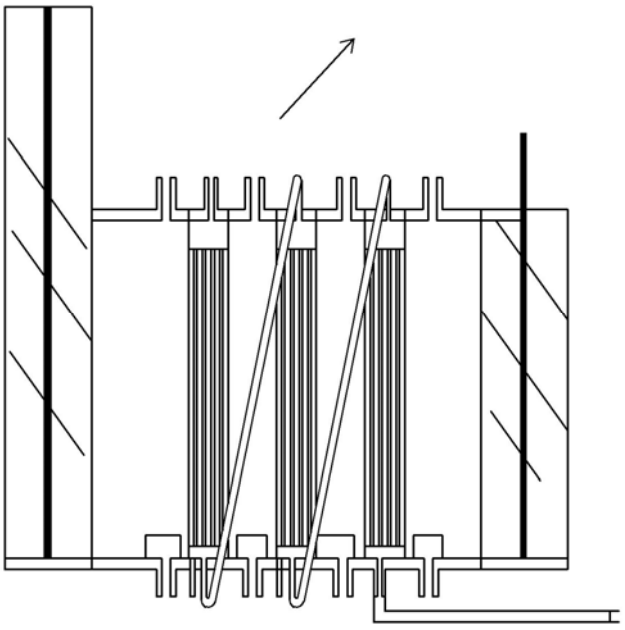

Fig. 1-3 The modified electrodecantation apparatus of Polson, 1953 [29]

In this modification, multi-chambers was connected by tubing and cooled by alternated cooling chamber. The resolution of electrophoresis was improved dramatically.

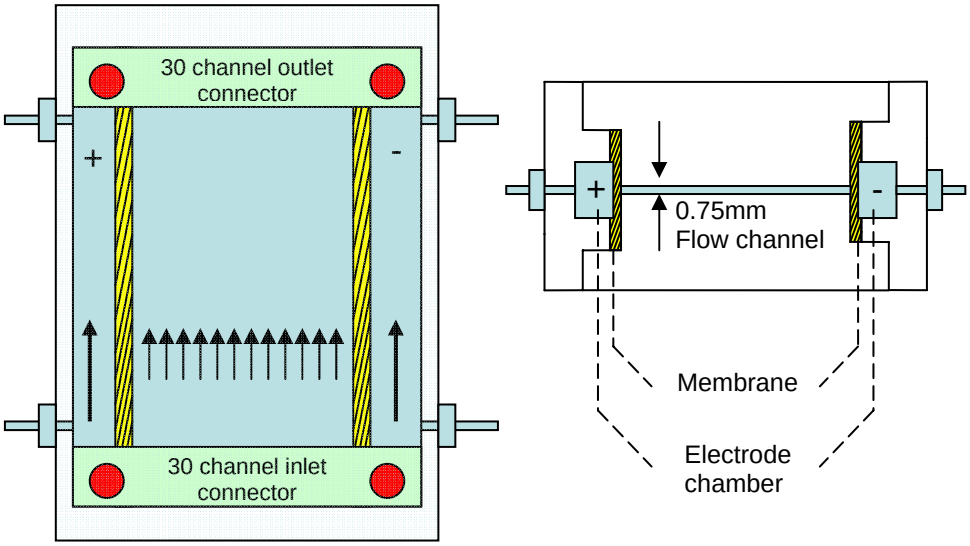

Fig.1-4 The free flow focusing apparatus RF3 and its cross-section view

generated the idea of "segmented immobilized pH gradients" [30, 31, 32] to maintain a protein's isoelectric point in a liquid stream. Therefore, in a feed buffer stream containing the desired protein and other impurities circulating orthogonally to an applied electric field, the impurities would migrate to the lateral gel phases delimiting the feed stream, while the desired protein maintained its isoelectricity in the feed chamber. The pH-imbedded gel-like membrane was later termed "Immobiline". Based on this technology, multi-chamber IEFs were conducted and multi-component protein mixtures were fractionated [33]. These pioneering works on pH-imbedded membranes revealed the determinant role of a charged barrier in protein separations, therefore implying that a possible route for multi-component protein separation could be realized by an ion-exchange membrane partitioned IEF.

1.2 Development of boundary layer theory

1.2.1 Hindered mass transfer

The mass transfer in liquid-filled pores of molecular dimension is of key importance in a membrane-based separation of colloidal solutes. The mass transfer of such a solute through the membrane will be much slower than that in bulk solution, particularly when the pore dimension is of the same order as that of a solute molecule. Through the efforts spanning over more than seven decades, mathematical models of hindered mass transfer elucidating the relationship between selectivity and membrane properties as well as solute molecules have been established [34]. These hindered mass transfer models have been used previously to understand the workings of biological membranes [35] and some physiological applications [36]. The link was only made later on that the hindered mass transfer model has extensive applications in separation engineering, e.g. characterization of membranes [37] as well as colloidal particle separations.

In practice, scientists have found that the surface charges on both the membrane pores and solute particles have been critical in membrane-based colloidal particle separation. It was noticed that the electrostatic and dispersion forces have large effects on hindered mass transfer through a membrane. Therefore, a new interest in the theory of electrostatic effects in hindered mass transfer was stimulated by the requirement of protein separation. Malone and Anderson proposed an approximate model taking into account the contributions of the electrostatic and dispersion forces to the partition coefficient [38, 39]. A more precise electrostatic effect for a spherical particle in a cylindrical pore was proposed later by Smith and Deen [40, 41]. In their model, the partition coefficient was correlated with relative pore size, pore surface charge, particle surface charge and Debye length (bulk concentration). For the first time, a theoretical prediction in the electrostatic effect on hindered mass transfer through a charged membrane was provided. In turn, the

partition coefficient of a membrane having precisely known properties could then be easily calculated and verified through experiments.

Nevertheless, the presented analytical model for electrostatic effects was derived by assuming the absence of an electric field. It has been noticed that the resistance of mass transfer through membranes driven by an electrical potential gradient imposed along the pore axis is much lower than mass transfer operations which are driven by hydraulic pressure [34]. After 1980s, the hindered mass transfer in electric field arose more attention, which was termed boundary effects in electrophoresis scope.

1.2.2 Thin double layer and protein separation

In 1985, Keh and Anderson analyzed [42] the boundary effect in the special case of a very dilute solution, which was also defined as a thin double layer. For colloidal spheres moving along the electric field across the membrane, the mobility is strongly dependent on the surface charge densities of both the membrane and the colloidal solute [A-1, in Appendix A].

Since mobility μ can be expressed in the form of $\mu = \upsilon / E_{\infty}$, the high ζ-potential of charged membranes in an IEM-FFIEF system would facilitate the particle's mobility and hence enhance the permeate flux during the separation process. On the other hand, according to the corrected Stokes' law proposed by Faxen [43], the Stokes' translation velocity can be written as a function of relative pore size $\lambda = a / b$, viscosity η, solute particle size a, and the force applied parallel to pore walls Fe_z [A-2]. By comparing the normalized electrophoretic mobility and Stokes' mobility, it was found that the hindrance in electrophoresis is much weaker than that in a pressure-driven filtration. This

comparison indicates that a lesser energy is required for an electric-force-driven mass transfer across a membrane. This phenomenon might explain the high efficiency of ion transfer through the in vivo cellular membranes. A pH difference exists across all of the living cells, and this pH difference produces an electric field as the driving force for mass transfer. In comparison with all the current technologies of membrane-meditated ion transfer, the membranes in living cells possess an untouchable efficiency in the absence of high pressure. The numerical comparison of the normalized electrophoretic mobility and Stokes' mobility were demonstrated in Fig. 1-5.

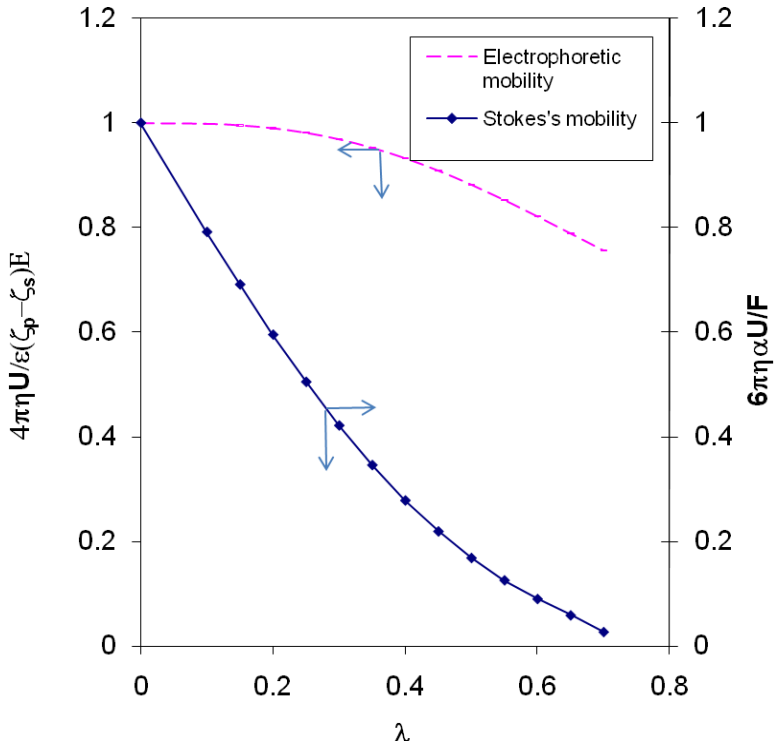

Fig. 1-5 Comparison between electrophoretic mobility and Stokes' mobility of a sphere on the axis of infinitely long pores [42]

Fig. 1-5 reveals that both the electrophoretic mobility and Stokes' mobility across a charged (positive or negative) membrane are monotonically decreasing functions of the relative pore size λ= a/b. From Fig. 1-5, one can find that the electrophoretic mobility

decreases much more slowly than the Stokes' mobility, indicating that the wall effect of hydrodynamic resistance overrides the wall effect of electrostatic benefits. In contrast, when the electrophoresis is performed parallel to a dielectric pore wall, the total wall effect of two opposite forces can speed up the migration of the particle [44]. However, it has to be noted that the electrophoretic mobility of a dielectric sphere can be improved dramatically by a lateral wall when the gap spacing is small. This is an important point to note when attempting to improve the mass transfer of membrane-based electrophoresis.

The accuracy of Eqn. (A-2) was proven to be extremely good and errors in this case were claimed to be less than 2.1 % if $\lambda \leq 0.7$ [45]. The accuracy deteriorated only under circumstances of very small pore size, i.e. $\lambda \geq 0.8$. However, membrane-based electrophoretic separations are rarely operated within infinitely dilute solutions ($\kappa a \rightarrow \infty$). Instead, most of membrane based electrophoretic separations are running under a reasonable higher concentration leading to a thick double layer ($\kappa a \leq 20$). Therefore, a mathematical model of a boundary effects (thick double layer) suitable for various double layer thicknesses had to be formulated to take operating conditions into account.

1.2.3 Thick double layer and protein separation

During the past two decades, a great deal of progress has been made in furthering the understanding of macromolecular electrophoretic motion in pores; in quantifying the effect of electro-osmosis; in defining the role of bulk concentrations; and in exploring the electrostatic effects on the mass transfer rates. The efforts in elucidating the role of solute concentration (thickness of double layer) provide a particularly profound and extensive change in membrane-based colloidal separation research. The theoretical study of

boundary effects with an arbitrary double layer thickness reveals that membrane-partitioned electrophoresis might have staged prior to the filtration process under any solute concentration. Therefore, the idea of membrane based electrophoresis for colloidal separation, which was once considered outdated, was revitalized by the development of the boundary effect theory.

In an electrophoresis separation process, the solute molecules which are large enough to behave as colloidal particles always are closely surrounded by other molecules or boundaries rather than isolated, which is similar to the case of a particle in a porous membrane. Hence, most of colloid electrophoreses are carried out in a system with thick double layer (low κa values). Furthermore, these charged colloidal particles and charged boundaries will impose a perturbation in the applied electric field, thus distorting the field and changing the mass transfer direction. Assuming a low surface potential and unrestricted double layer thickness, Ennis and Anderson [46] proposed an analytical solution for these circumstances [A-3].

Almost at the same time, Ennis et al. [47] proposed another mathematical model in the form of [A-4][48] concerning the mobility of protein through a porous membrane. In this solution, both the contributions from electro-osmosis and from Poiseuille flow to the average particle velocity were analyzed.

A comparison of eqns. [A-3] and [A-4] demonstrates that the only noticeable difference between these two equations lies in the [f (κa) – γ] term. Equation [A-4] provides for the first time a precise and explicit general solution for membrane-based protein electrophoresis by taking into account the quantified contributions of Poiseuille flow and

electro-osmotic flow to boundary effects. Following the method developed by O'Conner *et al.* [48], a verifying experiment test was performed in the study of Ennis *et al.* [47], showing an excellent agreement. Experiments showed that eqn. [A-4] does not merely provide an accurate calculation taking into account the various effects influencing mass transfer, but also implies that there can be a methodology development for the quantitative study of membrane-based electrophoresis.

The study of Ennis *et al.* triggered considerable interest in membrane-based electrophoresis, and multiple studies based on boundary effect simulations have been conducted thus far. Representative works have been contributed by Hsu and his associates [49, 50, 51, 52, 53]. Without experimental limitations arising from methodologies and conditions, these simulation works are capable of interpreting the boundary effects under various circumstances with numerical estimation. Hence, simulation works do play important roles in designing electrophoresis systems.

Recently, a more generalized analytical solution of the translation and angular velocities was developed by Keh and Hsieh [54]. Other than an evenly distributed surface charge, a dielectric particle and a spherical cavity with non-homogeneous surface zeta-potential on solid surfaces was analytically investigated by the using of the multipole expansions of the zeta-potential in the Poisson-Boltzmann equation. This result might overcome the limitation of eqn. [A-4] which was assumed suitable for a homogeneously distributed low surface zeta-potential.

1.3 Membrane technologies for protein separation

With a burgeoning demand from the life science industries, efficient membrane separation processes are required to meet the challenges faced by the pharmaceutical industry and in clinical practice. The immediate challenges faced by membrane separation processes including: high operation cost, low productivity, low selectivity and fouling. To conquer these difficulties, tailored membranes with well-designed biochemical and physical properties in conjunction with appropriate module design are recognized as the decisive factors. Since the separation performances are highly dependent on membrane properties, this study will inevitably take into consideration of material selections and fabrication technologies.

1.3.1 Membrane materials

Membrane electrochemical behavior relies principally on material selection [28]. The choice of material influences and constrains the membrane fabrication technique applied, physical property and morphology obtained, in turn influencing the membrane's electrochemical behavior during the separation process. The electrochemical behavior is generated from electrostatic interaction as well as boundary effects, influencing the overall separation efficiency of a process. However, the selection or the preparation of a suitable material with ideal physical properties and strong mechanical strength is not a trivial task. A few key factors originating from material nature have to be taken into consideration: 1) high charge rate; 2) strong mechanical strength; 3) low swelling rate; 4) low fouling; 5) good stability under both chemical and electrical environments; 6) manufacturing reproducibility; and 7) low cost. It is usually the case that natural materials, synthetic polymers, inorganic materials are applied for protein or other macrobiomolecule separations.

1.3.1.1 Natural materials

Natural materials derived from living beings have already been used over the ages as membrane materials for the dewatering of dairy products, e.g. the diverse use of animal bladders and leather have been applied as widespread tools for food preparation around the world. The study of membranes as a science was first conceived by Fick in 1855 [55]. The first record of the term "ultrafiltration" was conducted by Schmidt in 1856 [56] through filtering protein solutions across an animal membrane. At the early stages of membrane science development, many scientists adopted natural materials such as bladders, leathers, cow intestine, amnion and chorion as study objects [5]. The use of natural materials as membranes could generate high fluxes in MF and UF operations, and its use in electrodecantation (later termed as electrophoresis) for amino acids and protein separations produced excellent separation performance [28]. However, the limitations of membrane characterization technology during that period prevented the measurement of important membrane characteristics such as surface zeta potential, ion-exchange capacity, porosity and pore size or molecular weight cut-off. However, it was inevitable that synthetic polymer membranes would gradually replace natural membranes due to their ease of fabrication and excellent data reproducibility.

1.3.1.2 Organic (polymer) materials and their modifications

Polymeric materials are homogeneous and cost-effective with good processability and high reproducibility; hence they gradually became the dominant materials utilized for membrane fabrication. The first artificial membrane was made from collodion in dialysis

experiments [55]. At the early stages of membrane technology, most membranes for ultrafiltration were gelatinous [5]. Collodion sac artificial membranes were the first non-natural membranes to be extensively applied in various ultrafiltration processes, especially in protein separations and biological research. They were highly popular because of their easy processing, good data reproducibility and large filtration surface area. Other synthetic polymers were developed by the dozen for various membrane-based separation processes over the next seven decades. In spite of these developments, the development of protein separation and purification technology has been going at an extremely slow pace; only a few types of ionic polymer materials have proven worthy in protein separation over a long period of operations. The development of ion exchange membrane-based processes began in 1890, when the work of Ostwald [57] discovered that a membrane can exhibit impermeability towards certain electrolytes. It was discovered later that membranes with pore sizes in the order of 10^{-8} m (UF) or in the μm range (MF) could be applied satisfactorily in bioseparation processes. The most representative application, diafiltration technology, was the brainchild of Zydney's research group [6, 9, 10], which employed ion exchange membranes for protein separations in UF mode. These polymers can be charged by various chemical groups, such as strong acidic types (sulfonic groups), weak acidic types (carboxylic groups), strong base types (quaternary amine groups) and weak base types (primary, secondary and tertiary amine groups).

The primary choice of polymer backbones are those that can be easily grafted with charged groups, such the negative functional groups of $–SO_3^-$, $–COO^-$, $–PO_3^{2-}$, $–PO_3H^-$ and $–C_6H_4O^-$ etc. for cation exchange membranes, while positively charged groups, such as $–NH_3^+$, $–NRH_2^+$, $–NR_2H^+$, $–NR^{3+}$, $–PR^{3+}$ and $–SR^{2+}$ etc. are grafted to polymers for

anion exchange membranes [58]. Commonly used polymers include polyimides, PEK (polyether ketone), PEK-C, PSf (polysulfone), PES (polyethersulfone), PPO (poly p-phenylene oxide), PPS (poly p-phenylene sulfide) and their blends or block copolymers.

Most polymers used as the support layer of ion-exchange membranes are generally insoluble in any solvents, such as hydrocarbon PE and PP or fluorocarbon origin (PTFE, FEP, PFA, ETFE and PVDF). Three types of membrane fabrication technology are commonly used: 1) in casting modification, strong cation exchange membranes are prepared by the grafting of styrene on the given polymer films and the as-cast copolymer films are subsequently sulfonated, while the weak cation exchange membranes are prepared by grafting of epoxy acrylate monomers onto polymer films followed by the conversion of the epoxy group into carboxylic group. 2) phase inversion casting; 3) phase inversion spinning.

UF or MF membranes can principally be characterized as either hydrophilic or hydrophobic materials. Materials suitable for protein separations traditionally possess good hydrophilic properties and small contact angles. In comparison with hydrophobic membranes, hydrophilic membranes have a much reduced tendency to foul over long operation periods. This might be due to the fact that the ionic groups on a polymer chain form a water-rich environment inside the pores, which can facilitate the ionic interaction with protein molecules and prevent the formation of covalent bonds between membrane surface and protein molecules, such as a disulfide linkage. In the later operation steps, this interaction force can be easily overcome by varying the ionic strength or the strength of the applied electric field. On the contrary, hydrophobic membranes are characterized by a big contact angle ($> 90^{o}$), which can have hydrophobic interaction with protein

molecules thus forming an irreversible protein fouling layer on the membrane surface. Therefore, most hydrophobic membranes are not ideal for protein separations.

Following the development of electrophoretic technology, the gel-like membrane was slowly developed into a contemporary pH immobilized mixed matrix material as in the case of immobiline, which can effectively transfer protein molecules and accurately allocate them into different chambers according to their pI values (isoelectric point) [31,30, 31]. Nevertheless, the use of gel-like membranes presents a serious limitation in large scale fabrications; for example, the partitioning of electrolyzer cells required 3.5 m^2 of membrane area (standard electrolyzer size for Chloro-alkaline plants). However, gel-like membranes failed to meet the requirement of mechanical strength for installation and long term operations; therefore, the development of porous membranes with higher mechanical for such operations have received much more attention over the past half-century.

1.3.1.3 Inorganic material

The application of inorganic materials can be dated back to the 1920s, where Keil and Schieck (1928) [28] used porous earthenware as diaphragms in their protein isolation study, describing an immediate isolation of glycocholic acid from bile. In recent years, inorganic–organic composite materials are recognized as promising engineering materials due to their remarkable properties [59]. Organic materials provide high flexibility, good processability, tunable electrical properties, possible usage for semiconducting, and a certain degree of metallic behavior, while inorganic compounds provide the potential for high mobility, a range of magnetic and dielectric properties and

thermal and mechanical stability [58]. In spite of all these advantages, there have been few published studies investigating the application of inorganic membranes for protein separations. According to the known properties of such composite membranes shown in historical studies such as a high porosity, high mechanical strength and high electric conductivity etc., inorganic-organic membranes are very capable of developing a highly selective mass transfer for protein separation. Therefore, it is very possible that inorganic-organic membranes will replace gel-like immobiline materials and become an important medium for protein separations in free-flow electrophoresis.

1.3.2 Membrane fabrication

The performance of a membrane is heavily dependent on its structure and physical properties. The immediate challenges for industrial applications are the preparation of membranes possessing not only a good performance but a good durability in real process environments. Membrane fabrication is the critical step to pattern a material with a proper technique to develop the critical specific morphologies and requisite physical properties for optimal performance without neglecting mechanical strength. A number of techniques such as melt extrusion, compression modeling, stretching, track-etching, sol-gel process, vapor deposition, sintering, phase inversion spinning and solution casting have been developed to fabricate polymeric and inorganic membranes with the requisite pore sizes for separation purposes, and industry application demands of both performance and mechanical strength necessitate the formation of a thin selective skin on a strong porous supportive structure. In these membranes, the thin skin layers carry out the protein separation, and the porous structures provide sufficient mechanical support to withstand various impacts and vibrations generated by pumping actions.

Fig. 1-6 demonstrates the schematic diagram of the three types of porous membranes commonly used in protein separation processes: 1) a homogeneous porous membrane with pores in the range of 10 - 90 nm; 2) an integrally skinned asymmetric membrane, with homogenous pores in the range of 10 – 90 nm formed as the selective layer at the top of porous structure; 3) an integrally skinned asymmetric membrane or inorganic composite membrane sealed with a protective layer. A homogeneous porous membrane merely consists of a solid matrix with a porous structure uniformly dispersed throughout the whole membrane. Most symmetric microporous membranes are fabricated through the sintering of inorganic particles or phase inversion from a three-component dope (polymer-solvent-additive). Following the development of nanotechnology, the sintering of nanosized inorganic particles has become possible and symmetric membranes with pore sizes in the range of 10^{-8} m are available commercially.

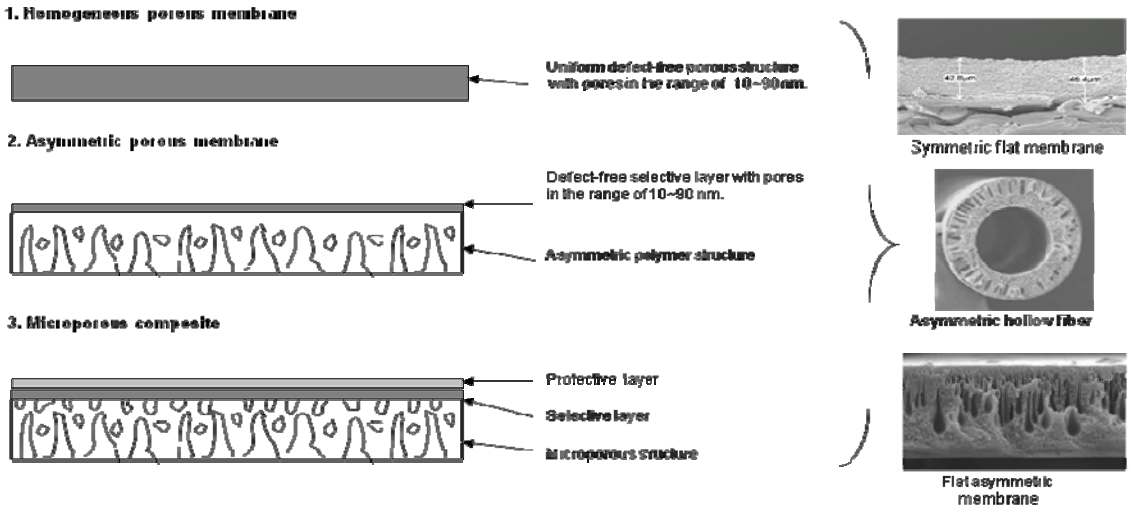

Fig. 1-6 Typical membrane structures

Asymmetric membranes can be formed in different geometries such as hollow fiber, flat sheet and tubing etc., by using an appropriate choice of fabrication equipment. Hollow

fiber membranes have been regarded as the most important membranes for filtration processes, mainly owning to their large membrane area per unit volume, good flexibility and self-contained mechanical support in industrial applications [60]. Asymmetric hollow fiber membranes are normally fabricated through phase inversion spinning. The composite hollow fiber membranes with protective layers are generally formed via a dip coating process as an additional treatment step to the phase inversion. Despite the many advantages attributed to hollow fiber membranes for various applications, they cannot be easily employed in electrophoresis due to their geometric limitations. Hence, the selection of membrane partitions for electrophoresis invariably ends up being flat sheet membranes.

Flat sheet membranes were once regarded as only useful for laboratory scale processes. However, in various industrial applications of electrodialysis and electrolysis, the flat sheet membrane became an indispensable requisite in an electrolyzer. For example, as shown in Fig. 1-7, flat-sheet Nafion membranes containing 3.5cm^2 of useful mass transfer area are applied in chloro-alkaline plants for the electrolysis of saturated sodium chloride solution into chlorine and sodium hydroxide. In every electrolyzer, 50 to 100 cells partitioned by identical membranes are arranged in series. Sodium ions selectively pass through the membrane to the cathode side of the cells, while chloride ions will be oxidized and form chlorine gas on the anodic side. As shown in Fig.1-8, another important application is the recovery of heavy metal or toxic electrolytes from industrial wastewater. Electrodialysis of waste water was performed through alternatively arranged cationic and anionic membranes. Based on the numbered examples available, it can be concluded that the role of flat sheet membranes are still very much invaluable in the area of electric field driven separation processes.

The formation of asymmetric porous membranes relies heavily on the phase inversion in the coagulant bath, very much similar to the spinning of hollow fiber membranes. Research in asymmetric membranes was first developed by Loeb and Sourirajan [61]. The phase inversion process has thus been formulated and standardized for industrial applications, whereby an integrally skinned asymmetric membrane can be fabricated in a singular step. Both the academic and industrial practices conclude that the key control parameters in membrane fabrication are that of pore size, the pore size distribution of the selective layer, as well as the thickness of the selective layer. In phase inversion membrane formation technologies, the manipulated variables for pore size and pore size distribution control include the chemical structure of polymer material, polymer solution concentration, diffusivity of polymer solution solvent in the nonsolvent, post-treatment membrane heating and cross-linking of the prepared membrane. For the fabrication of composite membranes, a layer of highly porous and inert material was coated on the top of asymmetric polymeric membranes or organic-inorganic mix matrix membranes for the purpose of protection from various frequent but minor damages, such as particles impact in the streams and pressure-induced vibrations.

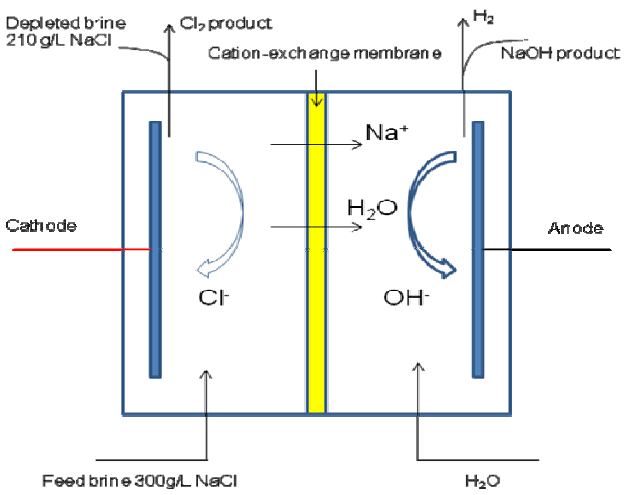

Fig. 1-7 Electrolysis of sodium chloride solution

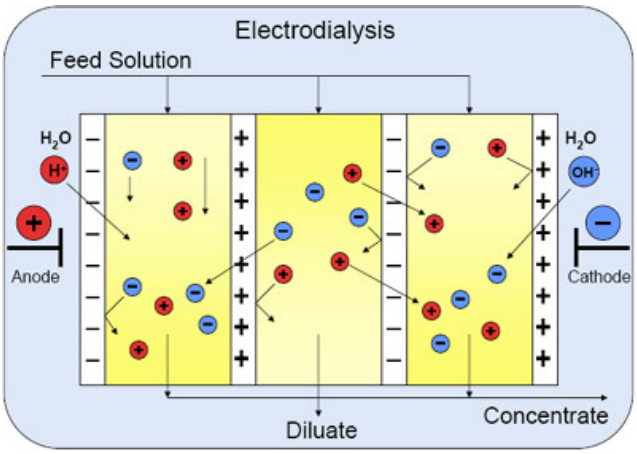

Fig. 1-8 Electrodialysis of waste water

1.3.3 Membrane module design and system design

Membrane-based protein separations provide a great opportunity to for increasing separation efficiency in the pharmaceutical industry. The membrane module is considered the crux of a separation system as it determines the overall productivity and efficiency of a separation process. The modules applied in industrial processes have traditionally been based on flat sheet and hollow fiber configurations. The vast majority of membrane modules are classified in five basic designs: hollow fiber, tubular, capillary, spiral wound as well as plate-and-frame. Generally, hollow fiber, tubular, capillary modules are applied in a filtration process which only have one feed and one permeate; the spiral wound module can theoretically align different membranes in series; thus it can perform multi-component separation within the same module. However, this operation is considerably constrained by pump capacities and membrane resistance, because stacked membranes in series provide a greater resistance to flow. In contrast, the plate-and-frame module is the only reliable choice for a multi-chamber, multi-component separation, which allows for the imposition of a homogeneous electric field on each membrane.

1.3.3.1The plate-and-frame module

A plate-and-frame membrane design consists of a package of flat-sheet membranes in repeat units between two electrodes. The plate-and-frame design may seem simplistic from an engineer's point of view, but it is sufficiently complex to act as robust and adaptive tools for multi-component protein separation. As shown in Figs. 1-7 and 1-8, the plate-and-frame design has been broadly applied in the electrochemical separation industry due to its high efficacy at such separations.

1.3.3.2 The spiral wound module

The spiral wound module maintains the simplicity of flat-sheet membranes, with a remarkably increased specific surface area of 300 m^2 / m^3 in comparison with the plate-and-frame module. As shown in Fig. 1-9, the assembly includes a sandwich of flat-sheet membranes with sieving or spacers between each sheet to offer permeate flow space and increase mechanical strength. The membrane envelope is wound around a collecting tube. When a spiral-wound module is running, the protein mixture is fed from the outside of the membrane, while the permeate is collected from the center collector. The spiral-wound module has been heavily employed in desalination plants for reverse osmosis operations. However, to the best of our knowledge, the application in electro-chemical scope has not been revealed. For our applications of protein purification, the use of a thin membrane stack might see the spiral-wound module being effective in multi-chamber electrophoresis operations.

1.3.3.3 The hollow fiber module

Hollow fiber membrane modules are assembled by packing a large number of spun fibers into a pressurized vessel. As shown in Fig. 1-10, the membranes are spun in the geometry of hollow cylindrical tubes with small diameters and adequate pore size, and most of these hollow fiber modules are used for filtration purposes. Its applications in biochemical processes are concentrated mainly in sterile filtration, tangential flow micro-filtration and virus filtration [6]. However, hollow fibers seem unsuited for multi-component protein separation due to the difficulty in imposing a homogeneous electric field across every hollow fiber. This difficulty lies in the assembly of electrodes in the large number of hollow fibers.

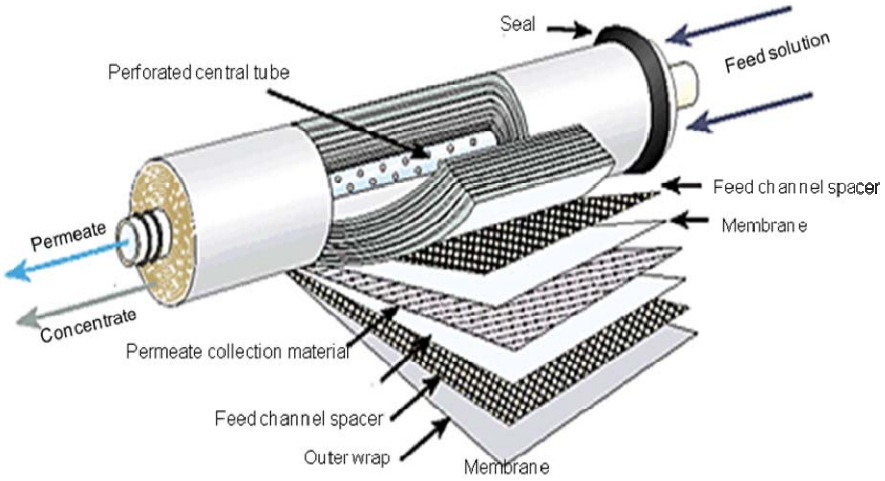

Fig. 1-9 The spiral-wound module and its assembly

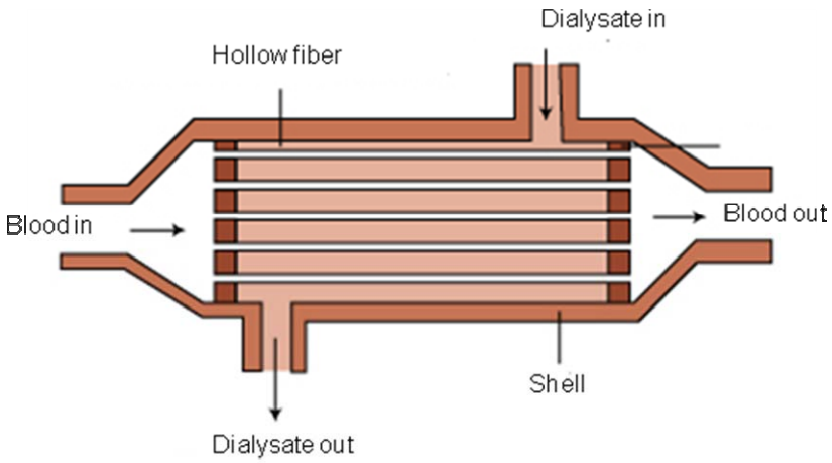

Fig. 1-10 The hollow fiber module of membrane based hemodialyzer

1.4 Research objectives

The main objective of my research is to develop a high performance protein separation process combining the advantages of membranes with current electrophoresis technologies aiming a feasible industrial operation process. High performance protein separation process is currently hindered by a few factors: 1) molecular size-based discrimination in the filtration process appears inadequate in distinguishing between protein molecules, as the feed mixture contains different protein molecules which are usually of similar molecular weight; 2) in comparison with electrophoresis, the hydraulic pressure driving force demands a high power consumption based on mole of protein molecules being transferred; 3) overlapping components will increase more production cost due to the further separation required; 4) the existing protein separation process based on a membrane-partitioned multi-chamber (MCE) was strongly challenged due to the low mechanical strength of the gel-like membrane presented in available literature. Therefore, this research study attempts to solve the above mentioned four difficulties in the following strategies provided:

1) Both charge and molecule size discriminations are adopted by applying adequate ion-exchange membranes;
2) The separation flux is improved to ten times that of an ultrafiltration process by enlarging membrane pores and imposing a larger electric field;
3) Overlapped components are separated into different chambers across the parallel aligned ion-exchange membranes and keep stationary in a specific chamber. The overlapped components produced in a non-membrane partitioned free-flow isoelectric focusing, such as in the case of Rorofor®, can be split effectively;
4) The theoretical explanations of membrane-base isoelectric focusing phenomena are mathematically derived and experimentally verified, providing a fundamental understanding of this complex process and a clue for further improvement.

In order to implement the above strategies, the research activities have been divided into four parts:

1) Fabrication and characterization of flat-sheet polysulfone cation-exchange membranes for the investigation of the effectiveness and efficiency of IEM-FFIEF (ion-exchange membrane partitioned free-flow isoelectric focusing).
2) Application of a series of membranes with different ion-exchange capacities and pore sizes in FFIEF, the analytical solution of boundary effects proposed by Ennis and Anderson et al. [46, 47] was proven to be capable of depicting the membrane based IEF electrophoresis. By introducing a new term - E_0 (the minimum electrical consumption for protein molecule to produce a flux breakthrough) and the effect of membrane structures, theoretical model can be compared with experimental results.
3) Study of the effects and improvement of mass transfer of a novel P84 polyimide membrane with a thin layer anionic modification on the membrane top surface.

4) Fabrication and characterization of aminated (polyphenylene oxide) PPO membranes for the triple-component protein separation and the key factors of self-sharpening phenomenon.

1.5 Organization of this research

This dissertation is organized in seven chapters and two appendices. Chapter one is the introductory chapter of this research dissertation. It provides the review of historical surveys, basic concepts, theoretical fundamentals, transport mechanisms and important industrial applications for membrane based protein separation. The research objectives, strategies and outlines of this dissertation are also demonstrated in this chapter.

The general experimental methodologies and approaches along with all materials applied in all areas are described in chapter two. This includes the polymer modification method, the polymer characterization method, the membrane fabrication methods, the membrane characterization methods, on-line pH control method, concentration monitoring methods and protein analysis methods etc.

Chapter three reports a combination of ion exchange membranes and free-flow isoelectric focusing (FFIEF) technology for high-selectivity and high-flux protein separation, in which ion exchange membranes are used as the separation media. The laboratory-prepared UF SPSf membranes have been proven a superior selectivity and flux to the two commercial benchmarks.

Chapter four investigates the protein mass transfer in the IEM-FFIEF process with the aid of boundary effect model contributed by Ennis et al. A fundamental understanding and analytical calculation method are provided.

Chapter five reveals the key factors of self-sharpening phenomenon by employing the aminated PPO membrane in IEM-FFIEF triple-component protein separation process.

Chapter six explores the effects and an approach of improvement of mass transfer through a novel P84 polyimide membrane with a thin top layer anionic modification.

Chapter seven summarizes the general conclusion drawn from this research and some recommendations for future work in this scope.

1.6 Reference

[1] T.E. Creighton, Protein fuction, second edition, W.H. Freeman and Company, New York, 1993.

[2] Report "Protein Purification Systems: Market Opportunities for Research Product Suppliers", Bioinformatics, issue of Genetic Engineering News, (2003), pg54-217.

[3] M. Kalyanpur, Downstream Processing in the Biotechnology Industry, Mol. Biotechnol., 22 (2002) 87.

[4] Report "Therapeutic Monoclonal Antibodies Report 2008-2023", (2008). http://www.bioportfolio.com/cgibin/acatalog/Therapeutic_Monoclonal_Antibodies_Report_2008-2023.html

[5] J.D. Ferry, Ultrafilter membranes and ultrafiltration, Chem. Rev., 18 (1936) 373.

[6] R. van Reis and A.L. Zydney, Bioprocess membrane technology, J. Membr. Sci., 297 (2007) 16.

[7] S. Sourirajan and T. Matsuura, Reverse osmosis/ultrafiltration process principles, National Research Council Canada (Ottawa, Canada), 1985.

[8]J.S. Hamada, Ultrafiltration for recovery and reuse of peptidoglutaminase in protein deamidation, J. Food Sci., 56 (2006) 1731.

[9] B. Cheang and A.L. Zydney, Separation of lactalbumin and lactoglobulin using membrane ultrafiltration, Biotech. and Bioeng., 83 (2003) 201.

[10]A.L. Zydney, Protein separations using membrane filtration: new opportunities for whey fractionation. Internat. Dairy J., 8 (1998) 243.

[11]M.E. Avramescu, Z. Borneman, and M. Wessling, Mixed matrix membrane adsorbers for protein separation, J. Chromato. A, 1006 (2003) 171.

[12]Y. Li, S.C. Soh and T.S. Chung, S.Y. Chan, Exploration of ionic modification in dual-layer hollow fiber membranes for long term high performance protein separation, AIChE J., 55 (2008) 321.

[13]S. Galier and H.R. Balmann, Study of the mass transfer phenomena involved in an electrophoretic membrane contactor, J. Membr. Sci., 194 (2001) 117.

[14]P. Wenger and P. Javet, Isoelectric focusing using non-amphoteric buffers in free solution: I. determination of stable concentration profiles, J. Biochem. & Biophys. Meth., 13 (1986) 259.

[15]P. Wenger and P. Javet, Isoelectric focusing using non-amphoteric buffers in free solution: II. apparatus and measures of pH stability, J. Biochem. & Biophs. Meth., 13 (1986) 275.

[16]P. Wenger and P. Javet, Isoelectric focusing using non-amphoteric buffers in free solution: III. Separation of amino acid, J. Biochem. & Biophs. Meth., 13 (1986) 289.

[17]W.J. Koros and G.K. Flemming, Membrane based gas separation, J. Membr. Sci., 83 (1993) 1.

[18]F.G. Smith, III and W.M. Deen, Electrostatic effects on the partitioning of spherical colloids between dilute bulk solution and cylindrical pores, J. Colloid Interf. Sci., 91 (1983) 571.

[19] R.H.C.M. van Eijndhoven, S. Saksena and A.L. Zydney, Protein fraction using electrostatic interaction inmembrane filtration, Biotechnol. Bioeng., 48 (1995) 406.

[20] A.L. Zydney and N.S. Pujar, Protein transport through porous membranes: effects of colloidal interactions, Colloid Surface A, 138 (1998) 133.

[21]D.B. Burns and A.L. Zydney, Contribution of electrostatic interactions on protein transport in membrane system, AIChE J., 47 (2001) 1101.

[22]Presentation Speech by Professor A. Westgren, Chairman of the Nobel Committee for Chemistry of the Royal Swedish Academy of Sciences, Copyright © The Nobel Foundation (1948).

[23]A. Tiselius, A new apparatus for electrophoretic analysis of colloidal mixtures, Trans. Faraday Soc.33 (1937) 524.

[24] W. Pauli, Untersuchungen an Elektrolytfreicn, Wasserlos]ichen Proteinkorpern, Biochem. Z., 152 (1924) 355.

[25]M. Bier, Recycling isoelectric focusing and isotachophoresis, Electrophpresis, 19 (1998) 1057.

[26] E.A. Murphy, Recent progress in latex technology, Ind. Eng. Chem., 44 (1952) 756.

[27] J.G. Kirkwood, A suggestion for new method of fractionation of proteins by electrophoresis convection, J. Chem. Phs., 9 (1941) 878.

[28] H. Svenson, Preparative electrophoresis and ionophoresis, Advances in Protein Chemistry.,volume IV,1948, pg 251.

[29] A. Polson, Multi-membrane electrodecantation and its application to isolation and purification of proteins and viruses, Biochimica et Biophysica Acta, 11 (1953) 315.

[30] P.G. Righetti, B. Barzaghi and M. Faupel, Protein desalting by isoelectric focusing in a segmented immobilized pH gradient, J. Biochem. Biophys. Methods, 15 (1987) 163.

[31] B. Barzaghi, P. G. Righetti and M. Faupel, Effect of salts on rat of contaminants' removal, J. Biochem. Biophys. Methods, 15 (1987) 177.

[32] P.G. Righetti, B. Barzaghi, M. Luzzana, G. Manfredi and M. Faupel, A horizontal apparatus for isoelectric protein purification in a segmented immobilized pH gradient, J. Biochem. Biophys. Methods, 15 (1987) 189.

[33] P.G. Righetti, Preparative protein purification in a multi-compartment electrolyser with immobiline membranes, J Chromat., 415 (1989) 293.

[34] W.M. Deen, Hindered transport of large molecules in liquid-filled pores, AIChE J., 33 (1987) 1409.

[35] A.K. Solomon, Characterization of biological membranes by equivalent pores, J. Gen. Physiol., 51 (1968) 335.

[36] W.M. Deen, M. P. Bohrer and B. M. Brenner, Macromolecule transport across glomerular capillaries: application of pore theory, Kidney Int., 16 (1979) 353.

[37] E. Klein, F. F. Holland, and K. Eberle, Comparison of Experimental and Calculated Permeability and Rejection Coefficients for Hemodialysis Membranes, J. Memb. Sci., 5 (1979) 173 (1979).

[38] D.M. Malone and J.L. Anderson, Diffusional boundary-layer resistance for membranes with low porosity, AIChE J., 23 (1977) 177.

[39] D.M. Malone and J.L. Anderson, Hindered diffusion of particles through small pores, Chem. Eng. Sci., 33 (1978) 1429.

[40] F.G. Smith III and W. M. Deen, Electrostatic double-layer interactions for spherical colloids in cylindrical pores, J. Colloid Interf. Sci., 78 (1980) 444.

[41] F.G. Smith III and W. M. Deen, Electrostatic effects on the partitioning of spherical colloids between dilute bulk solution and cylindrical pores, J. Colloid Interf. Sci., 91 (1983) 571.

[42] H.J. Keh, and J. L. Anderson, Boundary effects on electrophoretic motion of colloidal spheres, J. Fluid Mech., 153 (1985) 417.

[43] J. Happel, and H. Brenner, Low Reynolds Number Hydrodynamics, Kluwer Academic publisher group, Dordrecht, the Netherlands, 1983. Pg.318.

[44] H.J. Keh and S. B. Chen, Electrophoresis of colloidal sphere parallel to a dielectric plane, J. Fluid Mech., 194 (1988) 377.

[45] H.J Keh and J.Y. Chiou, Electrophoresis of a colloidal sphere in a circular cylindrical pore, AIChE J., 42 (1996) 1397.

[46] J. Ennis, and J.L. Anderson, Boundery effects on electrophoretic motion of spherical particles for thick double layer and low zeta potential, J. Colloid Interf. Sci., 185 (1997) 497.

[47] J. Ennis, H. Zhang, G. Steven, J. Perera and S. Carnie, Mobility of protein through a porous membrane, J. Membr. Sci., 119 (1996) 47.

[48] A. J. O'Connor, H. R. C. Pratt, and G. W. Stevens, Electrophoretic mobilities of proteins and protein mixtures in porous membranes, Chem. Eng. Sci., 51(1996) 3459.

[49] E. Lee, J. W. Chu, J.-P. Hsu, Electrophoretic mobility of a sphere in a spherical Cavity, J. Colloid Interf. Sci., 205 (1998) 65.

[50] A. Martín-Molina, M. Quesada-Pérez, F. Galisteo-González and R. Hidalgo-Álvarez, Electrophoretic Mobility and Primitive Models: Surface Charge Density Effect, J. Phys. Chem. B, 106 (2002) 6881.

[51] C.P. Tung, E. Lee and J.P. Hsu, Dynamic electrophoretic mobility of a sphere in a spherical cavity, J Colloid Interf. Sci., 260 (2003) 118.

[52] F. Carrique, F.J. Arroyo, M. L. Jiménez and Á. V. Delgado, Influence of Double-Layer Overlap on the Electrophoretic Mobility and DC Conductivity of a Concentrated Suspension of Spherical Particles, J. Phys. Chem. B, 107 (2003) 3199.

[53] J.P. Hsu, Z.S. Chen, M.H. Ku and L.H. Yeh, Effect of charged boundary on electrophoresis: sphere in spherical cavity at arbitrary potential and double –layer thickness, J. Colloid Interf. Sci., 314 (2007) 256.

[54] H.J. Keh and T.H. Hsieh, Electrophoresis of a colloidal sphere in a spherical cavity with arbitrary zeta potential distributions, Langmuir, 23 (2007) 7928.

[55] A. Fick, Über diffusion, Pogg. Ann. Phys. Chem., 94 (1855) 59.

[56] W. Schmidt, Experiments on the Velocity of Filtration of Different Liquids through Animal Membranes, Ann. Phys. Chem., 99 (1856) 337.

[57] W. Ostwald, Elektrische eigenschaften halbdurchl¨assiger scheidew¨ande, Z. Phys. Chem., 6 (1890) 71.

[58] T.W. Xu, Ion exchange membranes: state of their development and perspective, J. Membr. Sci., 263 (2005) 1–29.

[59] G. Kickelbick, Concepts for the incorporation of inorganic building blocks into organic polymers on a nanoscale, Prog. Polym. Sci., 28 (2003) 83.

[60] T. Matsuura, Synthetic membranes and membrane separations, Taylor and Francis group, CRC Press, 1994. Pg9.

[61] S. Loeb, S. Sourirajan, High flow porous membranes for separating water from saline solutions, US patent 3133132, 1964.

CHAPTER 2 MATERIALS AND EXPERIMENTAL PROCEDURES

This chapter describes the general experimental methodologies along with all materials involved in this study. Membrane materials, fabrication technologies, material and membrane characterization methods, as well as protein analysis methods are presented in different sections in this chapter.

2.1 Materials

2.1.1 Polymers

In chapters 3 and 4, polysulfone was chosen as the polymeric material for obtaining a charged material through sulfonation. Udel P3500NT polysulfone was provided by Solvay possessing a Mw of 141.5 kDa (GPC results from Peng Na) and a T_g of 190ºC. Polysulfone possesses superior mechanical strength and good processability for membrane formation.

In chapter 5, a modified polymer, brominated poly(2,6-dimethyl-phenylene oxide) (BPPO) was selected as basic material for the amination reaction. The BPPO with 90% bromination rate was obtained from Shandong Tianyi Imp. & Exp. Co., Ltd. China. The primary benzylic halide reagent, BPPO, is very reactive toward nucleophiles such as tertiary amines. The BPPO enables the modification of a currently uncharged polymer to a positively charged material.

In chapter 6, a BTDA-TDI/MDI co-polyimide commercially named P84 was chosen as the polymer material for the fabrication of porous ultrafiltration membrane. The P84

supplied by HP polymer (GmbH, Austria) possesses a Mw of 153.4 kDa (Peng Na GPC) and a T_g of 315ºC. The large amount of imide groups enables the easy modification and cross-linking of the membrane surface.The chemical structures and relevant properties involved in this dissertation are summarized in Table 2-1.

Table 2-1: Chemical structure and properties of applied polymer

Polymer material	Chemical structure	M_w (kDa)	Tg (ºC)	Density (g/cm^3)
Polysulfone	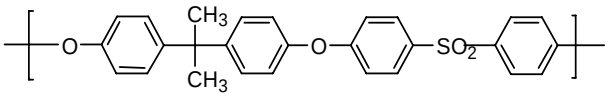	141.5	190	1.24
P84	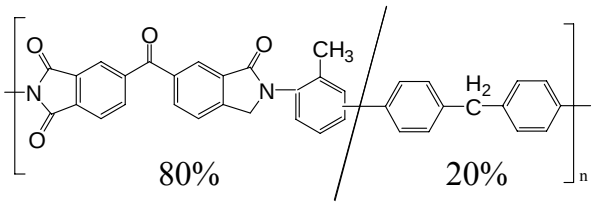	153.4	315	1.31
BPPO	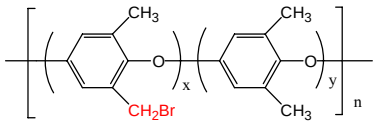	-	-	1.58

2.1.2 Polymer modification

In chapters 3 and 4, polysulfone (PSf) was sulfonated using the following procedure: 40 g PSf was dissolved in 400 ml dichloromethane and pre-cooled chlorosulfonic acid was gradually added into the polymer solution at −5 °C for a 45 min reaction. The reaction was then quenched in methanol. The final product, sulfonated polysulfone (SPSf), was

washed in methanol until the measured pH reached 5.5; finally, the SPSf was dried at temperature of 40 °C under a vacuum for 2–3 days.

In chapter 5, the following procedures were applied to BPPO for the preparation of a positively charged polymer: 1) BPPO and PSf were dissolved in THF to form 10% solutions and then filtered by a 300-mesh sieving. 2) For different amination rates, 20% of triethylamine (TEA in THF) solutions were added into the BPPO-THF polymer blend solution according to the ratios of TEA: BPPO in 1.0, 1.4 and 1.8, individually. 3) After 20 minutes of agitation under ambient temperatures, the solutions were quenched in methanol and the blended polymers were then precipitated. 4) Finally, the polymers with different amination rates were fully washed by methanol at least four times followed by drying in a vacuum oven under ambient temperature.

In chapter 6, the modifications were directly accomplished on the P84 membrane surface; hence no procedure was required to prepare a charged polymer material.

2.1.3 Proteins used as separation model

Bovine serum albumin (BSA) and hemoglobin (Hb) are used as a protein mixture model in chapter 3. While in chapter 4, BSA and myoglobin (Mb) were used as protein mixture model. In chapter 5, Mb, Lys and BSA were applied as the separation model mixed in random ratios. In chapter 6, the mixture of Mb and lysozyme (Lys) were used as the separation model. The above mentioned Hb, Mb, BSA and Lys were all procured from Sigma-Aldrich. The Mw and pI value of BSA are 66.5 kDa and 4.8, respectively; the Mw

and pI values of Mb are 17 kDa and 7.0, respectively; the Mw and pI values of Hb are 65 kDa and 6.8, while the Mw and pI value of Lys are 14.4 kDa and 11.0, respectively.

2.1.4 Other materials

Dense cation exchange membranes (CEX) and dense anion exchange membranes (AHA) were bought from Astom Corporation, Japan. All the water and acetonitrile (ACN) for HPLC analysis purposes were of GR grade (guaranteed reagent). All of reagents except ACN and trifluoro acetic acid (TFA) were of AR (analytical reagent) grade. The ultrapure water used for HPLC was produced by "Milli-Q plus 185" pure water system in our lab.

Other materials and chemicals used in chapters 3 and 4 are listed below: the microporous cation exchange membrane ICE450 was purchased from Pall with an IEC value of 9.6 meq per 47mm^2 disc and a pore size of 0.45 μm. The hydrophilic uncharged membrane C100F with a MWCO of 100 kDa was donated by Nadir Filtration GmbH. The ampholyte and tris were purchased from Bio-Rad. 0.01N NaOH solution was prepared from AR grade reagent provided by Chemicop. Iso-propanol (IPA) was from Infinity Laboratory Chemicals. N-methyl-2-pyrrolidone (NMP), dichloromethane (DCM), phosphoric acid (H_3PO_4), chlorosulfonic acid, trifluoroacetic acid (TFA), acetic acid (HAC) and phenolphthalein were provided by Merck, Singapore. Acetonitrile (ACN) was from Tedia Compony Inc. USA.

In Chapter 5, tetrahydrofurane (THF) and triethylamine (TEA) were from Fisher sientific, UK; NMP, IPA, methanol, H_3PO_4, NaOH, TFA, and KCl were all from the same source as above.

In chapter 6, ethylene diamine, diamino butane, polyethylene oxide (PEO) and polyvinylpyrrolidone (PVP) were obtained from Sigma-Aldrich. Iodomethane (CH_3I) was provided by Merck. Other materials such as NMP, IPA, methanol, H_3PO_4, NaOH, TFA, and KCl were all from the same source as above.

2.2 Membrane fabrication

In chapter 3 and 4, sulfonated polysulfone (SPSf) was used to fabricate the ion exchange flat-sheet membranes according to the following procedures: SPSf powder was first dissolved in NMP at different concentrations of 23, 24 and 25 wt%. The polymer solutions were then cast on a non-woven cloth with a casting gap of 250 μm, followed by immersion in IPA for 15 min and then in water for 1 day. These as-cast membranes were soaked in a glycerol/water (50/50 wt%) mixture for 1 day to maintain the pore structure, then dried in ambient air for long term storage. The stored membranes should be cleaned with deionized water before use.

In chapter 5, the following procedures were applied to BPPO for the fabrication of positively-charged membranes: 1) the three dried polymers with different amination rates were dissolved in NMP with the same concentration of 20% w/w; 2) the three polymer solutions were cast on non-woven clothes by a casting blade with a gap thickness of 250 μm; 3) the cast non-woven clothes were dipped in an IPA coagulant bath for 15 min and

followed by a water bath. The APPO-PSf membranes obtained were named as: M-A, M-B, and M-C which corresponded to 1.0, 1.4 and 1.8 times of TEA additions, respectively. The membranes with different amination rates were then post-treated with the following procedures: 1) soaking in a 0.5M HCl solution overnight to remove unreacted TEA followed by thorough rinsing with deionized water, and 2) soaking in a 0.5M NaCl solution overnight, followed by thorough rinsing with deionized water. After the post-treatments, the positively-charged group was determined to be $-CH_2N^+(C_2H_5)_3$.

In chapter 6, P84 was used to prepare anion exchange membranes with the following procedure: P84 powder was dissolved in NMP to a concentration of 23 wt%. The solution was then cast onto a piece of non-woven cloth with a gap thickness of 150μm. The as-cast non-woven cloth was immediately immersed in IPA for 20 minutes, followed by an immersion in methanol for a further 2 hours. The obtained P84 porous membrane was named M-O. Some M-O samples were directly soaked in a 5/5/90 (in V/V) ethylene diamine/ diamino butane/ methanol solution for a half-hour amination reaction. Capitalizing on the porous nature of the membrane surface and the short length of the diamine molecules, some diamine will end up cross-linking the membrane [1], while others can be utilized for further methylation to form quaternary amines. The unreacted diamine was then removed via washing with methanol and the modified membrane was named M-1. Some M-1 samples were subsequently dipped in a 20 wt% iodomethane solution in methanol for 12 hours. Iodomethane was chosen for the preparation of quaternary amine salts because of its high nucleophilicity [2]. Two different reaction temperatures (42°C and 48°C) were applied and the obtained membranes were named M-2 (42°C treatment) and M-3 (48°C treatment). All the membranes M-O, M-1, M-2 and M-3 underwent the same post-treatment routine: a soaking in 0.5 M HCl was first employed

for 12 hours followed by a full washing with deionized water; then a soaking in 1M NaCl for another 12 hours ensued followed by a full washing with deionized water. Membrane charge properties (IEC value and ζ-potential) will be shown later to increase with the degree of modification.

2.3 Membrane Characterization and Evaluation

2.3.1 FTIR

Fourier-transform infrared-Attenuated total reflection (FTIR-ATR) is an important and reliable characterization technique in organic chemistry. It offers an easy way to identify the presence of a certain functional group in a molecule. The unique collection of absorption bands in the FTIR database also enables the detection of grafted groups or specific impurities. Infrared spectroscopy reveals information about the vibrational states of a chemical bond. Intensity and spectral position of IR absorptions allow the identification of the structural elements of a molecule. Those absorptions locate at a unique wave-number and posses unique shape on a FTIR spectrum just like fingerprints of different chemical bonds. The typical vibrations of chemical bond make the infrared spectroscopy an important analytical tool for the confirmation of chemical structures [3].

Most of the time, a modified membrane will be directly fixed on the KBr holder. If the membrane is not transparent, ATR apparatus will be applied. For a modified membrane material, one dissolves a polymer in GR THF to a concentration of 0.5 wt%, and this solution will be dropped on a KBr holder. IR radiation is passed through the sample and the KBr. Some of the infrared radiation is absorbed by the sample and some of it is

transmitted. The resulting spectrum represents the molecular absorption and transmission, creating a molecular fingerprint of the sample.

2.3.2 XPS

X-ray Photoelectron Spectroscopy (XPS) is one of the surface analytical techniques that bombard a flat sample with photons, electrons or ions in order to excite the emission of photons, electrons or ions.

In XPS, the sample is irradiated with low-energy (~1.5 keV) X-rays, in order to provoke the photoelectric effect. The energy spectrum of the emitted photoelectrons is determined by means of a high-resolution electron spectrometer. Chemically modified dry membrane samples were directly analyzed by an AXIS HSi spectrometer (Kratos Analytical Ltd. England). There is a "survey scan", or "wide scan" spectrum, obtained at low resolution and covering the entire range of binding energies accessible with the X-ray source employed [4]. At high resolution, the spectrum demonstrates the chemical states of a given element, from which the changes in chemical bonds can be observed. In this dissertation, the C 1s, N 1s, O 1s, and Br 1s spectra were observed.

2.3.3 SEM or FESEM and EDX

Scanning electron microscopy (SEM) and field emission scanning electron microscopy are vast applied technologies used in the study of membrane morphologies. The SEM is a type of electron microscope that images the sample surface by scanning it with a high-energy beam of electrons in a raster scan pattern. The electrons interact with the atoms

that make up the sample producing signals that contain information about the sample's surface topography, composition and other properties such as electrical conductivity. A field-emission cathode in the electron gun of a scanning electron microscope provides narrower probing beams at low as well as high electron energy, resulting in both improved spatial resolution and minimized sample charging and damage.

In this research study, the SEM and FESEM are used to analyze the surface and cross-section morphology of various flat membranes. The SEM used in this study is JEOL JSM-5600LV and FESEM is JEOL JSM-6700F. The samples for SEM or FESEM need to be dried by freeze dryer to maintain the membrane structures. The samples for cross-section characterization were fractured in liquid nitrogen. After mounting all the specimens on the stub using a double-side conductive carbon adhesive tape, the specimens were further dried under vacuum for at least 20 min. All samples are sputter coated with platinum of 200 – 300 Å in thickness using the JEOL JFC-1200 Ion Sputtering device before testing.

The prepared SEM specimens are also used to measure the surface elemental content by Oxford INCA energy dispersion of X-ray (EDX). In this research, EDX was used to explore the distribution of the nitrogen element in the membrane cross-section.

2.3.4 Surface Zeta potential

The zeta potential of membrane surface was investigated through the SurPASS electrokinetic analyzer based on the streaming potential and streaming current method. The zeta potential is related to the surface charge at a solid / liquid interface and is a

powerful indicator for the surface chemistry (pH titration) and liquid phase adsorption processes, and the SurPASS helps in aiding the understanding of the surface properties of the fabricated membrane. The zeta potential is an interfacial property that is of great importance for understanding the behavior of solid materials in many technical processes. It gives insight into the charge and adsorption characteristics of solid surfaces. The structure of surface double layer is demonstrated in Fig. 2-1.

The Clamping Cell is the tool of the SurPASS for measuring planar surfaces like foils, polymer sheets, membranes, metals, ceramics or glass. Two different arrangements of planar samples are possible: in the symmetric configuration two identical surfaces are mounted and separated by a well-defined gap; the asymmetric geometry uses a reference surface and enables the non-destructive measurement of samples with different thicknesses [5]. As given by the Helmholtz–Smoluchowsky method, the apparent ζ-potential can be measured through eqn. (2-1):

$$\zeta_{apparent} = \frac{dU}{dP} \times \frac{\eta}{\varepsilon_r \times \varepsilon_0} \times \frac{L}{A \times R} \qquad (2\text{-}1)$$

It must be noticed that in order to mimic the real situations on membrane surface during the protein separation process, the buffer solution in streaming potential analysis was a 20 mM HCl-Tris solution, which led to much higher ζ-potential readings as compared to the literature reports. The high apparent ζ-potential is due to the fact that in dilute solutions, such as 1 mM KCl or 20 mM HCl-tris buffers, the conductivity of charged surface is not negligible, thus the ζ-potential results need to be corrected by 0.1M KCl through eqn. (2-2):

$$\zeta_{corrected} = \frac{dU}{dP} \times \frac{\eta}{\varepsilon_r \times \varepsilon_0} \times \frac{\kappa_{0.1MKCl} \times R_{0.1MKCl}}{R} \qquad (2\text{-}2)$$

where dU/dP is the slope of streaming potential versus pressure; η is the electrolyte viscosity; ε_r is the relative dielectric constant of electrolyte; ε_0 is the vacuum permittivity; L is the length of streaming channel; A is the cross-section area of the streaming channel; R is the resistance inside the measuring cell; $\kappa_{0.1MKCl}$ is the conductivity of 0.1M KCl; $R_{0.1MKCl}$ is the cell resistance when running 0.1M KCl. The sample for streaming potential measurements was titrated from pH 3 to pH 10 in a HCl-Tris buffer. This pH range covered all related pH values in the IEM-FFIEF separation process.

The interface between a solid surface and a surrounding liquid shows a charge distribution which is different from the solid and liquid bulk phases. In the model of the electrochemical double layer, this charge distribution is divided into a stationary and a mobile layer. A plane of shear separates these layers from each other. The zeta potential is assigned to the potential decay between the solid surface and the bulk liquid phase at this shear plane. The application of an external force parallel to the solid / liquid interface leads to a relative motion between the stationary and mobile layers and to a charge separation which gives experimental access to the zeta potential [5].

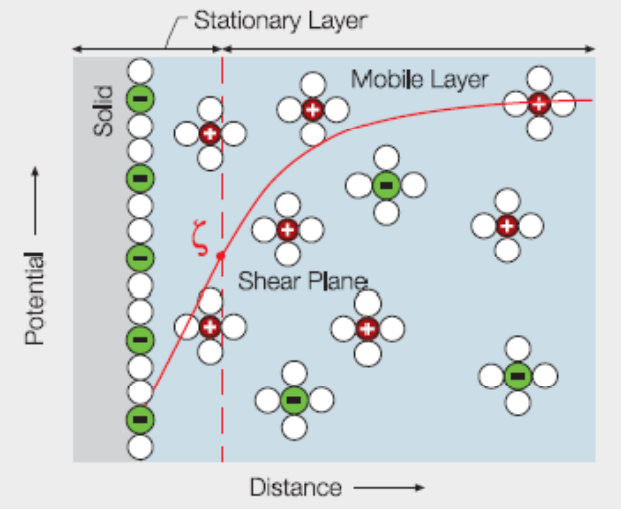

Fig. 2-1 The electrochemical double layer and measured surface zeta-potential [5]

2.3.5 Ion-exchange capacity

The ion-exchange capacity (IEC value) is an important parameter to characterize the electrical property of a membrane and is usually determined by the Mohr method. A Na type cation- exchange membrane with a known area was soaked in a 0.1M $CaCl_2$ solution overnight first, followed by fully washing with DI water, and the de-adsorbed Na element will be measured by either a Na^+ selective electrode or an ion-chromatography (IC) or inductive couple plasma (ICP). On the other hand, the Cl^- type anion-exchange membrane was soaked in a 0.1 M Na_2SO_4 solution first, and the Cl^- concentration as released was tested by either a Cl^- ion selective electrode [6], an IC or an ICP.

2.3.6 Pore size distribution

The characterization of pore size distribution provides key information for the membrane structure, thus playing an essential role in the understanding of the performance of a porous membrane. The pore size distribution was investigated by real solute rejection method [7].

Polyvinylpyrrolidone (PVP) with different MW of 10 kDa, 40 kDa, 360 kDa and 1300 kDa were used to prepare a series of feed solutions containing 200 ppm of PVP. The total organic carbon (TOC) of the solutions at both the feed and permeate sides of the ion exchange membrane were measured using a Shimadzu TOC-5000A analyzer. However, the TOC method is rather time-consuming process; hence, the Gel-Permeation Chromatography (GPC) method was proposed as an alternative. In order to obtain a high resolution in chromatography, it is crucial to maintain an at least fivefold difference in Mw between each subsequent component (the least Mw difference required by a satisfied

UF separation is tenfold). In this dissertation, PEG of Mw 2 kDa and PVP of 10 k, 55 k, 360 k and 1300 kDa were applied with the aid of the following relationship between Mw and Stokes' radius r [8]:

$$\begin{aligned} &For \quad PEG \quad r = 16.73 \times 10^{-3} \times Mw^{0.557} \quad nm \\ &For \quad PVP \quad r = 8.40 \times 10^{-3} \times Mw^{0.593} \quad nm \end{aligned} \qquad (2\text{-}3)$$

2.4 Protein Analysis Methods

2.4.1 HPLC

High performance liquid chromatography (HPLC) is widely applied for analysis of concentration of individual protein. An Agilent Technology 1200 HPLC with a VWD detector was used to determine the proteins' purity in the respective chambers. The C18 mass SPEC column was purchased from Grace Vydac Inc. The gradient elution was comprised by two mobile phases contained A: 100% ACN with 0.1% TFA; B: 100% water with 0.1% TFA. The protein sample analyses were conducted with the parameters as showing in Table 2-2:

Table 2-2 HPLC running conditions

HPLC Parameter	Controlled value
VWD wavelength	214 nm
Temperature	30 °C
Flow speed	1.0 ml / min
Running time	30 min
Post time	5 min
Injection	100 µl

2.4.2 Kinetic function of UV-Vis spectroscopy

In order to monitor real-time concentration changes, a UV–Visible spectrophotometer (BIOCHROM LIBRA S32) with kinetic function was used to test the online protein concentration. The protein solution between the permeate chamber and the UV spectrometer was circulated by a cartridge pump. Most proteins have absorbance at 280 nm, while few proteins such as hemoglobin and myoglobin have absorbance at 408 nm. Therefore, the total absorbance can be accessed at 280 nm. If protein 1 of a binary mixture has an absorbance at 408 nm, its concentration can be calculated through this reading. As a result, the concentration of another protein 2 can be calculated from the total absorbance of 280 nm following the eqn. (2-4):

$$A_{280} = (C_1 * b_1) + (C_2 * b_2) \qquad (2\text{-}4)$$

where A_{280} is the total absorbance at 280 nm; C_1 is concentration of protein 1, which can be obtained from the measuring at 408 nm; b_1 is the slope of standard calibration curve of protein 1 at 280 nm; C_2 is the concentration of protein 2; b_2 is the slope of standard calibration curve of protein 1 at 280 nm. Through a kinetic function, the Abs_{480} and Abs_{280} of the permeate chamber were measured in 5 mins time interval throughout the whole separation process. Therefore, a curve of concentration vs. time can be obtained, illustrating the changing trend of both C_1 and C_2 in permeate chamber. On the other hand, for multi-chamber on-line monitoring in chapter 5, the kinetic function was only applied at 280nm wavelength to display a total Abs changing trend in individual chambers.

2.4.3 Capillary Electrophoresis

A Beckman-Coulter P/ACE^{TM} MDQ capillary electrophoresis (CE) was used to measure the number of net charges carried by protein molecules in a 0.02 M HAC-tris buffer solution (pH = 4.8) in chapter 4. Through the measurement of mobility, the charge number can be calculated by eqns. (2-5) and (2-6) [9]. In our experiments, Mb and Hb were dissolved in a 0.02 M HAC-Tris buffer (pH = 4.8) and the mobilities were measured by a PDA (photodiode array) detector with varying wavelengths at 254 nm and 280 nm. The applied electrical field strength was 15 mA, and a 60 cm long neutral capillary with an inner diameter of 75 μm was used. The purpose for measuring Hb at pH = 4.8 was to compare the accuracy of the CE method with published data [10].

$$\zeta_s = f(\kappa a)\frac{q_s}{4\pi\varepsilon a_s}\exp(-\kappa a_s) \quad for \quad small \quad \kappa a < 20 \tag{2-5}$$

$$\mu_s = \frac{q_s}{6\pi\eta a_s} \tag{2-6}$$

2.5 Reference:

[1] B.T. Low, Y.C. Xiao, T.S. Chung and Y. Liu, Simultaneous occurrence of chemical grafting, cross-linking, and etching on the surface of polyimide membranes and their impact on H2/CO2 separation, Macromolecules, 41 (2008) 1297.

[2] F.A. Carey, Organic chemistry, 6th edition, Mc GRAW HILL, New York, 2006, pg967.

[3] G. Socrates, Infrared and Raman characteristic group frequencies, John Wiley & Sons, New York, 2004.

[4] G. Beamson, D. Briggs, High resolution XPS of organic polymer: the Scienta ESCA300 database, Wiley, New York, 1992.

[5] Manual of SurPASS electrokinetic surface analyzer, Anton Paar GmbH, 2008.

[6] B.B. Tang, T.W. Xu, M. Gong and W.H. Yang, A novel positively charged asymmetry membranes from poly(2,6-dimethyl-1,4-phenylene oxide) by benzyl bromination and in situ amination: membrane preparation and characterization, J. Membr. Sci., 248 (2005) 119.

[7] K.Y. Wang and T.S. Chung, The characterization of flat composite nanofiltration membranes and their applications in the separation of cephalexin, J. Membr. Sci., 247 (2005) 37.

[8] K.Y. Wang, T. Matsuura, T.S. Chung and W. F. Guo, The effects of flow angle and shear rate within the spinneret on the separation performance of poly(ethersulfone) (PES) ultrafiltration hollow fiber membranes, J. Membr. Sci., 240 (2004) 67.

[9] P.C. Hiemenz and R. Rajagopalan, Principles of colloid and surface chemistry, Marcel Dekker, 1997.

[10] J. Ennis, H. Zhang, G. Steven, J. Perera and S. Carnie, Mobility of protein through a porous membrane, J. Membr. Sci., 119 (1996) 47.

CHAPTER 3 HIGH-PERFORMANCE PROTEIN SEPARATION BY ION EXCHANGE MEMBRANE PARTITIONED FREE-FLOWISOELECTRIC FOCUSING SYSTEM

3.1 Introduction

With the advance in life science research, more and more biomolecules have been discovered to have pharmaceutical characteristics. The research of protein separation is stimulated by an increasing requirement for high-purity drugs in order to reduce the side effects induced by impurities [1]. Unfortunately, the protein separation is a difficult process due to the complexity of proteins themselves and their biological environments; therefore, the separation and purification often account for the major proportion of the production cost. The difficulties of protein separation includes: (1) Proteins are composed of a large amount of amino acids, and different amino acid sequences may lead to completely different properties and functions. (2) The same molecules may also express different activities when they are in different solution environments (e.g. different pH values). (3) Proteins in native environments always exist in a multi-component mixture, and some components may have very similar molecular weights (MW). (4) Some target protein molecules may bind with other protein molecules, thus resulting in the difficulty of separating them by a simple size exclusion method. (5) Protein solutions are a kind of colloidal solution, and the transport mechanism and selective affinity of proteins are related to their MW, charge characteristics, pH value of solution, and charge properties of separation media (e.g. solution, gel, membranes) and others. Hence, it seems to be

infeasible to find a universal separation principle for protein separation just based on single protein property.

In view of the above reasons, various protein separation processes have been developed based on different protein properties, including chromatography, membrane filtration [2], membrane chromatography, electrodialysis, electrophoretic contactor [3], protein immunoaffinity membrane [4], multi-compartment electrophoresis free-flow isoelectric focusing [5-25]. Among them, the membrane filtration may be a potentially attractive process for the separation of protein mixtures [2], where the separation mechanisms normally include the size exclusion and electrostatic exclusion. Since most ultrafiltration (UF) membranes fabricated by the phase-inversion method do not possess a very narrow pore size distribution on the selective skin, their separation performance is not high unless the ratio of MW of two proteins is larger than 10 [20]. Therefore, the electrostatic exclusion has been applied to assist the membrane-based protein separation when the difference in protein MW is small. Smith and Deen [26, 27] were the pioneers who studied the electrostatic exclusion and built a theoretical model to study the potential energy of the electrostatic double layer interaction between spherical colloids and cylindrical pores. They found that the double layer interaction potential is determined by the charge densities of both spherical particles and the cylindrical pore. Zydney and his coworkers have done a great amount of investigation on the effect of electrostatic interaction on protein transport in the membrane system [28-32]. It was found that high-selectivity protein separation could be achieved by adjusting the solution pH value and ionic strength because the electrostatic interactions between charged protein molecules and charged pores of membranes play a very important role to protein separation [33-36]. However, the

high-selectivity protein separation of UF membranes normally cannot last for a long time due to a significant fouling taking place after a certain operation time [37-40].

On the other hand, multi-compartment electrophoretic systems exhibit impressive performance to separate multi-component protein mixtures in one step with a high purity of about 99 % [5-25] Among these references, it has been proved that it is not necessary for the isoelectric focusing to be performed on a continuous gel media. It can be performed well through a thin film. Nevertheless, most multi-compartment electrophoretic systems have used pH immobile gel-like membranes which have a low mechanical strength. These membranes may potentially lose the immobilized ions under a long time operation, thus greatly reducing the practicability of this approach. In order to prolong the life time, a neutral UF membrane with good mechanic strength has been proposed and embedded in the system [7-9, 20]. A long life time was achieved but the introduction of neutral UF membranes may compromise the electrostatic selectivity.

Therefore, the purpose of this work is to combine the UF ion exchange membranes (i.e. charged membranes instead of neutral membranes) and the free flow isoelectric focusing (FFIEF) technology to enhance protein separation. It is believed that the charged membrane surface may lead to an electrostatic selectivity to the charged protein molecules. Namely, the protein molecules with the same charge sign as the membrane may be repulsed, while the protein molecules with the opposite charge sign may pass through the membrane. To our best knowledge, so far there is no academic literature available on applying UF ion exchange membranes in the free flow isoelectric focusing system. A series of characterizations were done for the home-made ion exchange membrane by FTIR, SEM, titration, and polyvinylpyrrolidone (PVP) solute rejection

method. The protein separation performance was measured by a kinetic UV-Visible spectrometer and a high performance liquid chromatograph (HPLC).

3.2. Working principle of the IEM-FFIEF system

The isoelectric focusing (IEF) technology has been extensively used in the protein separation with a great success, and its performance is mainly determined by the net charge of proteins and separation media. The net charge of proteins is the sum of all positive and negative charges provided by amino acid chains. When the pH value of a protein solution is lower than the isoelectric point (pI) of the protein (i.e., pH < pI), the protein molecules carry positive charges, as shown in eqn. (3-1). On the contrary, when the pH value of a protein solution is higher than the pI value of the protein (i.e., pH > pI), the protein molecules bring negative charges, as shown in eqn. (3-2) [41]:

$$\begin{aligned} &R-NH_2+H^+ \rightarrow R-NH_3^+ \\ &R-COO^- + H^+ \rightarrow R-COOH \end{aligned} \qquad (3\text{-}1)$$

$$\begin{aligned} &R-NH_3^+ + OH^- \rightarrow R-NH_2 + H_2O \\ &R-COOH + OH^- \rightarrow R-COO^- + H_2O \end{aligned} \qquad (3\text{-}2)$$

The theoretical principle of the IEM-FFIEF system is illustrated in Fig. 3-1. The feed and permeate chambers are partitioned by a UF ion exchange membrane (IEM) which only allows the ions with the opposite charge to pass through due to the electrostatic attraction [3,42]. Meanwhile, this membrane may prevent the backflow from the permeate side. When bovine serum albumin (BSA) and hemoglobin (Hb) proteins are mixed in the feed chamber with a pH value of 4.8, BSA molecules carry zero charge because its pI value is equal to 4.8, while Hb molecules take positive charges due to its pI value of 6.8. Therefore, BSA molecules stay at the feed chamber due to zero electric driving force,

whilst Hb molecules with positive charges diffuse through the porous ion exchange membrane under the electric driving force and reach the permeate chamber with a pH value of 6.8. The net charge of Hb molecules reduces to zero in the permeate chamber, thus preventing Hb molecules from further migration. Therefore, in principle, a high-purity Hb may be obtained at the permeate chamber.

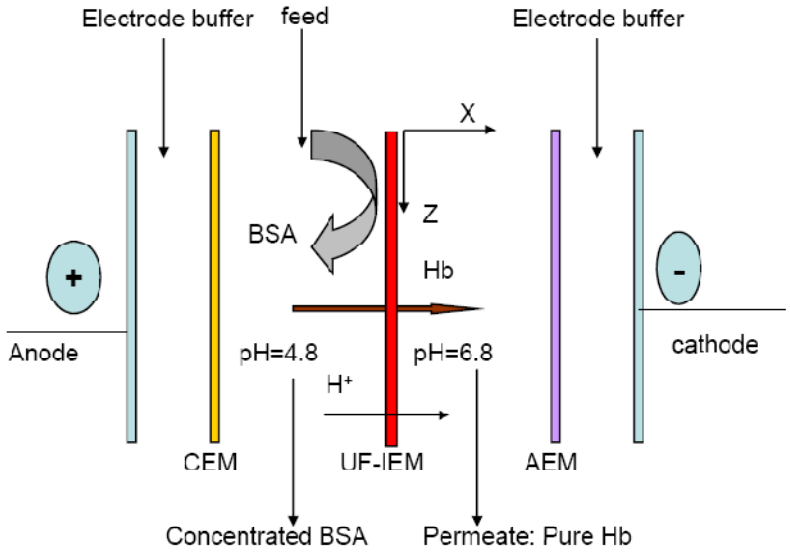

Fig.3-1 Theoretical schematic of the IEM-FFIEF method [3].

UF-IEM: ultrafiltration cation exchange membrane;
CEM: dense cation exchange membrane;
AEM: dense anion exchange membrane.

For a high resolution protein separation, a stable and continuous pH gradient with constant conductivity and high buffer capacity is requested. Ampholyte has been commonly used to perform a stable pH gradient in the traditional isoelectric focusing system due to various advantages, such as high buffer capacity, high solubility and good conductivity at pI values of proteins, absence of biological effect, and low molecular weights [41]. However, the extremely high price limits its application in the FFIEF system. Therefore, an acetic acid-tris buffer with the similar properties was adopted in our work to substitute the ampholyte. In order to maintain a relatively stable pH gradient across the

membrane, two additional chambers (i.e. chambers 1 & 4 in Fig. 3-2) are incorporated. A relatively constant pH gradient and conductivity across the membrane may be achieved by controlling the pH values in chambers 1 & 4 through a combination of manual adjustment and utilization of circulating tanks containing a large volume of buffer solution.

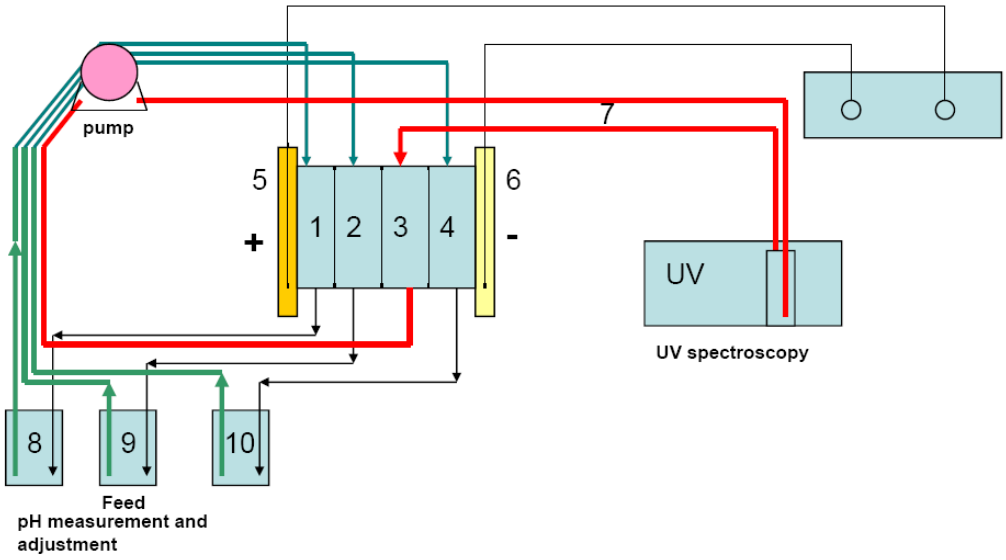

Fig.3-2 Experimental set up.

1 the chamber 1 with pH = 3.2~3.3; 2 the chamber 2 (feed chamber) with pH = 4.8;
3 the chamber 3 (permeation chamber) with pH = 6.8;
4 the chamber 4 with pH = 8.7~8.8;
5 the anode chamber; 6 the cathode chamber; 7 the permeation test circuit;
8 the measurement and adjustment tank of pH value in chamber 1;
9 the measurement and adjustment tank of pH value in chamber 2;
10 the measurement and adjustment tank of pH value in chamber 4.

3.3 Experimental

3.3.1 Materials

The microporous cation exchange membrane ICE450 was bought from Pall with an IEC value of 9.6~31 meq per 47 mm disc and a pore size of 0.45 μm. The hydrophilic

uncharged membrane C100F with a MWCO of 100kDa was donated by Nadir Filtration GmbH. The dense cation exchange membrane and anion exchange membrane were bought from Astom Corporation. Udel P3500NT polysulfone was provided by Solvay. The ampholyte and tris were bought from Bio-Rad. The bovine serum albumin (BSA) and hemoglobin (Hb) were bought from Sigma-Aldrich. The molecular weight (M_w) and pI values of BSA are 66.5k Da and 4.8, respectively; while M_w and pI values of Hb are 65k Da and 6.8, respectively. 0.01 N NaOH solution was prepared from AR grade reagent provided by Chemicop. Iso-propanol (IPA) was purchased from Infinity Laboratory Chemicals. N-methyl-2-pyrrolidon (NMP), dichloromethane (DCM), phosphoric acid, chlorosulfonic acid, trifluoroacetic acid, acetic acid, phenolphthalein and acetoniltrile (ACN) all were provided by Merck.

3.3.2 Sulfonation procedure of polysulfone

In order to obtain the charged membrane material, polysulfone (PSf) was sulfonated using the following procedure: Firstly, 40 g PSf was dissolved in 400 ml dichloromethane; secondly, a pre-cooled chlorosulfonic acid was gradually added into the polymer solution at -5 ^{o}C for a 45 min reaction; thirdly, the reactants were quenched in the methanol; fourthly, the product, sulfonated polysulfone (SPSf) was washed by methanol until pH values reached to 5.5; finally, SPSf was dried at room temperature under vacuum for 2-3 days [43-47]. FTIR Bio-Rad FTS3500 was used to identify the sulfonated polysulfone structure at 1030 cm^{-1} wave number [42-46].

3.3.3 Membrane fabrication

SPSf was used to fabricate the ion exchange membranes as the following procedures: 1) SPSf powder was dissolved in NMP with the concentrations of 23 wt%, 24 wt% and 25 wt%; 2) The polymer solutions were cast on a non-woven cloth with a 250 μm casting knife followed by the immersion in IPA for 10min and then in water for 1 hr; 3) These as-cast membranes were soaked in a glycerol/water (50/50 wt%) mixture for 1 day to hold the pore structure of membranes and dried at atmosphere; 4) These membranes were cleaned with deionized water before use.

3.3.4 Characterizations

A titration method was applied to measure the ion exchange capacity (IEC) of SPSf materials and various membranes. 0.25 g SPSf powder or a piece of 5 cm×5 cm membrane was dissolved in 10 ml NMP and 0.1 N NaOH was used to titrate with the phenolphthalein as an indicator. The IEC values of SPSf materials and membranes were formulated as follows [44]:

$$DS = 0.442*N*V/(W-0.081*N*V) \quad (3\text{-}3)$$

$$IEC = 1000*DS/(442+81*DS) \quad (3\text{-}4)$$

where DS is the degree of sulfonation in %, N is the concentration of standard NaOH in mole/L, V is the consumed volume of standard NaOH in ml, W is the weight of samples in gram, IEC is the ion exchange capacity in meq / g for SPSf materials or meq / m^2 for membranes.

The electron micrographs of ion exchange membranes were examined by a scanning electron microscope (SEM) on a Jeol JSM-5600LV and JSM-6700F to estimate the pore size on the membrane surface and the effective cross-sectional thickness.

The pore size distribution of ion exchange membranes (IEMs) were characterized by the solute rejection method and the detailed procedure has been described elsewhere [48-50]. Polyvinylpyrrolidon (PVP) with different MWs of 10k Da, 40k Da, 360k Da and 1300k Da were used as the solutes and then a series of PVP solutions with a concentration of 200 ppm were prepared as the feed solutions in this work. Each PVP feed solution was pumped into the upstream of the ion exchange membrane and the permeate solution was collected at the downstream of the ion exchange membrane. The total organic carbon of solutions at the feed and permeate sides of the ion exchange membrane were measured using a Shimadzu TOC-5000A to obtain the separation data as a function of different PVP molecule sizes, thus estimating the mean pore size and pore size distribution of the ion exchange membrane.

3.3.5 The protein analysis method

An ultraviolet (UV) visible spectrophotometer (BIOCHROM LIBRA S32) with a kinetic function was used to test the protein concentration online. It is well known that the Hb solution displays two absorbance wavelengths at 280 and 408 nm, while the BSA solution only exhibits an absorbance wavelength at 280 nm. Therefore, the Hb concentration in the Hb-BSA mixture was determined directly from the absorbance at 408 nm. The BSA concentration at 280 nm was obtained by subtracting the Hb contribution at this position from the total absorbance at 280 nm, which was assessed from the Hb concentration. Generally, comparing with HPLC, the commonly used UV method for testing protein concentration may cause a bigger measurement error because the HPLC technology can first separate the different molecules (including buffer and protein molecules) and then

detect their signals in sequence, thus avoiding the disturbance among them. However, the UV technology can only detect their signals when these molecules are still in a mixture. This drawback might lead to an artificially negative BSA concentration due to the application of the deduction method in the calculation of protein concentrations, especially when a high-purity Hb solution with a much lower BSA concentration was obtained at the permeate side of membranes. However, despite the disadvantages of the UV method, it was still applied to test the protein concentration in this work because it is helpful to monitor the changing trend of protein concentrations during the whole experimental running through its on-line kinetic function.

Meanwhile, Hewlett Packard 1050 HPLC instrument with a VWD detector was also applied to offset the disadvantages of the UV method and obtain the more accurate protein concentration in this work. The column Grace Vydac C4 mass SPEC was purchased from Grace Vydac Inc. The gradient elution solution as a mobile phase in the HPLC system contained A: 20 % acetonitrile aqueous solution with 0.05 % trifluoroacetic acid and B: 45 % acetonitrile aqueous solution with 0.05 % trifluoroacetic acid. To prevent BSA and Hb peaks from overlapping to notable extent in HPLC spectra, enough amount of 1,4-dithioerythritol (0.001g in 2ml sample) was used to react with permeate samples. After few minutes of reaction, the Hb peak can be separated from BSA peak, thus can accurately determine the concentration of these two proteins.

3.3.6 Protein separation experiments in the FFIEF system

The experimental setup shown in Figs. 3-2 and 3-3 was an IEM-FFIEF system which consists of four pH gradient chambers and two electrode buffer chambers. The water

splitting was inevitable in both electrode chambers due to the application of a high voltage. The migration of [H^-] generated by the water splitting from the anthodic chamber to the permeate chamber easily resulted in a fluctuation in pH values, thus influencing the protein separation performance. In order to address this issue, two extra chambers 1 & 4 were added between electrode chambers and protein chambers as shown in Figs. 3-2 and 3-3. A pseudo-stable pH could be automatically obtained in the protein chambers by keeping the pH values in chambers 1 & 4 constant even at a high voltage (e.g. 200V), thus avoiding the effect of electrode reactions on pH values. The magnitude of water splitting could be calculated from the amount of tris used to offset the increase in pH in chamber 1 induced by the [H^-] migration. Typically, 0.0275 mole tris (0.5 M * 55 ml) was needed for membrane A in a 100-min operation.

Chambers 1~4 and two electrode chambers all are in the same size of 42.9 cm^2 cross-section and 4.0 cm thickness. The effective area of all types of membranes used in the IEM-FFIEF system is 38.6 cm^2. As shown in Fig. 3-3, the anode chamber was filled with 0.2 M H_3PO_4 buffer, and the cathode chamber was filled with 0.2 M NaOH. Two Ti metal flat plates were placed inside the two electrode chambers, separately, and these two electrodes were connected to a direct current (DC) power supply from Bio-Rad with an accuracy of 0.1 V. Between the anode chamber and chamber 1, a dense cation exchange membrane was inserted to prevent the protein molecules from attaching the electrode. Similarly, between the chamber 4 and cathode chamber, an anion exchange membrane was inserted to prevent the protein molecules from attaching the cathode. Therefore, 3 circulating buffer tanks were provided and their pH values were measured and adjusted online as shown in Fig. 3-2.

The pH values of solutions were tested using a pH meter (HORIBA F-23II E) with an accuracy of 0.01. In order to keep the stable pH values in the chambers 2 and 3, it was necessary to keep stable pH values in the chambers 1 and 4. The large volumes of buffer solutions in the circulating tanks might supply enough buffer capacities to prevent the changes in pH values of chambers 1 and 4. Commercial or self-made membranes were inserted between every pair of chambers, and 200 ml HAC-Tris buffers with different pH values were fed in corresponding chambers as shown in Fig. 3-3. A UV-visible spectrophotometer was used to test the protein concentration at the permeate side of membranes on-line [50]. The protein solution between the permeate chamber and the UV spectrometer was circulated by a peristaltic pump. In this work, at least 2-3 pieces of membranes were parallel tested for each experimental condition to ensure reproducibility.

For the simple batch operation, ICE450, Nadir C100F and self-made membrane B were tested for protein separation at different voltages of 60 V, 100 V and 200 V, where the membrane B was cast using a 23 wt% SPSf solution. A 30 ml protein mixture (Hb 1 g/L : BSA 1 g/L) was pumped into the chamber 2 (i.e., the feed compartment) with a volume of around 200 ml for conditioning. After conditioning, another 30ml protein mixture was fed into the same chamber for testing (0.15 mg/ml Hb in the feed chamber). The protein concentration at chamber 3 (i.e., the permeate chamber) was on-line analyzed with the aid of kinetic function of the UV-visible spectrophotometer. In order to overcome the effect of electro-osmotic phenomenon, all of air holes were sealed except one at the feed chamber as shown in Fig. 3-3. Under this situation, there was no net water flow in the permeate chamber, and thus protein Hb could be concentrated in the permeate chamber.

For the semi-batch operation, ICE450, Nadir C100F, self-made membranes A, B and C were tested for protein separation at a voltage of 200 V, where the membranes A, B and C were fabricated using a SPSf solution of 25 wt%, 23 wt% and 24 wt%, respectively. The difference between the semi-batch and batch operations was that three batches of fresh Hb/BSA protein mixtures were consecutively filled into the feed chamber with an interval of ~30 min for testing, instead of only one batch in the batch operation. In addition, this semi-batch operation was consecutively repeated three times without changing and cleaning the membrane to test and ensure high stability and reproducibility of the system. In other words, both protein solutions in the feed and permeate chambers were discharged after the first round of semi-batch operation, and 200 ml fresh buffer solutions with the fresh protein mixture were directly re-fed into the corresponding chambers for the second round of testing without any membrane cleaning process between two rounds.

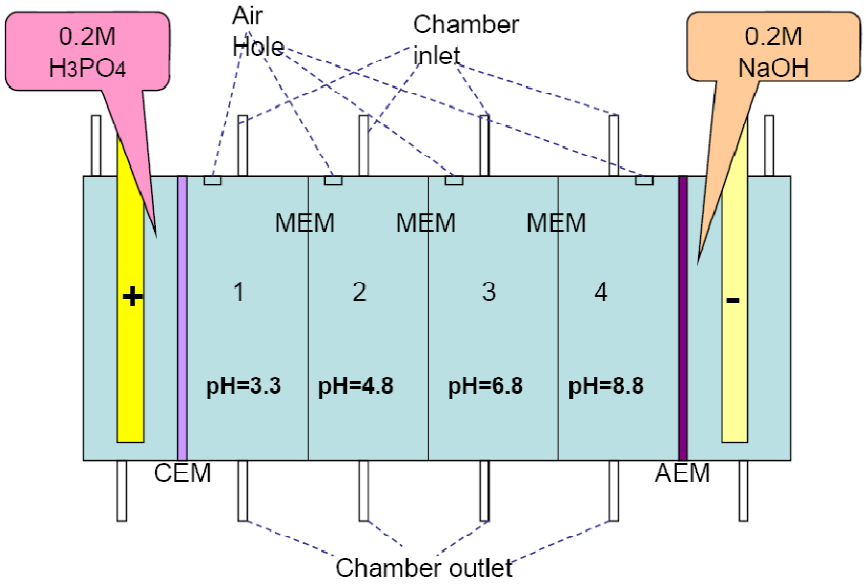

Fig.3-3 Schematic of the IEM-FFIEF device.

Where CEM is a commercial dense cation exchange membrane which resists the protein from the anode; AEM is a commercial dense anion exchange membrane which resists the protein from the cathode.

3.4. Results and discussion

3.4.1. Characterizations of polymer materials and membranes

The FTIR spectra of polysulfone and sulfonated polysulfone materials are given in Fig. 3-4. Compared to PSf, the SPSf spectrum shows a new transmission peak at around 1030 cm−1, which suggests a successful graft of sulfonated groups. The IEC values of SPSf materials and various membranes are shown in Table 3-1. Nadir C100F is an uncharged membrane. The IEC value of ICE450 membrane is provided by Pall. IEC results of self-made SPSf materials and membranes A, B, and C were calculated using the titration method. FESEM images of three self-made SPSf ion exchange membranes are exhibited in Fig. 3-5. It can be found that the thickness of SPSf cross section is around 80μm and the pore size on the membrane top-surface (cutoff pore size) is about tens of nanometers which may be in the suitable range for the Hb and BSA separation.

The solute rejection curves of different membranes from the PVP transport experiments are summarized in Fig. 3-6, where the mean pore size at 50% rejection and MW cut-off (MWCO) at 90% rejection can be determined. Figs. 3-7 and 3-8 exhibit the probability density function curves and the cumulative pore size distributions of three self-made membranes A, B, and C, respectively, which were generated from the real rejection curves in Fig. 3-6. It can be seen that the pore size distribution of self-made membranes is wide, and there are ~ 60% small pores with diameters of lower than 5 nm and also 20–30% large pore with diameters of higher than 10 nm.

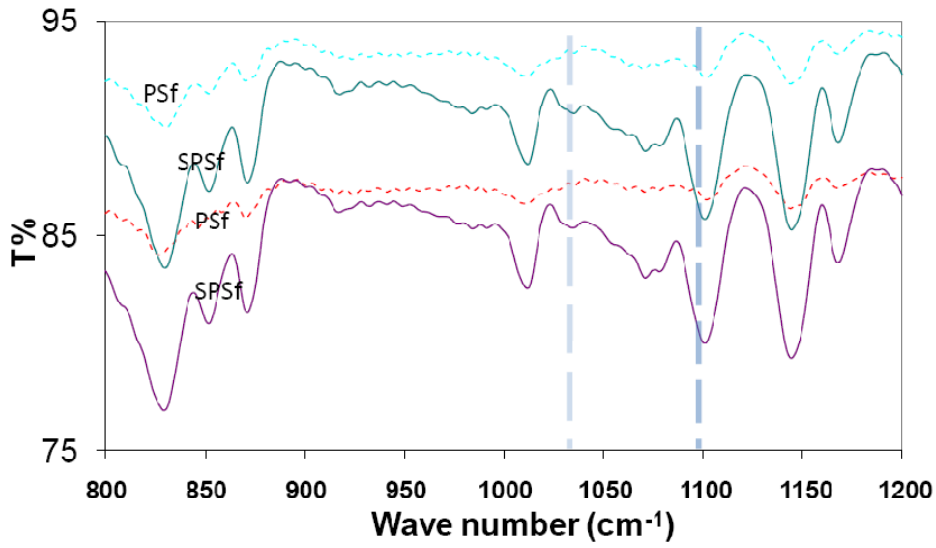

Fig.3- 4 FTIR spectra of polysulfone (PSf) and sulfonated polysulfone (SPSf).

Table 3-1 Ion exchange capacity results of SPSf materials and various membranes

Membrane ID	Membrane IEC (meq/m^2)	SPSf IEC (meq/g)
Nadir C100F	NA	NA
Pall ICE450	5.5~17.8	NA
A [a]	6.9	0.72
B [b]	6.5	0.70
C [c]	5.9	0.66

[a] membrane A with 25% SPSf polymer;
[b] membrane B with 23% SPSf polymer;
[c] membrane C with 24% SPSf polymer.

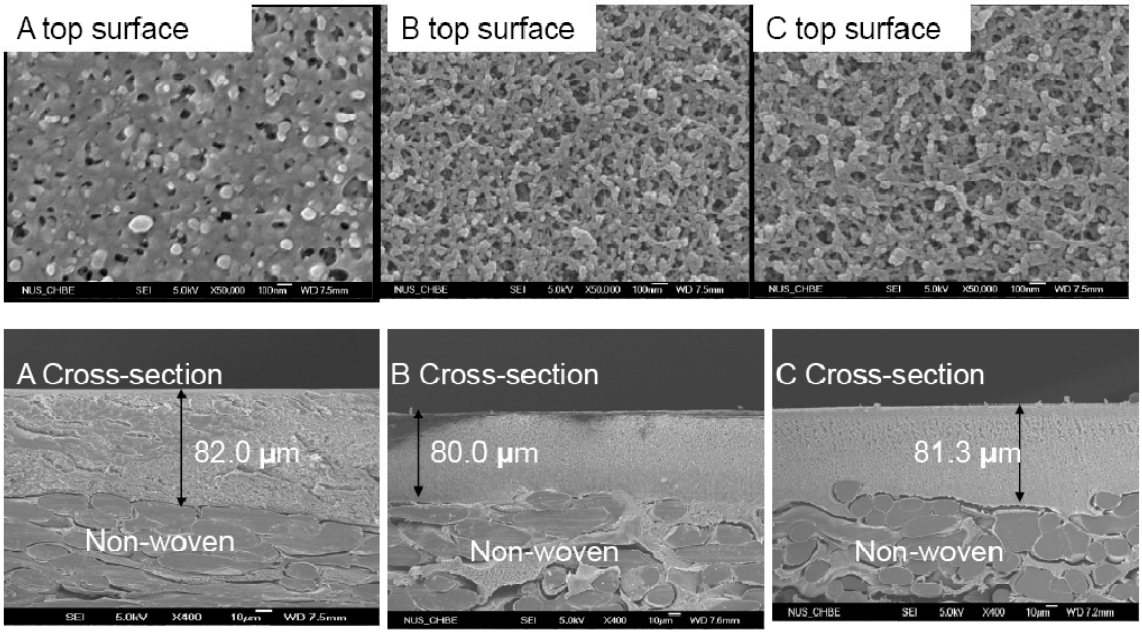

Fig.3-5 SEM images of self-made membranes A, B and C

(A: 25% SPSf polymer; B: 23% SPSf polymer; C: 24% SPSf polymer)

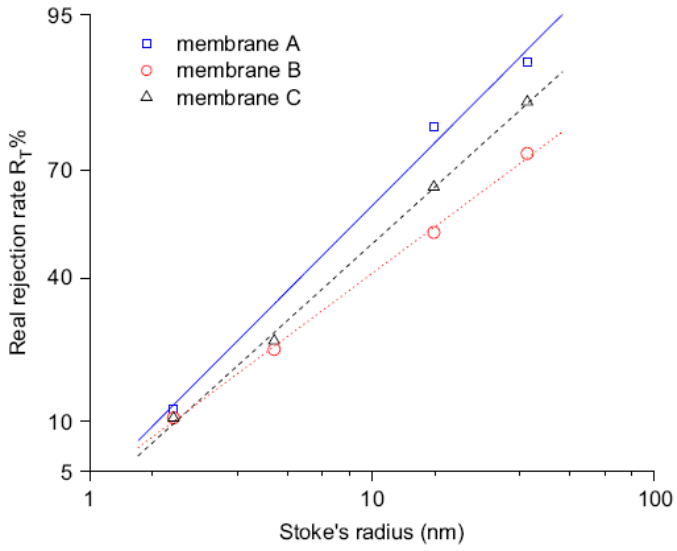

Fig. 3-6 Real rejection curves, plotted on the log-normal probability coordinate system

(A: 25% SPSf polymer; B: 23% SPSf polymer; C: 24% SPSf polymer).

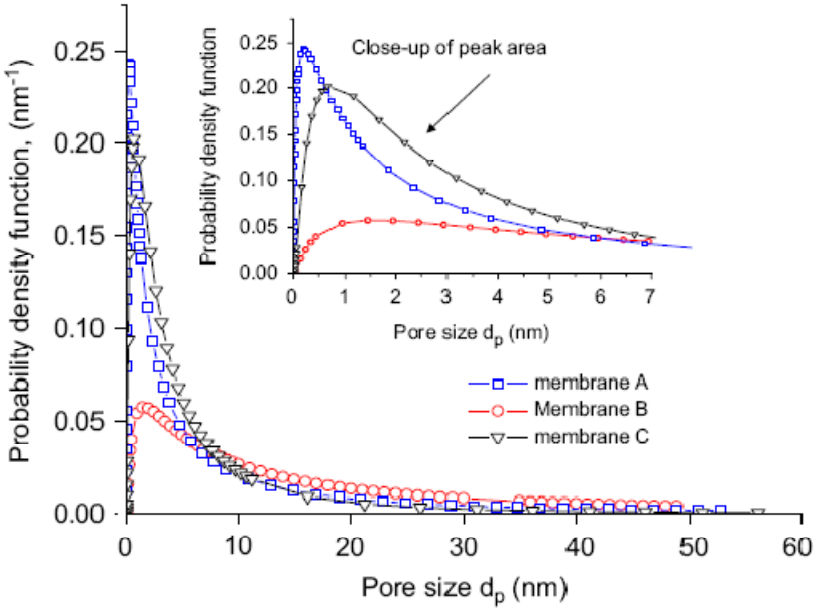

Fig.3-7 Probability density function curves of self-made membranes A, B and C (A: 25% SPSf polymer; B: 23% SPSf polymer; C: 24% SPSf polymer).

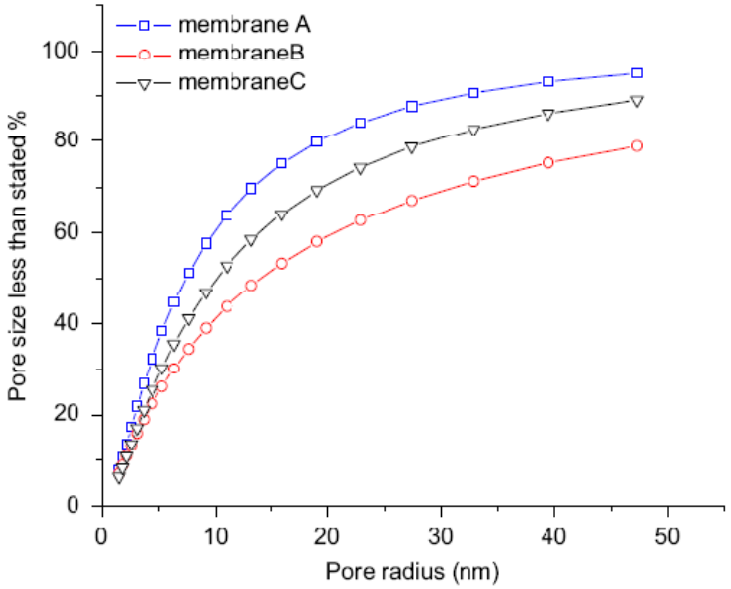

Fig. 3-8 Cumulative pore size distributions of self-made membranes A, B and C (A: 25% SPSf polymer; B: 23% SPSf polymer; C: 24% SPSf polymer).

3.4.2 Protein separation performance under the batch operation

Three different types of membranes were tested under 200 V using the batch operation. The changes in Hb and BSA concentrations at the permeate side of membranes (chamber 3) vs. time is shown in Fig. 3-9. It can be seen that the Hb concentration in chamber 3 increases nearly linearly for all three membranes, while the BSA concentration in chamber 3 exhibits a different trend. For ICE450 and Nadir C100F membranes, the BSA concentration at chamber 3 shows an apparent increment after 30min, leading to a large reduction in Hb/BSA separation performance, whilst for membrane B, BSA molecules hardly transport through it during the entire experimental running so that a high-purity Hb may be collected at the permeate chamber. The possible reasons that resulting in different separation performance among these three membranes may arise from different IEC values and pores sizes on the membrane surface. The Nadir C100F membrane is an uncharged one; therefore, it may not provide a help through the electrostatic interaction in preventing the transport of BSA molecules. For the ICE450 membrane, although it possesses a moderate IEC value and presents a negatively-charged surface, its huge pore size (~450 nm) may dramatically reduce the effect of electrostatic interaction between proteins and negatively-charged sulfonic groups on the transport of BSA molecules. Therefore, only membrane B with a moderate IEC value and suitable pore sizes displays the best protein separation performance among these three membranes.

The effect of different voltages on the protein separation performance of Nadir C100F membrane and membrane B is shown in Fig. 3-10 which is under the batch operation without topping up the feed solution into chamber 2. It can be found that Hb and BSA fluxes through both membranes increase with increasing voltage; however, for these two

membranes, BSA emergence time at the permeate side is much different even at the same voltage of 200 V. Nadir C100F membrane needs 50min, while membrane B needs 90 min. This may be due to the fact that the negative charges in membrane B play a very important role in enhancing the capability to hold the cations in the membrane so that a relatively stable pH gradient can be formed along the membrane B. In addition, the Nadir C100F membrane shows a poor ability to maintain a stable pH gradient due to the lack of negative charges; therefore, the pH value of 4.8 in the feed chamber may drop faster. When there is a decrease in pH values in the feed chamber, BSA molecules are not no longer neutral, but positively charged. Hence, they can more easily pass though the membrane together with Hb molecules, thus leading to a significant reduction in Hb/BSA separation performance. Even though the membrane B can hold a relatively stable pH gradient for a longer time than the commercial membranes, its protein separation performance becomes deteriorated because of the change in pH values in the feed and permeate chambers result in the migration of more BSA molecules.

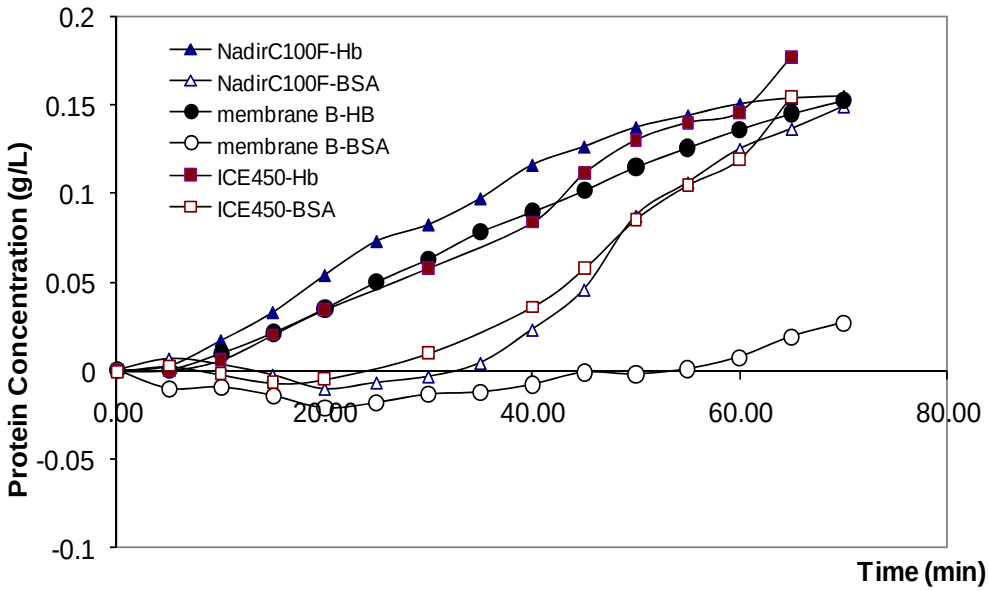

Fig. 3-9 Comparison of protein separation performances of different membranes under 200V and the batch operation (B: 23% SPSf polymer)

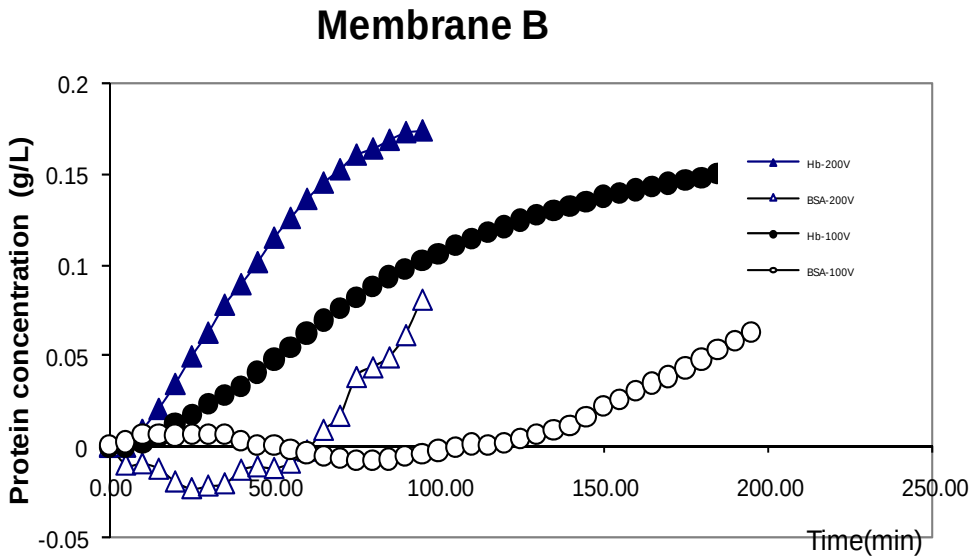

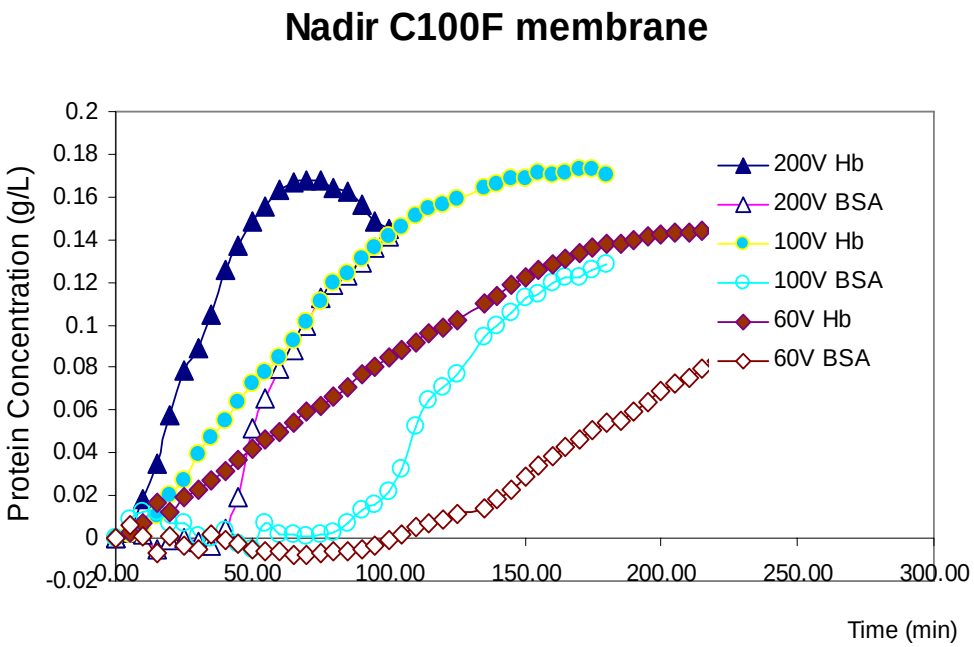

Fig. 3-10 Effect of different voltages on the protein separation performances of membranes under the batch operation (B: 23% SPSf polymer)

3.4.3 Protein separation performance under the semi-batch operation

In order to solve the problem that the protein separation may deteriorate after a certain period of time due to the unstable pH gradient, a semi-batch operation was designed. In this operation, three batches of fresh Hb/BSA mixture were filled into the feed chamber in sequence with an interval of ~30 min. The newly fed protein mixture may ensure the enough concentration of Hb in the feed chamber, thus retaining the original pH values in the feed and permeate chambers and extending the period of stable pH gradient. As shown in Fig. 3-11, Hb molecules pass through membranes B and C continuously, and meanwhile, BSA molecules are kept in the feed chamber due to a stable pH gradient. As a result, a high-purity (> 90 %) Hb is obtained at the permeate chamber in the semi-batch operation if membranes B and C. However, for both Nadir C100F and ICE450 membranes, the system shows a large flux of BSA molecules, indicating a poor Hb/BSA separation. These results are in good agreement with those in the batch operation. Clearly, the negatively charged membranes with a proper pore size distribution are the keys to prevent the transport of BSA molecules.

In order to investigate the current changing tendency in whole semi-batch period, the current was measured as a function of time and voltage during the experimental process. Fig.3-12 illustrates the current flowing with time through the IEM-FFIEF system at given voltage V = 200V. No obvious change in the current with time can be seen after conditioning when a constant voltage is applied. This is mainly due to the fact that the pH values in the corresponding chambers 1~4 were kept constant, thus leading to a relative stable conductivity in the whole buffer system. On the other hand, the current tendency as a function of applied voltage for membrane A is plotted in Fig. 3-13, wherein the data

were collected after conditioning. Current is increasing with applied voltage but not linearly related.

In order to test the stability and reproducibility of the IEM-FFIEF system, two or three rounds of semi-batch operations were consecutively performed for membranes A and C without the cleaning process. Fig. 3-14 shows the results. One slope curve represents one round of semi-batch operation, including the feeding of 3 x 30 ml fresh protein mixtures. It is obvious that a high-purity Hb is continuously collected at the permeate chamber after two or three rounds of semi-batch operations even though there is no membrane cleaning step between two consecutive rounds. This suggests that the membrane fouling phenomenon does not apparently happen during our semi-batch operation, and a reasonable stability and reproducibility can be realized in our designed IEM-FFIEF system.

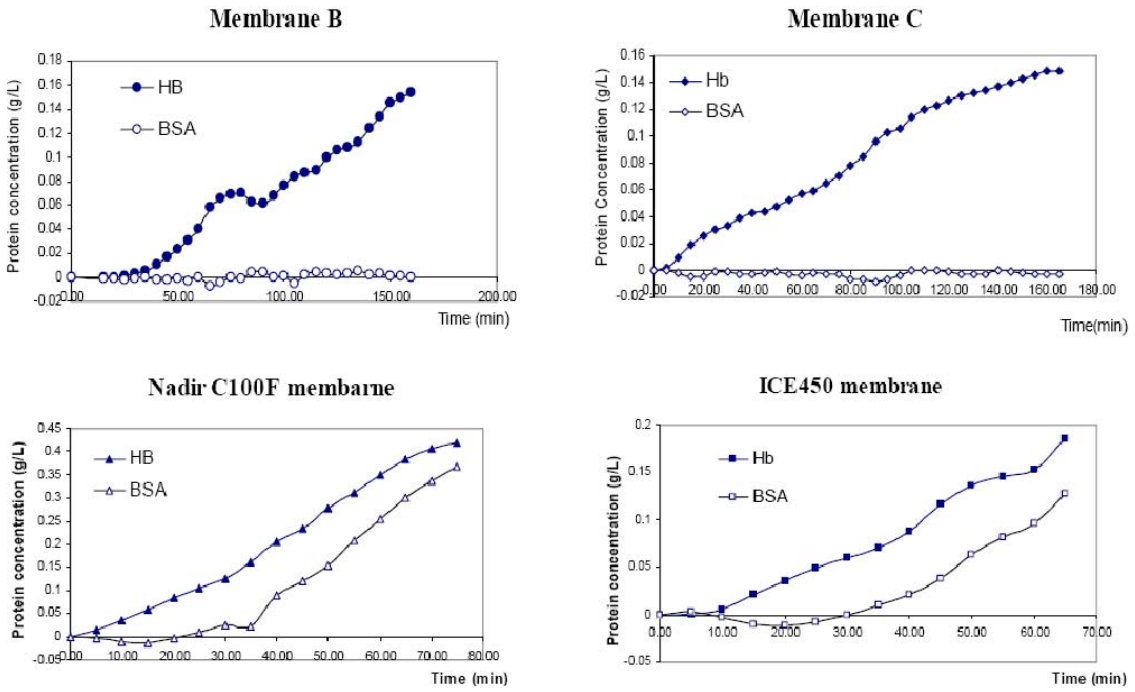

Fig.3-11 Protein separation performance different membranes under 200V and the semi-batch operation. (B: 23% SPSf polymer; C: 24% SPSf polymer)

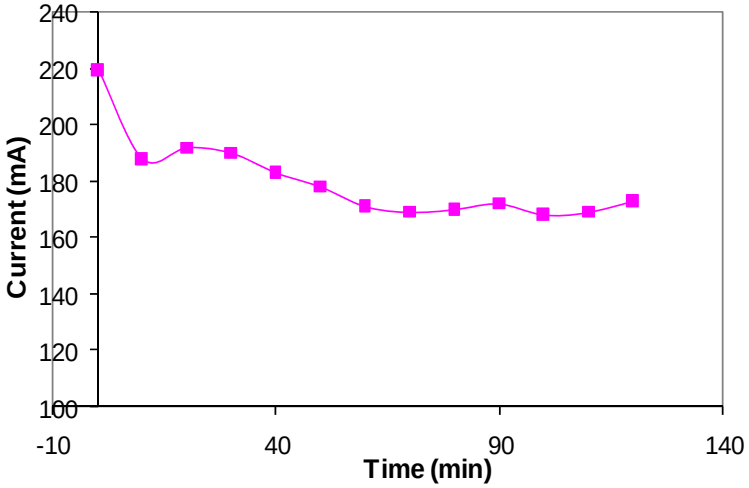

Fig.3-12 The current flowing through the system at given voltage V=200V.

The current drop with time during conditioning period, as more and more protein adsorbed on to membrane pores; when adsorption reach to maximum, the mass transfer started, and the current tend to be stable.

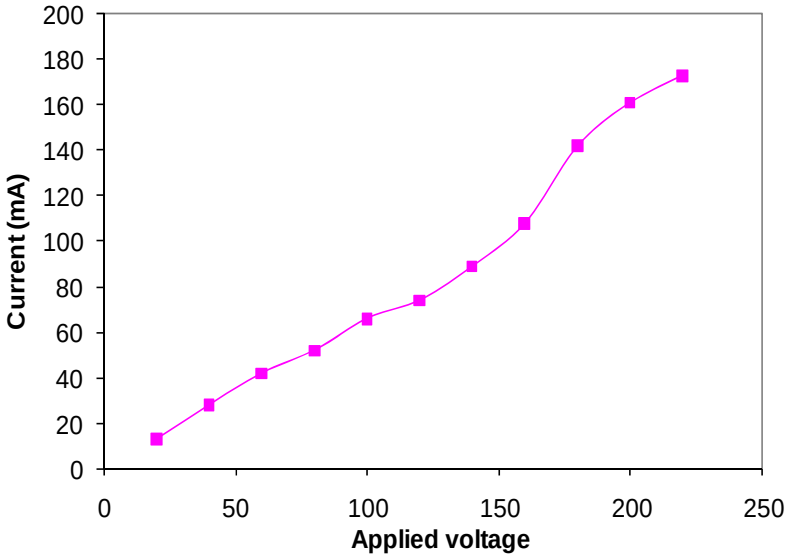

Fig.3-13 Current tendency vs. applied voltage.

After conditioning, the current was measured vs. voltage for FFIEF protein separation process. pH of chamber 1 & 4 were adjusted; constant pH was maintained in every chamber.

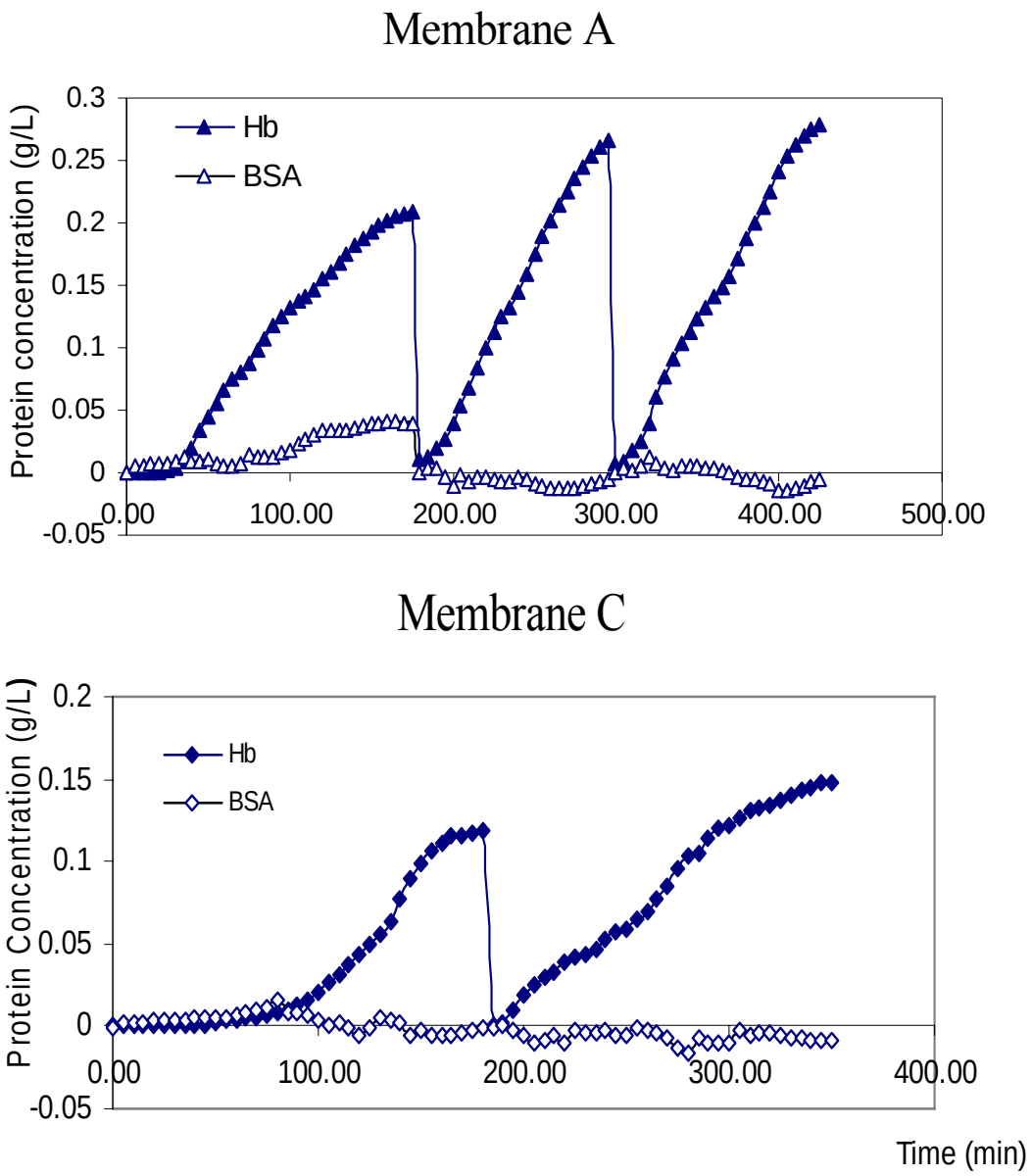

Fig.3-14 Results of stability and reproducibility measurement of membranes A and C under 200V and the semi-batch operation

(A: 25% SPSf polymer; C: 24% SPSf polymer)

During the experimental measurement of the stability and reproducibility of the IEM-FFIEF system, the solution samples at the feed and permeate chambers were collected after each round of semi-batch operation for the protein concentration testing using HPLC. Results are shown in Table 3-2, where Hb/BSA separation factor was calculated using eqn. (3-5):

$$\text{Separation factor} = \frac{(C_{Hb}/C_{BSA})_{\text{permeate chamber}}}{(C_{Hb}/C_{BSA})_{\text{feed chamber}}} \qquad (3\text{-}5)$$

It can be seen that a permeate solution with a 0.3 g/L Hb concentration and a 90-99 % Hb purity is achieved. For membrane A the yield of a semi-batch maximum is 70~75% in Fig.3-12, membrane B & C yields are around this value. This demonstrates that IEM-FFIEF system developed in our study can exhibit a much higher separation performance for Hb/BSA protein mixture by combining the features of free flow isoelectric focusing technology and ion exchange membranes.

3.5. Conclusions

A high performance protein separation process for Hb-BSA mixture has been developed using porous ion exchange membranes partitioned free flow isoelectric focusing system. FTIR spectra suggest a successful graft of sulfonated groups on the polysulfone backbone due to the appearance of a new peak at 1030 cm^{-1}. Titration method and SEM pictures show that the self-made membranes possess a moderate IEC value and suitable pore sizes, respectively.

The protein separation results in the batch operation show that the home-made UF SPSf membranes have the superior selectivity to commercially available membranes. This is

due to the fact that both the pH gradient across the membranes and the electrostatic interaction between the protein molecules and membrane surface play important roles in the protein separation, thus demonstrating the importance of employing charged membranes in the FFIEF system to obtain high protein separation.

High purity (> 90 %) and relative higher concentration of Hb has been obtained at the permeate side of ion exchange membranes during the semi-batch operation. This work clearly demonstrates the great potential of FFIEF for industrial applications. Moreover, experimental results in the consecutive semi-batch operations suggest that the membrane fouling phenomenon is not severe, and high reproducibility in targeted products can be realized in our designed IEM-FFIEF system.

Table 3-2 HPLC test results for protein concentration

Sample ID	Chamber 3		Chamber 2		Separation Factor
	BSA (g/L)	Hb (g/L)	BSA(g/L)	Hb(g/L)	
Mem A [a]	0.0330	0.2082	0.1994	0.0935	10.65
peak a	13.70%	86.30%	68.08%	31.92%	
Mem A [a]	0.0212	0.2908	0.1686	0.0978	23.64
peak b	6.8%	93.2%	63.30%	36.70%	
Mem A [a]	0.0289	0.3180	0.2288	0.0924	27.20
peak c	8.34%	91.66%	71.22%	28.78%	
Mem C [b]	0 [c]	0.1092	-	-	Extremely
peak a	0%	99.9%			large
Mem C [b]	0 [c]	0.1605	-	-	Extremely
peak b	0%	99.9%			large

[a] Mem-A with 25% SPSf polymer;
[b] Mem-C with 24% SPSf polymer;
[c] data were guessed values because the BSA was not detectable in these samples.

Acknowledgement:

The authors would like to thank A-star and National University of Singapore (NUS) for funding this research with the grant number of R-279-000-164-305. Thanks are due to Solvay Advanced polymers L.L.C. and Nadir Filtration GmbH for their donations of polysulfone materials and NF membranes, respectively. Special thanks are given to Drs. Y. C. Xiao, Q. Yang, K. Y. Wang and B. Cao for their valuable assistance.

3.6 References

1. A.L. Zydney and N.S. Pujar, Protein transport through porous membranes: effects of colloidal interactions, Colloid Surface A, 138 (1998) 133.

2. R.H.C.M. van Eijndhoven, S. Saksena and A.L. Zydney, Protein fractionation using electrostatic interactions in membrane filtration, Biotechnol. & Bioen., 48 (1995) 406.

3. S. Galier and H.R.Balmann, Study of the mass transfer phenomena involved in an electrophoretic membrane contactor, J. Membr. Sci., 194 (2001) 117.

4. C. Charcosset, Z. Su, S. Karoor, G. Daun and C.K. Colton, Protein A immunoaffinity hollow fiber membranes for immunoglobulin G purification: Experimental characterization**,** Biotechnol. & Bioeng., 48 (1995) 415.

5. Z. Prusik, Free-flow electromigration separations, J. Chromato. A, 91 (1974) 867.

6. C. Hanning, Continuous free-flow electrophoresis as an analytical and preparative method in biology, J. Chromato. A, 159 (1978) 183.

7. P. Wenger and P. Javet, Isoelectric focusing using non-amphoteric buffers in free solution: I. determination of stable concentration profiles, J. Biochem. & Biophys. Meth., 13 (1986) 259.

8. P. Wenger and P. Javet, Isoelectric focusing using non-amphoteric buffers in free solution: II. apparatus and measures of pH stability, J. Biochem. & Biophys. Meth., 13 (1986) 275.

9. P. Wenger and P. Javet, Isoelectric focusing using non-amphoteric buffers in free solution: III. Separation of amino acid, J. Biochem. & Biophys. Meth., 13 (1986) 289.

10. P. Wenger, M. Zuanni and P. Javet, Amphoteric isoelectric immobiline membranes for preparative isoelectric focusing, J. Biochem. & Biophys. Meth., 14 (1987) 29.

11. M. Bier, G.E. Twitty and J.E. Sloan, Recycling isoelectric focusing and isotachophoresis, J. Chromato. A, 470 (1989) 369.

12. J. Lucas, M. Faupel, C. Goecking and R.S. Explorat, Preparative separation of pyrogens from proteins by isoelectric focusing using a multi-compartment electrolyzer with Immobiline membranes, Electrophoresis, 11 (1990) 981.

13. S. Cherkaoui, P. Zell and P. Javet, Characterization of immobiline membranes for application in a multi-compartment electrolyzer for protein purification, J. Biochem. & Biophys. Meth., 25 (1992) 61.

14. G. Motonobu, N. Toshio and H. Tsutomu, Protein separation by preparative multicompartment electrolyzer secluded by isoelectric membranes, Sep. Sci. & Technol., 28 (1993) 1947.

15. M. Chiari, M. Nesi, P. Poncada and P.G. Righetti, Preparative isoelectric focusing in multi-compartment electrolyzers: Novel, hydrolytically stable and hydrophilic isoelectric membranes, Electrophoresis, 15 (1994) 953.

16. J. Watson, Continuous, free-flow electrophoresis: A modified approach, Sep. Technol., 4 (1994) 239.

17. A. Bossi and P.G. Righetti, Fractionation of carrier ampholytes in multi-compartment electrolyzers with isoelectric membranes, Electrophoresis, 16 (1995) 1930.

18. A.N. Cherkasov and A.E. Polotsky, The resolving power of ultrafiltration, J. Membr. Sci. 110 (1996) 79.

19. J.C. Baygents, B.C.E. Schwarz, R.R. Deshmukh and M. Bier, Recycling electrophoretic separations: modeling of isotachophoresis and isoelectric focusing, J. Chromato. A, 779 (1997) 165.

20. C.A.P.M. van Nunen, Design of Large Scale Membrane, Electrophoresis Module for Separation of Proteins, PhD. thesis, University of Eindhoven, (1997).

21. D.B. Rylatt, M. Napoli and D. Ogle, Electrophoretic transfer of proteins across polyacrylaminde membranes, J. Chromato. A, 865 (1999) 145.

22. C. Tragas and J. Pawliszyn, On-line coupling of high performance gel filtration chromatography with imaged capillary isoelectric focusing using a membrane interface, Electrophoresis, 21(2000) 227.

23. P. Hoffmann, H. Ji, R.L. Moritz and L.M. Connolly, Continuous free-flow electrophoresis separation of cytosolic proteins from the human colon carcinoma cell line LIM 1215, A non two-dimensional gel electrophoresis-based proteome analysis strategy, Proteomics, 1 (2001) 807.

24. Z.J. Wang, G.W. Le, Y.H. Shi and W. Grzegorz, Purification of plasmid DNA using a multi-compartment electrolyzer separated by ultrafilter membranes, Biotechnol. Lett. 24 (2002) 121.

25. M. Cretich, G. Pirri and G. Carrea, Separation of proteins in a multi-compartment electrolyzer with chambers defined by a bed of gel beads, Electrophoresis, 24 (2003) 577.

26. F.G. Smith III and W.M. Deen, Electrostatic double layer interactions for spherical colloids in cylindrical pores, J. Colloid & Interf. Sci., 78 (1980) 444.

27. F.G. Smith III and W.M. Deen, Electrostatic effects on the partitioning of spherical colloids between dilute bulk solution and cylindrical pores, J. Colloid & Interf. Sci., 91 (1993) 571.

28. N.S. Pujar and A.L. Zydney, Electrostatic and electrokinetic interactions during protein transport through narrow pore membranes, Ind. & Eng. Chem. Res., 33 (1994) 2473.

29. D.B. Burns and A.L. Zydney, Contributions to electrostatic interactions on protein transport in membrane system, AIChE J., 47 (2001) 1101.

30. C.C. Ho and A.L. Zydney, Transmembrane pressure profiles during constant flux microfiltration of bovine serum albumin, J. Membr. Sci., 209 (2002) 363.

31. B. Cheang and A.L. Zydney, Separation of α-lactalbumin and β-lactoglobulin using membrane ultrafiltration, Biotechnol. & Bioeng., 83 (2003) 201.

32. A.L. Zydney, Protein separations using membrane filtration: new opportunities for whey fractionation, Int. Dairy J., 8 (1998) 243.

33. J.E. Sader and D.Y.C. Chan, Electrical Double-Layer Interaction between Charge Particles near Surfaces and in Confined Geometries, J.Colloid & Interf. Sci., 218 (1999) 423.

34. Z.R. Ulberg and L.G. Marochko, The electrophoretic properties and stability of the cell suspensions, Colloid Surface A, 159 (1999) 513.

35. R.X. Zhuo and W. Li, Preparation and characterization of macroporous poly(nisopropylacrylamide) hydrogels for the controlled release of proteins, J. Polym. Sci. A, 41 (2003) 152.

36. P.K. Das and S. Bhattacharjee, Electrostatic double-layer interaction between spherical particles inside a rough capillary, J. Colloid & Interf. Sci., 273 (2004) 278.

37. N.F. Gordon, C.M.V. Moore and C.L. Cooney, An overview of continuous protein purification process, Biotechnol. Adv., 8 (1990) 741.

38. K.J. Kim, P. Sun, V.A. Chen and G. Fane, The cleaning of ultrafiltration membranes fouled by protein, J. Membr. Sci., 80 (1993) 241.

39. N.A. Ochoa, M. Masuelli and J. Marchese, Development of charge ion exchange resinpolymer ultrafiltration membranes to reduce organic fouling, J. Membr. Sci., 278 (2006) 457.

40. Y. Wan, J. Lu, Z. Su and Z. Cui, Evaluation of fouling and concentration polarization during protein ultrafiltration by pulsed sample injection technique, Desalination, 199 (2006) 539.

41. R. Westermerier and V.C.H. Weinheim, Eletrophoresis in Practice, New York published, 1993.

42. J.A. Wesselinggh and J.C. Bosma, Protein ion exchange adsorption kinetics, AIChE J., 47 (2001) 1571.

43. I.C. Kim, J.G. Chio and T.M. Tak, Sulfonated polyethersulfone by heterogeneous method and its membrane performances, J. Appl. Polym. Sci., 74 (1999) 2046.

44. J.K. Fang, H.C. Chiu, J.W. Wu and S.Y. Suen, Preparation of polysulfone base cation exchange membranes and their application in protein separation with a plate-and-frame module, React. Funct. Polym., 59 (2004) 171.

45. Y. Mastumoto and M. Sudoh, Preparation of composite UF membranes of sulfonated polysulfone coated on ceramics, J. Membr. Sci.,158 (1999) 55.

46. I.S. Byun and I.C. Kim, Pervaporation behavior of asymmetric sulfonated polysulfones and sulfonated poly(ether sulfone) membranes, J. Appl. Polym. Sci., 76 (2000) 787.

47. R. Guan, H. Zou, D.P. Lu, Polyethersulfone sulfonated by chlorosulfonic acid and it membrane charateristics, Euruop. Polym. J., 41 (2005) 1554.

48. K.H. Youm, W.S. Kim, Prediction of intrinsic pore properties of ultra-filtration membrane by solute rejection curves: effects of operating conditions on pore properties. J. Chem. Eng.Japan 24 (1991) 1.

49. K.Y. Wang, T. Matsuura, T.S. Chung and W.F. Guo, The effects of flow angle and shear rate within the spinneret on the separation performance of poly(ethersulfone) (PES) ultrafiltration hollow fiber membranes, J. Membr. Sci., 240 (2004) 67.

50. K.Y. Wang and T.S. Chung, The characterization of flat composite nanofiltration membranes and their applications in the separation of cephalexin, J. Membr. Sci., 247 (2005) 37.

CHAPTER 4 INVESTIGATION OF MASS TRANSFER IN THE ION-EXCHANGE MEMBRANE PARTITIONED FREE-FLOW ISOELECTRIC FOCUSING SYSTEM (IEM-FFIEF) FOR PROTEIN SEPARATION

4.1. Introduction

The separation of bio-molecules such as proteins and pharmaceuticals from native mixtures is a technology-intensive process. For protein separation, membrane technology coupled with electrophoresis has been considered as a potential approach [1]. The most attractive characteristics of electrophoresis are continuous mass transfer and sharp separation in the presence of a direct current driving force. Hybrid membrane technologies utilizing either electrostatic effects [2-11] or electrophoresis [12, 13] have been proposed in order to overcome the problems in membrane based ultra-filtration e.g. fouling, efficiency decline and low selectivity. Therefore, the combination of both electrostatic effects and electrophoresis for protein separation process may generate some synergistic results.

Among various electrophoresis methods, isoelectric focusing (IEF) exhibits the highest resolution and may be the most suitable method for preparative purposes [13-17]. IEF has been developed for the separation of different types of protein molecules according to their pI values [18-30]. Generally, IEF employed for analytical purposes uses gel materials as the separation media. Bier and his associates made significant contributions to the IEF process by controlling the flow pattern in each partitioned chamber of recycle-flow IEF (RIEF or free-flow isoelectric focusing (FFIEF)) in multi-compartments [31-34]. RIEF has been commercialized by Bio-Rad under the trade name of Rotofor™ for laboratory

preparative applications. However, it still has limitations in resolving protein separation. One of the major drawbacks is that the proteins do not be fully focused, and the fractioned species would distribute over a series of neighborhood chambers [30]. The high cost of the ampholyte used to stabilize the pH gradient in the isoelectric focusing cell is another drawback hindering the scaling up of RIEF [18-20].

To overcome these limitations, Wenger and Javet employed neutral ultra-filtration membranes with acetic acid-sodium acetic acid buffers in the FFIEF system to force pH adjustment in the two end buffer chambers [18-20]. This approach has been proven beneficial for amino acid separation in their works and in our protein separation through ion-exchange-membrane-partitioned free-flow isoelectric focusing (IEM-FFIEF) system using self-fabricated ion-exchange ultrafiltration membranes [35]. Another approach is to use immobiline in FFIEF. Immobiline is a gel-like membrane that has its own pI value. Due to the buffer capacity provided by the charged materials constituting immobililine, it is able to maintain a certain pH during the process and gives rise to distinct and sharp fractioned species in a series of specific chambers [23-29]. However, the immobiline membrane has poor mechanical strength and relatively short life span, thus limiting its application in industrial process.

Capitalizing all the advantages of different IEF devices and immobiline membranes, we intend to utilize solid phase porous sulfonated polysulfone (SPSf) membranes in multi-compartment electrophoresis (MCE) to achieve protein separation and concentration. The differences between the current study and the conventional immobiline membranes partitioned MCE are (1) the SPSf cation-exchange membranes have much stronger mechanical strength than gel-like immobiline membranes and (2) the SPSf membranes

can perform the selective function of immobiline membranes with high reproducibility and without ion depletion [35]. For applications in industrial scale electrolyzers, membranes with high mechanical strength and reproducibility are needed and the SPSf porous membranes developed by Chung's group are appropriate for commercial use [35, 36]. The structure of the SPSf membranes is significantly different from the gel like immobilines and its influences on mass transfer have not been fully revealed. Thus, a large portion of this work aims to combine the membrane methodology with the boundary effect theory to study the basic phenomena of mass transfer in IEM-FFIEF process. It is generally accepted that a pH jump occurs at the surface of "dense" ion-exchange membranes. The existence of a pH gradient across the membranes is highly debatable within the membrane community. However, we believe that there is a pH gradient across the microporous cross-section when different pHs are applied on the two sides of an ion-exchange membrane. In addition, it is necessary to prove the existence of a "minimal effective pore radius" (R_e) above which the free movement of protein molecules occurs.

In order to prove our hypotheses and to verify the applicability of boundary effect theory in IEM-FFIEF system, protein separation experiments were performed. A series of characterizations were conducted on the fabricated SPSf membranes by FTIR (Fourier transform infrared spectroscopy), FESEM (Field emission scanning electron microscopy), EDX (Energy dispersive X-ray spectroscopy), streaming potential measurement and solute rejection methods. To study the mass transfer phenomena, a simple model comprising of a binary mixture of bovine serum albumin (BSA) and myoglobin (Mb), was separated by the IEM-FFIEF system and the real velocities of Mb were compared with the calculated values obtained from the boundary effect theory.

4.2. Theoretical background

The mass transfer of protein through an ion exchange membrane in the IEM-FFIEF process is a complicated science of boundary effects which involves surface electrical properties, double layer thickness, micro-structure of membranes, applied electric field and electrostatic interaction between the particle and membrane pore surface. In order to correlate mobility with surface charge properties and membrane structure, this section focuses on introducing the theoretical background of boundary effects and deriving the measurable parameter E_0 which indicates the minimal electric field strength necessary for flux breakthrough.

4.2.1 Isoelectric focusing for protein separation

The fundamentals of IEM-FFIEF technology has been introduced in our previous work [35]. Basically, the IEM-FFIEF performance is mainly determined by the net charges on the particle surface and separation media. The net charge of protein particles is the sum of all positive and negative charges provided by amino acid units. Fig. 4-1 shows the experimental set up and Fig. 4-2 shows the principle of the IEM-FFIEF separation. The feed and the permeate chambers are separated by a sulfonated polysulfone (SPSf) ultrafiltration (UF) membrane, which allows only the positively charged ions to pass through while the negatively charged ions are rejected. Under the given conditions, BSA is slightly negatively or zero charged while Mb is positively charged in feed chamber. As a result of the electrostatic effect, Mb will be transferred to the permeate chamber and BSA will be rejected and remained in feed chamber.

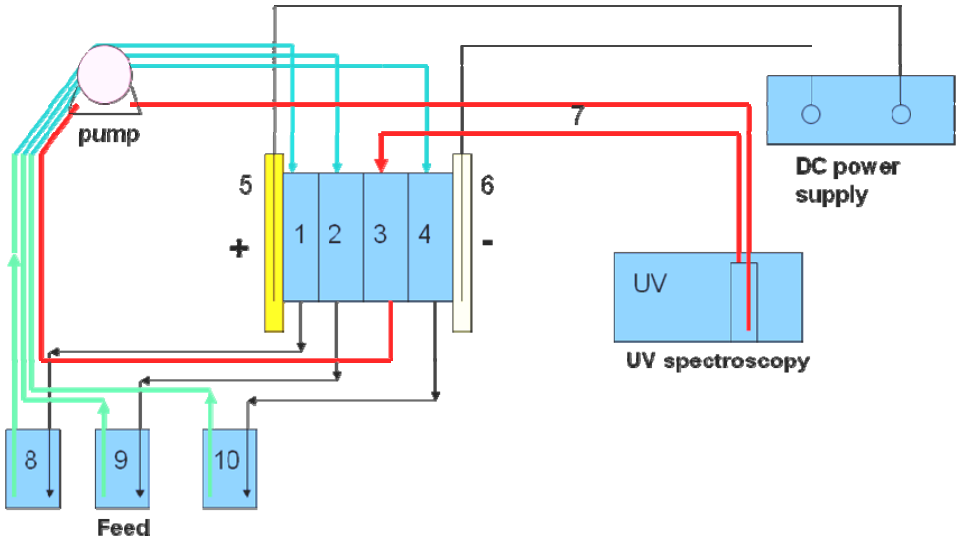

Fig. 4-1 Experimental set up

1: the chamber 1 with pH = 3.2~3.3;
2 :the chamber 2 (feed chamber) with pH = 4.8;
3 :the chamber 3 (permeation chamber) with pH = 6.8;
4 :the chamber 4 with pH = 8.7~8.8;
5 :the anode chamber; 6: the cathode chamber;
7 :the permeation test circuit; 8, 9, 10 the measurement and adjustment tanks of pH values in chamber 1, 2 and 4 individually.

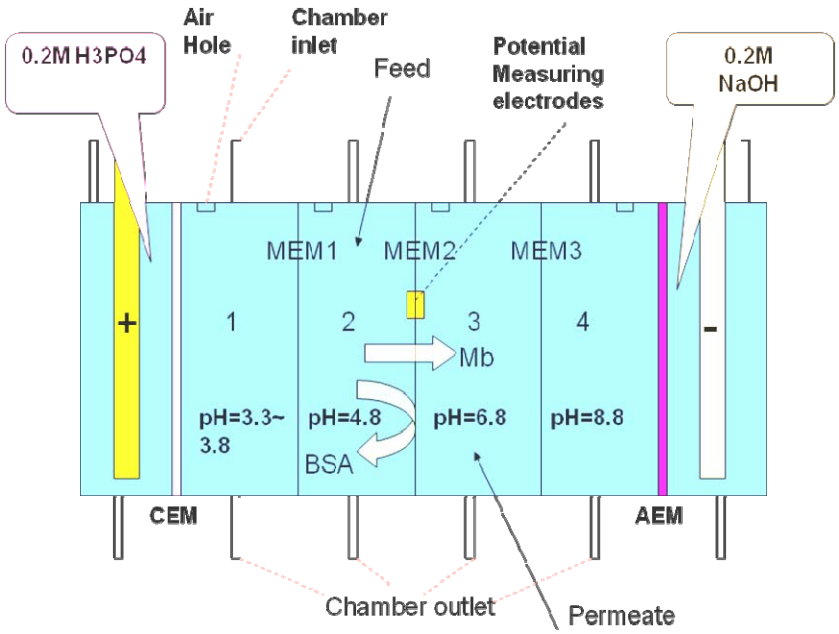

Fig. 4-2 Schematic of the IEM-FFIEF device

CEM: dense cation exchange membrane; AEM: dense anion exchange membrane.

4.2.2 Boundary effects of the membrane

The electrophoretic motion of charged particles in the presence of a confined boundary has been broadly studied and numerous analytical expressions and simulations have been derived in a wide range of double layer thickness [37-41]. Among these vast studies, Ennis, Keh and Anderson have contributed massive fundamental works on mathematic modeling, provided various clues for further understanding of the membrane based electrophoresis. Particularly the assumptions presented in Ennis et al. work [39] are closest to the reality of our membrane based electrophoresis. By assuming a thick double layer, an analytical expression of translation velocity (υ) of a charged particle through a charged cylindrical pore was proposed by Ennis et al. [39]. Their studies clearly demonstrated that the mass transfer through a membrane based electrophoresis is determined by the surface ζ-potentials (of both particles and membrane pores), pore sizes, particle size, buffer concentration and undisturbed applied electric field E_∞, as shown by eqn. (4-1):

$$\begin{aligned}\upsilon = \frac{\varepsilon\zeta_s}{4\pi\eta} E_\infty e_z \{ & f(\kappa a) + \gamma \left(g(0,\kappa b) \frac{1+3.867\lambda-1.907\lambda^2-0.834\lambda^3}{1+1.867\lambda-0.741\lambda^2} - g(\lambda,\kappa b) \right) \\ & + \lambda^3 (0.79683 \times [f(\kappa a) - L(\kappa a)] - 1.28987 \times [L(\kappa a) - \gamma]) \\ & + 1.89632\lambda^5 [L(\kappa a) - \gamma] \\ & + \lambda^6 (0.63494 \times [f(\kappa a) - L(\kappa a)] - 1.02781 \times [L(\kappa a) - \gamma])\}\end{aligned} \tag{4-1}$$

$$\kappa \approx 3.288\sqrt{I} \quad in \quad (nm) \tag{4-2}$$

$$I = \frac{1}{2}\left(n_i^z C_i^f z_P^2 + \sum C_{bi} z_{bi}^{\ 2} \right)^{1/2} \tag{4-3}$$

$$g(\lambda,\kappa b)=1-\frac{2I_1\left(\kappa b(1-\lambda)\right)}{\kappa b(1-\lambda)I_0\left(\kappa b\right)}$$
$$-\frac{\lambda^2}{3(1-\lambda)^2 I_0\left(\kappa b\right)}\{I_0\left[\kappa b(1-\lambda)\right] \qquad (4\text{-}4)$$
$$-1+\kappa b(1-\lambda)I_1\left[\kappa b(1-\lambda)\right]\}$$

All the symbols in the equations are listed in the nomenclature. The functions *L(κa) and f(κa)* are given in appendix A. The term $4\pi\eta\upsilon/(\varepsilon E_\infty \zeta_s)$ is defined as relative mobility. I_0 *and* I_1 are the zero and first order terms of the first kind of modified Bessel functions. The function $g(\lambda,\kappa b)$ represents the effects arisen by the charged pore surface. When λ = *0,* $g(0,\kappa b)$ represents this effect at the centre of the pore. Correspondingly, the function $\gamma g(\lambda,\kappa b)$ represents the contribution of electro-osmosis to the average particle velocity (at the particle surface enclosed in the pore); and the $\gamma g(0,\kappa b)$ term represents the contribution of Poiseulle flow (at the centre of the pore) to the average velocity [39]. Eqn. (4-1) is particularly appropriate for protein electrophoresis via a porous membrane in a system with a low κa value (i.e., thick double layer) and minimal overlapping of the double layers between particles and pore surface.

4.2.3 Minimal electric field strength E_0 for flux breakthrough

As a result of electrostatic effect, a certain amount of applied energy is consumed for making flux breakthrough - we call it the minimal electric field strength E_0. The expression of E_0 can be simply derived from the governing equation of IEF and the Einstein's equation. The governing equation of IEF is a special form of Nernst-plank equation at steady state and can be written in the form of eqn. (4-5):

$$-D_{im}\frac{dC_{im}}{dx}=E\mu_{im}C_{im} \qquad (4\text{-}5)$$

The solution to eqn. (4-5) has been discussed in details by Svensson and is represented by eqn. (4-6) [42]:

$$C_{im} = C_0 \exp(-\frac{p\imath x^2}{2A\kappa_0 D_{im}}) = C_0 \exp(\frac{\mu_{im} E_\infty x}{2D_{im}}) \qquad (4\text{-}6)$$

According to Svensson's results, when μ_{im} is a known function of pH and when the conductivity κ_0, the diffusivity D_{im} and $p = - d\mu_{im}/dx = -d\mu_{im}/d(pH)*d(pH)/dx$ can be regarded as constants within the IEF medium, then $\mu_{im} = - px=\upsilon/E$. The $x = 0$ is defined at the isoelectric point of component i as shown in Fig. 4-3 (because BSA has been rejected, i refers to Mb only). Therefore, at the permeate side of membrane we have $z_i = 0$, $\mu_{im} = 0$ and C_0 = maximum.

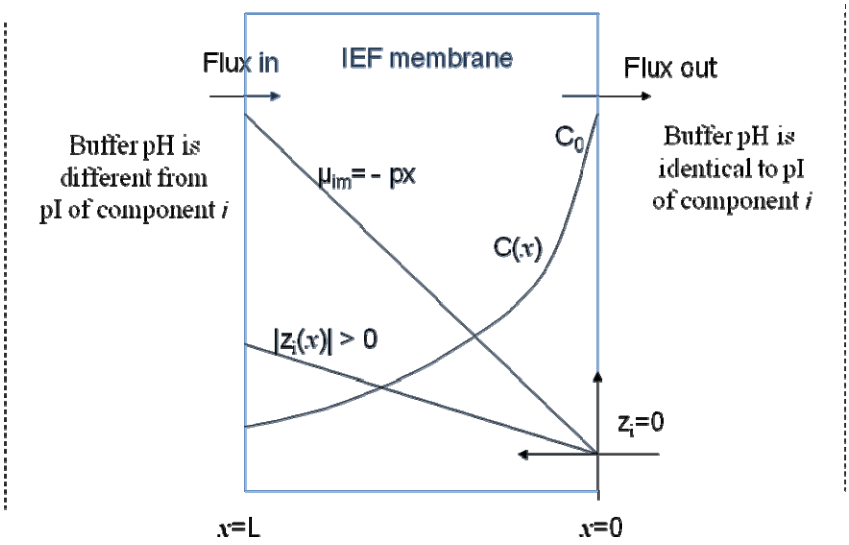

Fig. 4-3 Illustration of mass transfer in the ion exchanged membrane of FFIEF

On the other hand, the relationship between diffusivity, D_{im}, and mobility, μ_{im}, is given by eqn. (4-7) [43]:

$$\mu_{im} = \frac{z_i F D_{im}}{RT} \qquad (4\text{-}7)$$

As defined by Svensson, the diffusion coefficient in eqns. (4-6) and (4-7) corresponds to

the ion with mobility μ_{im} and thus, this D_{im} is not the "self-diffusion coefficient" [42]. In eqn. (4-7), the effective valence per unit site is defined as the average charge over the whole macromolecule:

$$z_i = \frac{\sum z_p n_i^z}{N_i} \qquad (4\text{-}8)$$

where z_p is the valence per charge site, n_i^z is the net charge on one protein molecule under a specific pH; N_i is the total number of amino acid units.

Meanwhile when considering the local electrostatic effect, the concentration of component i inside a pore is determined by the electrostatic potential relative to the pore surface [44], where the local electrostatic potential ζ_t is a function of location x. The local concentration of ionic constituent i is given by the Boltzmann equation [45, 46]:

$$C_{im} = C_0 \exp\left(-\frac{z_i(x) F \zeta_t(x)}{RT}\right) \qquad (4\text{-}9)$$

where $\zeta_t(x) = \zeta_s(x) - \zeta_w$ is the electrostatic potential between the protein molecule surface (ζ_s) and the pore surface (ζ_w). A new expression can be derived by substituting eqn. (4-7) into eqn. (4-6). Eqn. (4-10) is obtained by equating the resultant equation to eqn. (4-9).

$$E_0 = -\frac{2\left(\zeta_s^{\,f} - \zeta_w^{\,f}\right)}{L} \qquad L > x > 0 \qquad (4\text{-}10)$$

where ζ_s^f and ζ_w^f are the ζ-potentials of Mb surface and pore surface at the feed side ($x = L$), respectively. Since BSA is supposed to be fully rejected by the membrane, E_0 can be considered as the minimum electrical consumption for Mb to overcome the electrostatic effect and to produce a flux breakthrough.

4.2.4 Undisturbed electric field strength E_∞ and disturbed electric field strength E_∞'

The electrical potential across the membrane is contributed by three components; namely, the external power supply, the electrostatic potential, and the pH gradient. The E_∞ in eqn. (4-1) is given by eqn. (4-11) [39]:

$$E_\infty = \frac{\iota}{\varepsilon_p \kappa_0 A} \qquad (4\text{-}11)$$

In order to determine the real experimental velocity (υ_{real}) of Mb molecules,

$$\upsilon_{real} = \mu_{real} \times E_\infty' \qquad (4\text{-}12)$$

the disturbed electric field strength, E_∞' is required:

$$E_\infty' = \vec{E}_\infty + \vec{E}_0 = \frac{\iota}{\varepsilon_p \kappa_0 A} - \frac{2\left(\zeta_s^{\,f} - \zeta_w^{\,f}\right)}{L} \qquad (4\text{-}13)$$

The real average mobility μ_{real} in eqn. (4-12) is given by eqn. (4-14) [39]:

$$\mu_{real} = \frac{V_f \kappa_w}{\iota C_{i0}^{\,f}} \left(\frac{dC_i^{\,f}}{dt} \right) \qquad (4\text{-}14)$$

where V_f is the volume of feed chamber; ι is the applied current; κ_w is the overall conductivity and is given by $\kappa_w = \iota/Vl$; l is the total length between two electrodes; $C_{i0}^{\,f}$ is the original Mb concentration in feed chamber; $dC_i^{\,f}/dt$ is the rate of change of concentration over time. Since all of the parameters at the right hand side of eqn. (4-14) are experimentally measurable, the real mobilities and hence, the real velocities of Mb through different membranes can be calculated from protein separation experiments.

4.2.5 Surface ζ-potentials for a thick-double layer

The apparent zeta-potential, $\zeta_{apparent,}$ can be determined from the following Helmholtz-Smoluchowski equation using streaming potential measurements for a thin double layer

[47]:

$$\zeta_{apparent} = \frac{\Delta E_s}{\Delta P}\frac{\eta \kappa_0}{\varepsilon_0 \varepsilon_r} \qquad (4\text{-}15)$$

The $\zeta_{apparent}$ can be corrected by 0.1M KCl through eqn. (16) [42, 43]:

$$\zeta_{corrected} = \frac{dU}{dP} \times \frac{\eta}{\varepsilon_r \times \varepsilon_0} \times \frac{\kappa_{0.1MKCl} \times R_{0.1MKCl}}{R} \qquad (4\text{-}16)$$

However, the surface streaming potential can not represent the ζ-potential inside the pores. Particularly when κb < 20, the pore surface has a thick double layer (i.e., the double layer thickness of pore surface is of the same order as the particle), and the ζ-potential on pore surface will be dramatically affected by the pore size. Fortunately, the ζ-potential inside the pore can be derived from the measurement of streaming potential at the membrane surface as follows [48, 49]:

$$\zeta_w = \frac{\Delta E_s}{\Delta P}\frac{\eta \kappa_0}{\varepsilon_0 \varepsilon_r}\frac{1}{g(0,\kappa b)} \qquad (4\text{-}17)$$

where the *g(0, κb)* is a special form of eqn. (4-4) at $\lambda = 0$, which physically represents a correction factor of surface ζ-potential induced by the pore curvature.

On the other hand, the ζ-potential at the surface of the protein molecule, ζ_s can be calculated based on the simplified equations for thick double layer (small κa) as shown by eqn. (4-18) [50]:

$$\zeta_s = f(\kappa a)\frac{q_s}{4\pi\varepsilon a_s}\exp(-\kappa a_s) \quad for \quad small \quad \kappa a < 20 \qquad (4\text{-}18)$$

$$\mu_s = \frac{q_s}{6\pi\eta a_s} \qquad (4\text{-}19)$$

where μ_s is the particle mobility in a solution which is easily measured using capillary electrophoresis. Therefore, the charge quantity carried by the protein

molecules, q_s, can be obtained.

4.3. Experimental

4.3.1 Materials

The dense cation and anion exchange membranes were purchased from Astom Corporation. Udel P3500NT polysulfone was provided by Solvay. Tris ($H_2NC(CH_2OH)_3$) was purchased from Bio-Rad. Bovine serum albumin (BSA), myoglobin (Mb) and polyvinylpyrrolidon (PVP) with different molecular weights (M_w) of 10k Da, 40k Da, 360k Da and 1300k Da were obtained from Sigma-Aldrich. The molecular weight (M_w) and pI values of BSA are 66.5k Da and 4.8, respectively, while the M_w and pI values of Mb are 17.8k Da and 6.8, respectively. Sodium hydroxide, iso-propanol (IPA), N-methyl-2-pyrrolidon (NMP), dichloromethane (DCM), phosphoric acid, chlorosulfonic acid, trifluoroacetic acid, acetic acid, phenolphthalein were of AR grade. Acetonitrile (ACN) was of GR grade.

4.3.2 Membrane fabrication

The procedure to synthesize a charged polymer with different extent of sulfonation has been described elsewhere [35]. A series of casting solutions containing the same polymer concentration (23 wt% 1:1 blend of PSf and SPSf) but different charge density were prepared to cast membranes A, B, C and D. The polymer solution was cast upon a non-woven cloth using a 250 μm blade; followed by immersing the as-cast membrane including the non-woven cloth into an iso-propanol coagulant bath for 15 min. The prepared membranes were then post-treated by 0.5M hydrochloride acid and fully rinsed

by deionized water.

4.3.2.1 Measurement of the electrical properties of membranes

A titration method was applied to measure the ion exchange capacity (IEC) of SPSf materials. 0.25 g SPSf powder or a piece of 5 cm x 5 cm membrane was dissolved in 10 ml NMP. The resultant solution was titrated using 0.1000 M NaOH with the aid of phenolphthalein as an indicator. An Anton-Paar streaming potential analyzer was utilized for the surface ζ-potential analysis on membrane surface. Auto-titration of a tris-acetic acid (0.02 M) buffer with pH 7.0 was performed using 0.5 M acetic acid (HAC) as titrant. A series of ζ-potential data were collected as a function of pH in the range of 4.7 to 7.0. The apparent ζ-potential data later was corrected by 0.1M KCl. To measure the electrical resistance, membranes A, B, C, D were immersed into 0.1 M KCl for 24 hrs, followed by sandwiching them in an electrical testing cell where the electrodes were mechanically tighten. The resistance was measured at 25°C through a multi-meter. The repeatabilities are good if the membranes are prepared under identical conditions.

4.3.2.2 Pore size distribution and porosity measurements

The pore size distributions of ion exchange membranes (IEMs) were characterized by the solute rejection method which has been described elsewhere in details [51]. Polyvinylpyrrolidon (PVP) with different M_w of 10 kDa, 40 kDa, 360 kDa and 1300 kDa were used to prepare a series of feed solutions containing 200 ppm of PVP. The total organic carbon (TOC) of the solutions at both the feed and permeate sides of the ion exchange membrane were measured using a Shimadzu TOC-5000A analyzer.

The porosity was measured by a weight reduction method. The free water on the membrane surface was removed using tissue paper before weighing the membrane. After that, the membrane was dried at 60°C under vacuum for 24 hrs and the mass of the dried membrane was obtained. The membrane porosity is determined using the followed eqn. (4-20):

$$porosity = \frac{(m_1 - m_2)/\rho_w}{(m_1 - m_2)/\rho_w + m_2/\rho_p} \qquad (4\text{-}20)$$

where m_1 and m_2 are the mass of the membrane before and after drying, respectively; ρ_w and ρ_p are the density of water and polymer, respectively.

4.3.2.3 Verification of the trans-membrane pH gradient

An energy dispersive X-ray (EDX) analysis was carried out to verify the existence of a pH gradient in the membrane. Since the employed buffer system is acetic acid – tris ($H_2NC(CH_2OH)_3$) pair, the nitrogen element in the tris molecules can be used as an indicator of the local tris concentration. Hence, the nitrogen distribution in the membrane cross-section was obtained via EDX analysis. If there is a gradient distribution of nitrogen in the membrane cross-section, it indicates the existence of a trans-membrane pH gradient.

A schematic of the IEM-FFIEF experimental set-up is shown in Fig. 4-1. Fresh membranes were mounted in the separation chamber as shown in Fig. 4-2 and buffers of different pH were introduced into the chambers. A 200 V electric power was applied to the IEM-FFIEF device for 40 min to equilibrate the membrane with the buffers. Upon

terminating the electrical supply, the membrane between chambers 2 & 3 was carefully and rapidly removed from the device. The membrane was immediately immersed in liquid nitrogen to freeze the liquid inside the membrane. Finally, the frozen membrane was placed in a freeze dryer till thoroughly dried. The sample for the EDX study was fractured in liquid nitrogen and observed by a scanning electron microscopy.

4.3.2.4 Protein separation

Following the aforementioned method in section 4.3.2.3, the set-up for protein separation was prepared, and the protein mixture was introduced into chamber 2. During the IEF period, the protein concentration in chamber 3 was monitored by ultraviolet (UV)-visible spectrophotometer (BIOCHROM LIBRA S32) with a kinetic function. The mobility and flux were determined by the rate of change of protein concentration with time in the permeate chamber. The real average mobility was given by eqn. (4-14). Since the FFIEF is a quasi-steady state process, the rate of change of protein concentration in the permeate chamber will be identical to that in the feed chamber i.e. $dC_i^f/dt = dC_i^p/dt$.

4.3.3 Analysis of proteins

A Beckman-Coulter P/ACE^{TM} MDQ capillary electrophoresis (CE) was used to measure the net charges carried by protein molecules in 0.02 M HAC-tris buffer solution (pH = 4.8). Through the measurement of mobility, the charge number can be calculated by eqn. (4-19). In our experiments, Mb and Hb were dissolved in 0.02 M HAC-tris buffer (pH = 4.8) and the mobilities were measured by a PDA (photodiode array) detector with varying wavelengths at 254 nm and 280 nm. The applied electrical field strength was 15 mA, and

a 60 cm long neutral capillary with an inner diameter of 75 μm was used. The purpose for measuring Hb at pH = 4.8 was to compare the accuracy of the CE method with published data [39].

A Hewlett Packard 1200 HPLC with a VWD detector was used to determine the protein purity in the respective chambers. The C18 mass SPEC column was purchased from Grace Vydac Inc. The gradient elution was comprised by two mobile phases contained A: 100% acetonitrile aqueous solution with 0.1% trifluoroacetic acid; B: 100% water with 0.1% trifluoroacetic acid.

4.4. Results and discussions

4.4.1 Confirmations of sulfonation and verification of pH gradient across the membrane

A FTIR Bio-Rad FTS3500 was used to characterize the sulfonated polysulfone structure at 1030 cm^{-1} and 1096 cm^{-1} [52]. Fig. 4-4 illustrates the FTIR spectra of polysulfone and sulfonated polysulfone membranes. Compared to PSf, the SPSf exhibits new transmittance peaks at around 1030 cm^{-1} and 1096 cm^{-1} which are representative of the sulfonated groups. Fig. 4-5 shows the signal strength of nitrogen across the membrane cross-section which was obtained from the EDX analysis. The observed profile is approximately exponential and this indicates the existence of a linear pH gradient across the membrane thickness because pH is defined as –log $[H^+]$. Therefore, the fundamentals of isoelectric focusing can be applied to the mass transfer study across the membrane in the IEM-FFIEF system.

On the other hand, the EDX results also qualitatively demonstrate that the SPSf membrane is the medium with dominant pH gradient in IEM-FFIEF, while the free flow buffers between two membranes can be regarded as pH homogenous. When identical SPSf membranes are applied in a series of buffers with different pHs, as shown in Fig. 4-2, different pH gradients with discontinuous pHs are formed in the individual membranes. Therefore, the SPSf- membrane are capable of performing the selective function of immobiline membranes without the need to incorporate chemical constituents with different pI values in fabrication process. Furthermore, since ion depletion does not pose a problem for the solid phase SPSf ion-exchange membrane, good reproducibility can be achieved even after long term operation and regeneration.

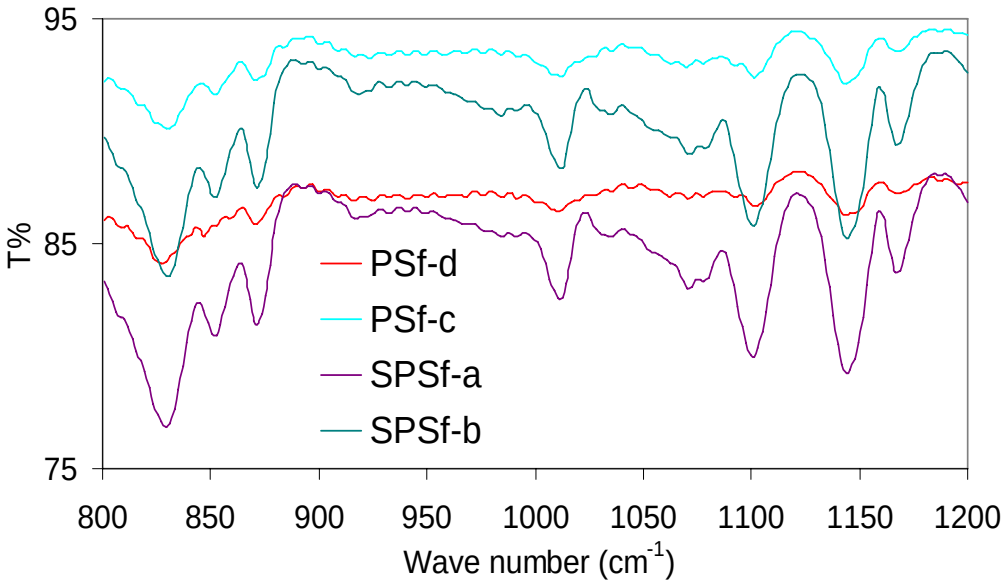

Fig. 4-4 FTIR spectra of polysulfone (PSf) and sulfonated polysulfone (SPSf)

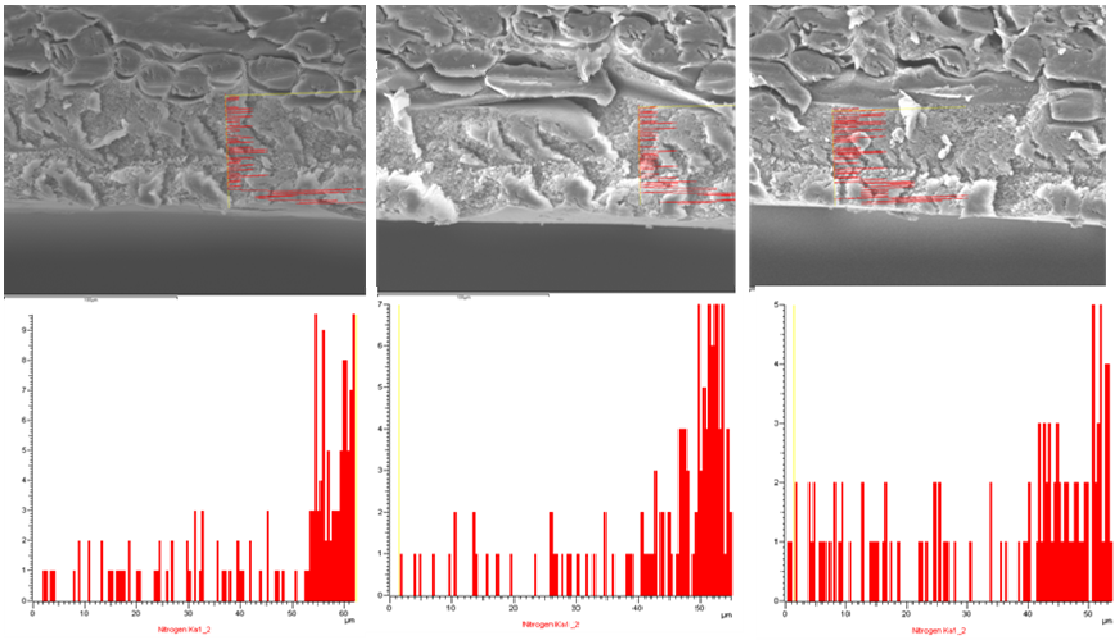

Fig. 4-5 pH gradient profiles across membrane cross-sections which is masured by the signal strength of nitrogen element.

4.4.2 Micro-structure characterizations of membranes

Fig. 4-6 a) shows the rejection vs. Stoke radius (r_s), from which the mean pore sizes of the membranes are taken as the r_s values at 50% rejection and the molecular weight cut-offs (MWCOs) are taken as the molecular weight at 90% rejection. It can be observed that the higher the charge density (IEC) of the membrane materials, the larger is the mean pore size. With reference to Table 4-1, the pure water flux (PWP) of the membrane becomes very small at low charge density. Fig. 4-6 b) exhibits the cumulative pore size distribution. Table 4-1 summarizes the measured porosity of various membranes and its trend is consistent with the conclusion of the higher charge density results in higher porosity, which is drawn from Fig. 4-6 b).

4.4.3 Physical properties of protein molecules

The molecular weights and dimensions of the related proteins are given in Table 4-2. The surface charge number (at pH = 4.8) was calculated according to the capillary electrophoresis results as discussed in Section 4.2.5.

4.4.4 Electrical properties of membranes

Table 4-1 summarizes the electrical properties of the SPSf membranes with varying degrees of sulfonation. Table 4-1 shows that a SPSf membrane with a higher IEC value exhibits a larger ζ-potential value. Fig. 4-7 displays the plot of ζ-potential vs. pH in the range of 4.7 ~ 7.0 for these membranes. The ζ-potential does not vary much between pH 4.8 and pH 6.8. This information is very important for the local zeta potential inside the membrane because ζ-potential in our experiments may not vary much in the pH range of 4.7 ~ 7.0 and can be assumed as constant during calculations.

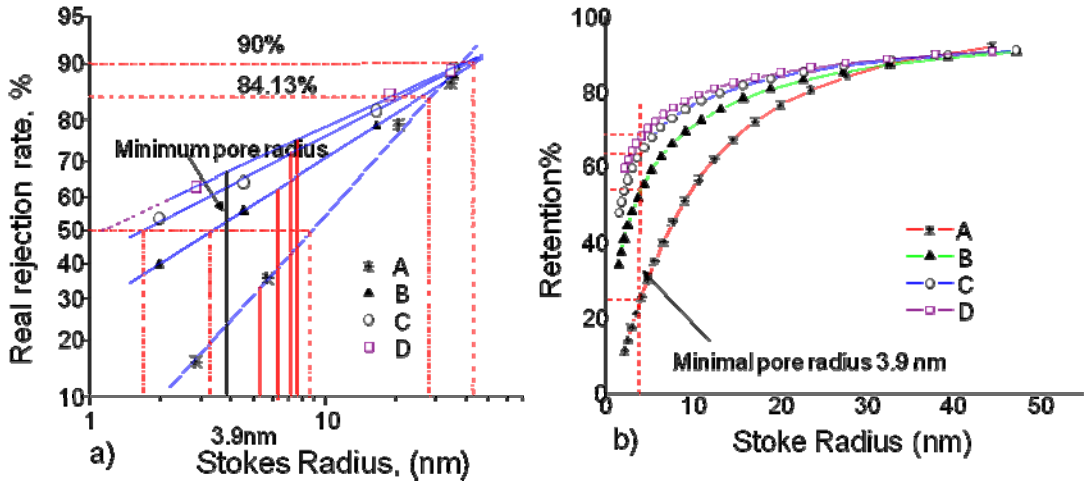

Fig. 4-6 Pore size distribution and effective pore size

a) is the real rejection vs. Stokes radius; b) is the cumulative pore size distribution.
in a), the red dot-dash lines at 50% are the mean pore sizes; the red solid lines are the effective pore size above the minimal pore radius R_e=3.9nm.
in b), the percentage of pores above the minimal pore radius (*Fp*) for A is 75%, for B is 54%, for C is 38% and for D is 32%.

As given by eqn. (4-17), the pore curvature dramatically affects the ζ_w of the pore wall. The ζ_w value cannot be represented accurately by the surface streaming potential if the membrane pore size and protein molecule size are of the same order of magnitude. To calculate ζ_w inside the pores, we need to have the surface ζ-potential and the "mean pore size". One point to highlight here is that our SPSf membranes compared to commercial membranes exhibit a relatively scattered pore size distribution and a considerable quantity of the pores is smaller than the protein molecular size. If these small pores are included as accessible mass transfer channels for the proteins in eqn. (4-1), (e.g. taking the pore size corresponding to 50% rejection as the mean pore size, as shown in Fig. 4-6), it will lead to a noticeable discrepancy from the experimental results. Therefore, to calculate the surface potential ζ_w inside the pores, the pore size distribution of different membranes, a "minimal pore radius R_e" and an "effective pore radius" must be defined. Using eqn. (4-1), a chart of relative mobility as a function of λ can be drawn as shown in Fig. 4-8. Since the effective pore radius for protein mass transfer must be bigger than a minimum pore size R_e which can allow the protein molecules to pass through, the calculation of the minimum pore size becomes necessary. To calculate the R_e, one must consider the condition of least overlapping of the double layers. In our system, the buffer solution has an initial ionic strength of $I = 0.02\ M$ and a protein molecule radius of $a = 2.1\ nm$. Thus, following eqn. (4-2), the calculated relative double layer thickness is $\kappa a = 1$. However the double layer thickness will gradually reduce in the IEF process due to the increased ionic strength arising from the pH adjustment. In our case, a rough evaluation of the total amount of buffer addition results in $\kappa a \approx 4$. Therefore, it is more reasonable to consider a range of double layer thickness from $\kappa a \approx 1$ to 4. According to Fig. 4-8, when $\kappa a = 1$ and $\gamma = -2$, $\upsilon = 0$ occurs at $\lambda = 0.40$. Based on the theoretical calculations by Ennis and

Zhang et al. [39], $\upsilon = 0$ occurs at $\lambda = 0.53$ if $\kappa a = 4$, $\gamma = -2$. Since a = 2.1 [53] nm and λ varies from 0.4 to 0.53, b is determined from the relation $b = a/\lambda$ as 3.9 ~ 5.25 nm. Therefore, with varying double layer thickness, R_e falls in the range 3.9 ~ 5.25 nm. As a conservative estimation, the smaller R_e value was adopted. Therefore, the effective pore radius is taken as the mid-value between the R_e of 3.9 nm and the Stoke's radius which corresponds to 100% rejection (red solid lines in Fig. 4-6).

Table 4-1 Membrane characterizations

Sample ID	A	B	C	D
Membrane IEC (meq/m^2)	7.50	6.385	5.5	4.71
$\zeta_{corrected}$-potential (mV)	-41.4	-30.5	-22.1	-16.3
ζ_w in pores (mV) κb (above r=3.9nm)	-62.2 5.4	-42.5 6.5	-29.8 7.2	-21.4 7.9
Electric resistance (MΩ)	6.55	8.45	9.35	10.68
d_p- MWCO (nm)	38.7	44	42.5	40.3
Mean pore size d_p (nm) R_e above d_p=7.8nm	17.70 25.32	6.54 28.8	3.4 32.10	2.3 34.90
PWP (m^3/m^2.sec)	5.792E-5	2.286E-5	7.078E-6	9.494E-7
F_p Percentage of Pores above d_p=7.8nm	75%	54%	38%	32%
Top layer thickness L (μm)	59.0	65.2	72.8	74.0
ε_p Porosity	0.685	0.650	0.620	0.585

Table 4-2 Protein molecule sizes and charge numbers

Protein	MW (Da)	Stocks radius [a]	ζ_S (mV) [b]	Charge number [c]	Number of amino-acid [d]	Effective valence [e]
Mb	17800	2.10	+19.4	+14.0	153	0.0915
Hb [f]	68000	3.13	+17.1	+20.4	574	0.0355
BSA	66000	3.55	0	0	0	0

[a.] the molecule size data come from ref. [53];
[b.] ζ_S which is determined by Capillary Electrophoresis as showing in eqn.(4-18);
[c.] the charge number were calculated from eqn.(4-19) by dividing elementary electric amount;
[d.] from ref. [54,55] http://en.wikipedia.org/wiki/
[e.] the effective valence z_i calculated from eqn.(4-8);
[f.] the purpose of measuring Hb is to confirm the accuracy of CE method by comparing the measured Hb z-potential with published data ref.[39].

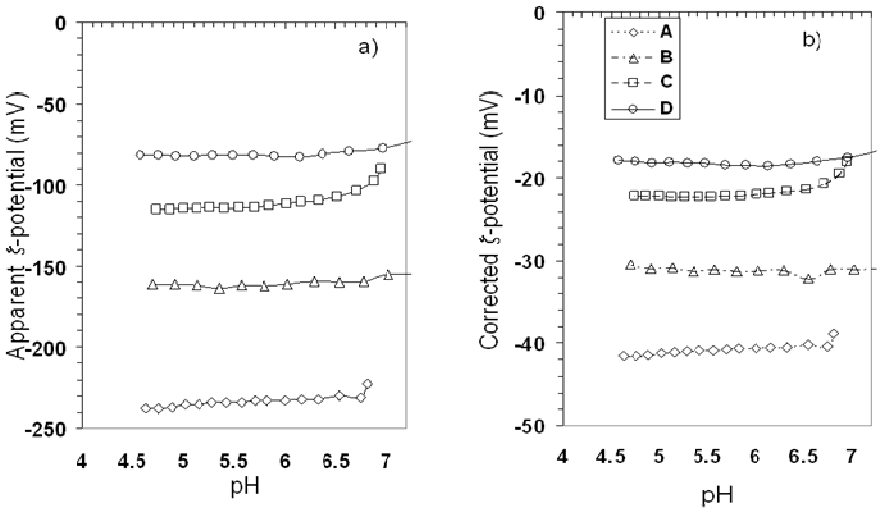

Fig. 4-7 ζ-potentials as a function of pH

where a) is apparent streaming potential without correction;
b) is the corrected streaming potential calculated from eqn.(4-16), where 0.1M KCl was used to correct the surface charging effect on ζ-potential.

As demonstrated in Fig. 4-6 (a) and Table 4-1, the mean pore size, *b* above 3.9 nm is significantly different from the mean pore size given at 50% of rejection. In Table 4-1, the corresponding κb values were given together with ζ_w values and the observed trend for these two parameters is D >C > B > A. With reference to Fig. 4-6 (b), the percentage of pores above 3.9 nm is in the order of A > B > C > D. This implies that for membrane D, the pore size distribution is broader and is dominated by the small pores. On the other hand, for membrane A, the pore size distribution is much narrower and is dominated by bigger pores. As shown in Table 4-1, the range of calculated κb satisfies the requirement of least overlapping of the double layer: κ(b-a) > 4~5 [37] which in turn validate the application of eqn. (4-1) in this study. Therefore, the discrepancy of eqn. (4-1) due to the largely scattered pore size distribution can be corrected by simply multiplying a correction factor F_p from Fig. 4-6 (b), where F_p is the percentage of pores above the minimum pore radius for a specific membrane.

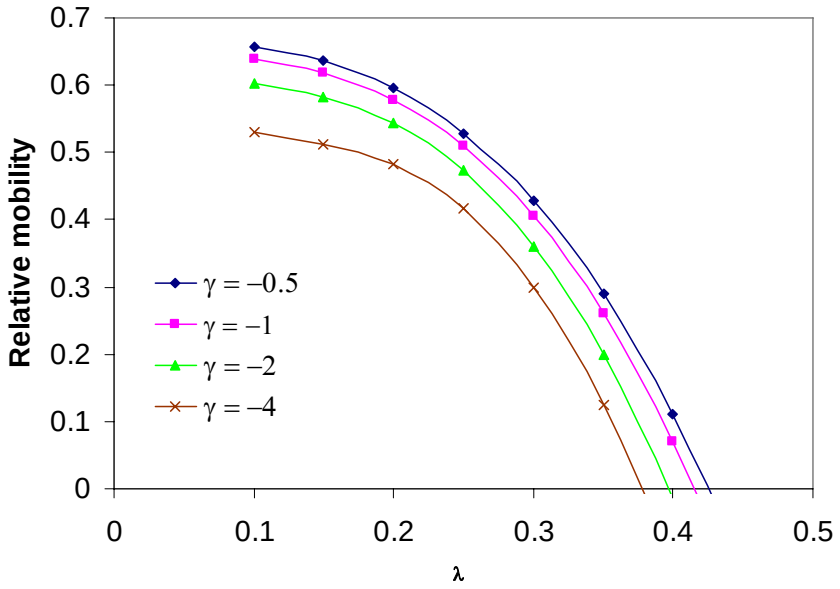

Fig. 4-8 Relative mobility of proteins as a function of λ calculated from the Ennis's theory for κa=1.

4.4.5 Comparison of theoretical and experimental velocities

For the theoretical calculation of relative mobility, one important parameter that needs to be known is the undisturbed electric field strength, E_∞. The E_∞ could be directly calculated from eqn. (4-11). The disturbed electric field strength E_∞' is necessary for the calculation of real velocity. Table 4-3 summarizes the measured data required for electric field strength calculations. The calculated velocities and mobilities from Ennis's theory are listed in Table 4-4, where ζ_s in eqn. (4-1) is an average value over the membrane cross-section which equals to $0.5 \times \zeta_s^f$. The influence of heterogeneous pore size distribution on the mass transfer of protein molecules has been considered for relative mobility calculation by including the correction factors F_p and porosity into eqn. (4-1). The real mobility in eqn. (4-14) can be calculated through the determination of dC_i^f/dt (see Fig. 4-9) from the kinetic UV-Vis results. The experimentally determined mobilities and velocities are listed in Table 4-4. The comparisons of mobilities and velocities vs. ζ_w are demonstrated in Figs. 4-10 and 4-11, respectively.

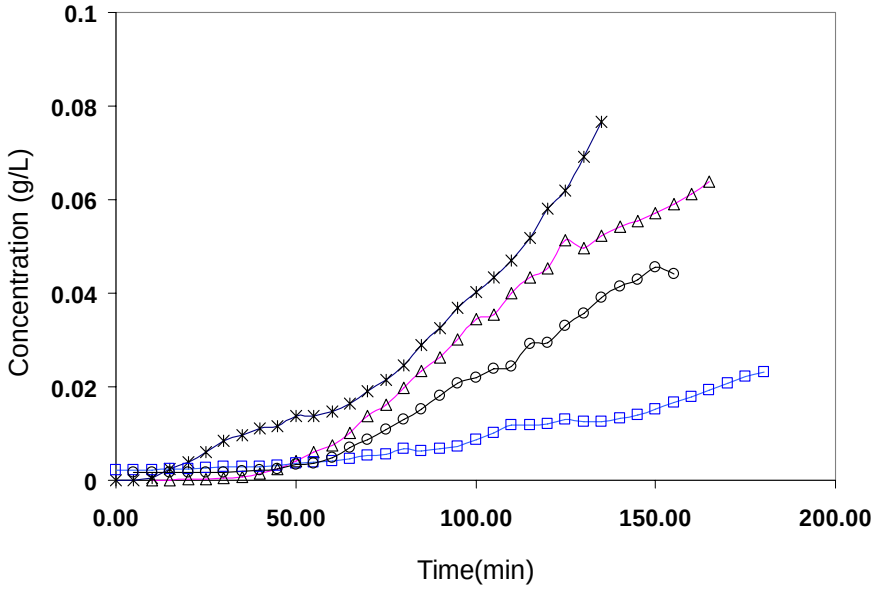

Fig. 4-9 dC/dt monitored by UV-Vis spectrometer kinetic function

As shown in Fig. 4-10, both the experimental and theoretical mobilities exhibit linear relationships with ζ_w, and the two trend lines are amazingly close if we use $\mu = \upsilon_{theo} / E_\infty'$ to calculate the μ_{theo}. On the contrary, if $\mu = \upsilon_{theo} / E_\infty$ is applied in the μ_{theo}'s calculation, the μ_{theo} will be underestimated compared with the experimental values as shown in Fig. 4-10.

Table 4-3 The calculation of undisturbed electric field E_∞ and disturbed electric field E_∞'

Parameters	A	B	C	D
Voltage applied	200	200	200	200
Current (mA) [b]	311	195	124	84
Overall Resistance	643.1	1025.6	1612.9	2380.9
κ_0 ($mS.m^{-1}$) [d]	23.63	23.63	23.63	23.63
E_∞ (mV) [e]	4478.8	2959.5	1973.0	1416.5
L (μm) [f]	96	107	129	140
E_∞' (mV) [g]	2637.8	1812.9	1226.2	879.3

[a] is applied constant voltage;
[b] is current measured from DC power supply;
[c] is electric resistance calculated from Ohm's law;
[d] is the conductivity of the fluid in the pore, given by $\kappa_0=\lambda_0 * l/A$, λ_0 is original conductance of buffer at pH=4.8, measured value is 0.465ms. l is the length between two electrodes, l=0.218m, A is the cross-section area of every chamber; A=0.00429m^2.
[e] is given by eqn.(4-11);
[f] is given by t+0.30* L_c, L_c is non-woven cloth thickness, L_c=93μm; t is the measured SEM thickness.
[g] is given by eqn.(4-13).

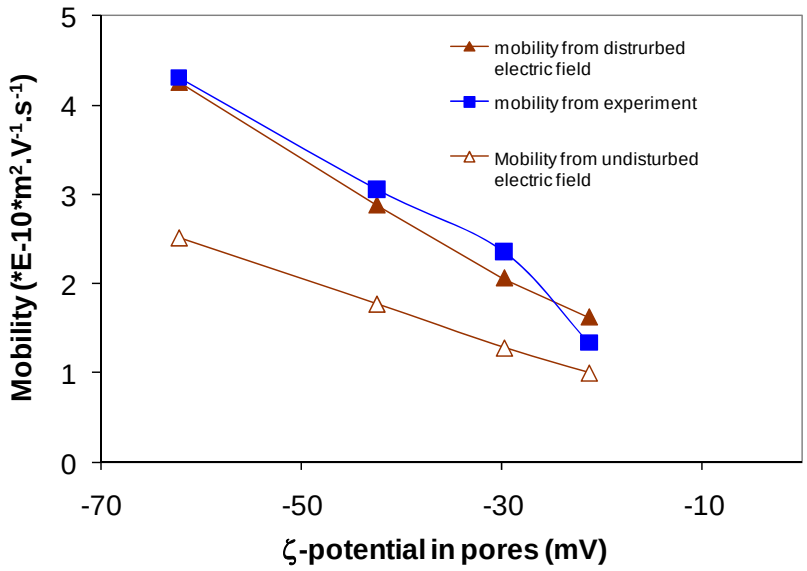

Fig. 4-10 Comparison of mobilities from experiments and theoretical predictions

This is due to the fact that only the E_{∞}' contributes to the migration of protein molecules; while a part of energy, E_0, is the energy consumption for overcoming the electrostatic effect. On the other hand, based on Einstein's equation, the linearity in Fig.4-10 implies that the diffusivity, D_{im} is a linear function of ζ_w in the charged cylindrical pore. Thus, the mass transfer can be improved by increasing the membrane IEC value. This phenomenon can be explained by the Ohm's law. Since the mass transfer of protein can be regarded as a process of charge migration through a conductive substance (membrane), a lower resistance leads to higher current electric field under the same applied voltage. The resistance data in Tables 4-1 and 4-2 clearly shows that the lower resistance is a consequence of the higher IEC value. The higher IEC value in turn leads to higher charge migration.

With reference to Fig. 4-11, the trend line for the theoretical prediction of velocity vs. ζ_w even more surprisingly overlaps with the experimentally measured results after inserting

the F_p and porosity in eqn.(4-1). On the contrary, if we neglect the F_p and porosity, there is a distinct deviation between the theoretical and experimental velocities. In fact, the results obtained are in reverse direction as shown in Fig. 4-11 and Table 4-5. This observation indicates that the theoretical prediction proposed by Ennis and Zhang et al. (eqn.(4-1)) is only sufficient to depict one particle and one pore electrophoresis through a membrane. In other words, the pore size distribution and the effective pore size play crucial roles in the application of eqn.(4-1) in the heterogeneous membrane. This is because the pore size distribution and minimal effective pore size R_e determine the stereo-hindrance of the membrane structure. The stereo-hindrance of the membrane structure dramatically influences the translation velocity and should be included in eqn. (4-1). The pore size distribution and the effective pore size can simplify the complicated pores population into a statistical model, which can represent the membrane characteristics and be applied in a theoretical model based on a single pore.

Table 4-4 Comparison of the velocities from experiments and from theoretical prediction

Mem ID	dC/dt [a] ($g.L^{-1}.s^{-1}$)	μ from expt [b] ($m^2.V^{-1}.s^{-1}$)	u from expt [c] ($m.s^{-1}$)	μ from theory [d]	u from theory [e,f]
A	1.26E-5	4.31E-10	1.14E-6	4.02E-10	1.12E-6
B	8.94E-6	3.06E-10	5.54E-7	2.82E-10	5.23E-7
C	6.90E-6	2.36E-10	2.89E-7	1.95E-10	2.53E-7
D	2.80E-6	1.34E-10	8.41E-8	1.41E-10	1.42E-7

a. The concentration changing rate calculated from Fig.4-9.
b. In eqn.(4-14),the initial feed concentration is 0.134g/L, and κ_w'/i is 22.9 $V^{-1}.m^{-1}$; the κ_w is given by $\kappa_w=i/V/L_e$.
c. The real velocities calculated by multiplying E_∞' with measured motilities.

d. The mobility calculated from theoretical velocity divided by E_∞ .
e. The theoretical velocity calculated by eqn.(4-1) multiplying the percentage of pores above d_p=7.8nm.
f. The ζ_s in eqn.(4-1) is a average value given by $\zeta_s = 0.5\zeta_s^f$

Table 4-5 Comparison of the relative velocities

Different approaches	A	B	C	D
Relative velocity (mean pore size above r=3.9nm)	0.5882	0.5756	0.5931	0.5889
Relative velocity (mean pore size at 50% in Fig.6)	0.4603	-0.0255	-2.078	-6.932

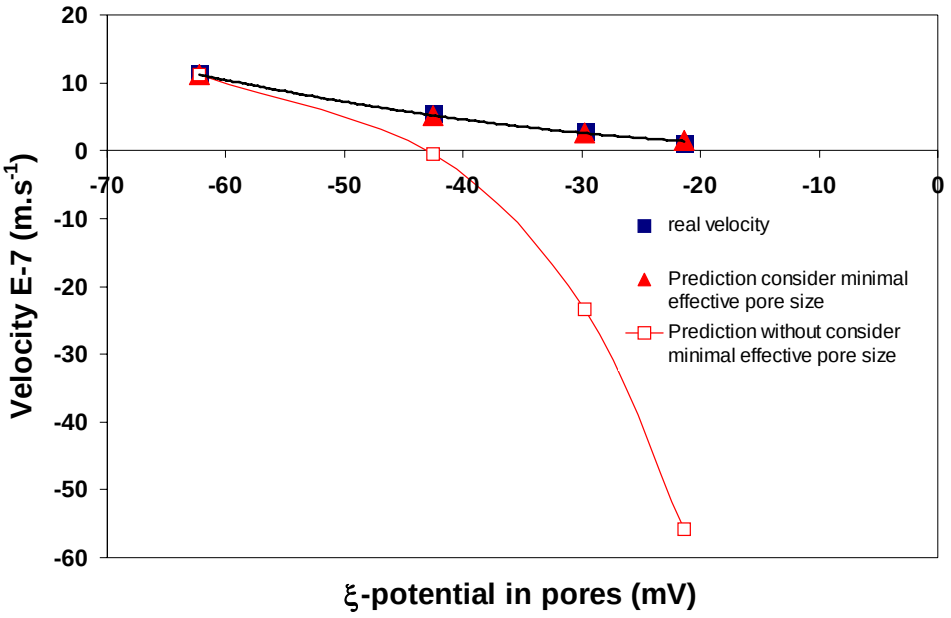

Fig. 4-11 Comparison of velocities from experiments and theoretical predictions

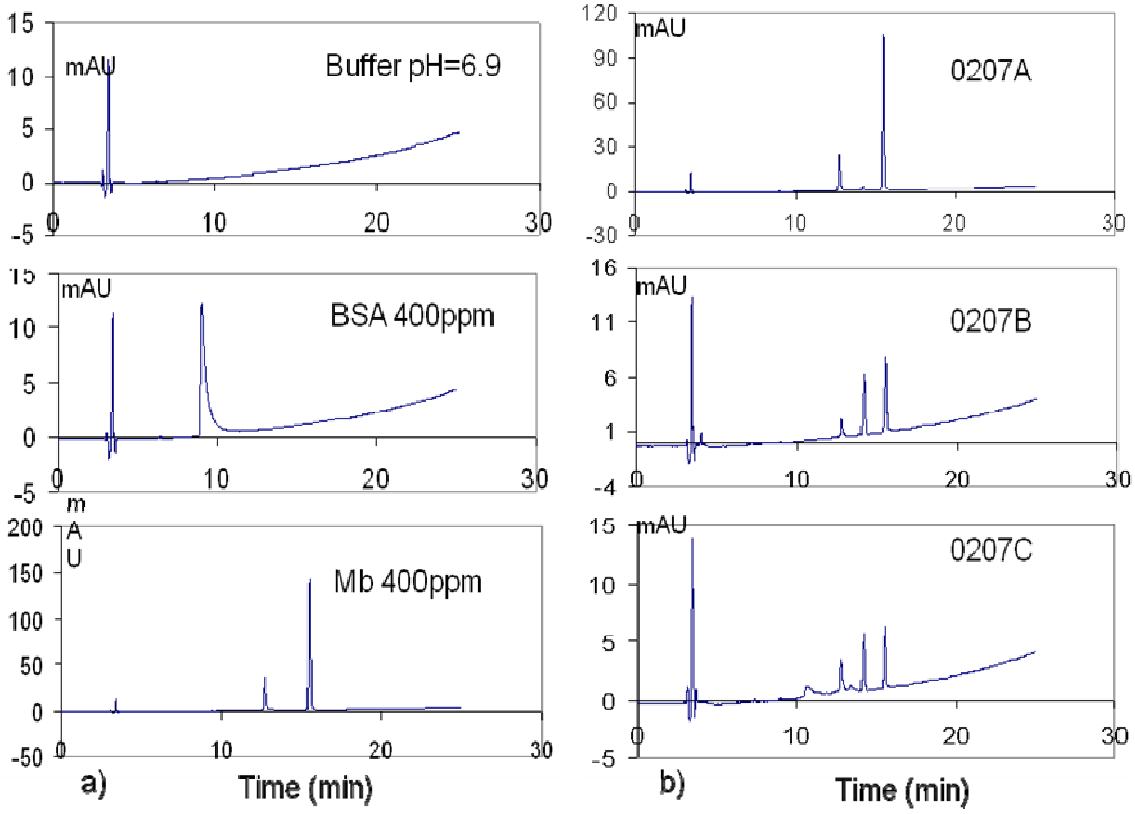

Fig.4-12 The HPLC results of protein separation

a) HPLC standards' retention time; b) IEM-FFIEF performance results tested by HPLC

4.4.6 Protein separation experiments

HPLC analysis results for the standard pure proteins and samples collected from permeates are given in Figs. 4-12 a) and 4-12 b), respectively. Referring to Fig. 4-12 a), the retention time of tris, BSA, and Mb are 3.5 min, 9.5 ~10.5 min and 12.5~15.2 min, respectively. It is obvious that: 1) there was no BSA signal in the permeate sample when membranes A and B were applied for the separation of the protein mixture (BSA + Mb); 2) a small BSA signal presented in the permeate sample when membrane C was applied; 3) the Mb signal for membrane A is much higher than that of membranes B and C. 4)

three peaks exhibits in permeate samples are due to the fact that protein molecules carrying different number of charges (different polarity) appeared in permeate chamber. The HPLC results implies that high purity Mb can be obtained in permeate chamber with high flux; an infinity in separation factor can be achieved by increasing the membrane IEC value, where the separation factor can be expressed in eqn. (4-21), indicating the extent of separation is extremely high:

$$Separation\ factor = \frac{(C_{Mb}/C_{BSA})_{permeate}}{(C_{Mb}/C_{BSA})_{feed}} \qquad (4\text{-}21)$$

Therefore, a comparison of HPLC results reveals that the Mb product with both high concentration and high purity can be obtained through tailoring the membrane surface charge and pore size for the FFIEF process.

4.5 Conclusions

The following conclusions can be drawn from this study:

1) For the first time, by means of SEM-EDX results, we have proven that a pH gradient exists in the membrane cross-section when the IEM-FFIEF process is in operation. Thus, the IEF theory is applicable not only in conventional macro-sized gel media but also in the micro-scale range of the membrane cross section.
2) We have derived and quantitatively calculated the minimum electrical consumption (interaction potential) for Mb, E_0, and thus the disturbed applied electric field, E_∞' through measurable parameters. This in turn verifies the applicability of the Ennis's equation.
3) We have experimentally proven that Ennis and Zhang's et al. theoretical prediction for protein velocity and mobility through a porous membrane is applicable in the ion-

exchange membrane partitioned free-flow isoelectric focusing system (IEM-FFIEF) after considering the effects of pore size distribution and effects of disturbed electric field.

4) The charge properties of the membrane surface, in particular the IEC value (indicated by ζ-potential), plays a major role in determining the membrane's pore size, porosity, mobility and velocity for ion exchange membrane mediated electrophoresis. Comparing to the uncharged polymer solution, the charging sites on modified polymer chains have dramatically changed the phase inversion process and formed different membrane structures.
5) For the separation of BSA and Mb, permeates with high protein purity can be achieved under stable pH gradient.

4.6 References:

1. S. Galier and H.R. Balmann, Study of the mass transfer phenomena involved in an electrophoretic membrane contactor, J. Membr. Sci. 194 (2001) 117.

2. F.G. Smith III and W.M. Deen, Electrostatic double layer interactions for spherical colloids in cylindrical pores, J. Colloid Interf. Sci. 78 (1980) 444.

3. F.G. Smith III and W.M. Deen, Electrostatic effects on the partitioning of spherical colloids between dilute bulk solution and cylindrical pores, J. Colloid Interf. Sci. 91 (1993) 571.

4. D.B. Burns and A.L. Zydney, Contributions to electrostatic interactions on protein transport in membrane system, AIChE J. 47 (2001) 1101.

5. N.S. Pujar and A.L. Zydney, Electrostatic and electrokinetic interactions during protein transport through narrow pore membranes, Ind. Eng. Chem. Res. 33 (1994) 2473.

6. R. van Reis and A.L. Zydney, Membrane separations in biotechnology, Curr. Opin. Biotech. 12 (2001) 208.

7. A.L. Zydney and N.S. Pujar, Protein transport through porous membranes: effects of colloidal interactions, Colloid Surface A. 138 (1998) 133.

[8] B. Cheang and A.L. Zydney, Separation of α-lactalbumin and β-lactoglobulin using membrane ultrafiltration, Biotechnol. Bioeng. 83 (2003) 201.

[9] A.L. Zydney, Protein separations using membrane filtration: new opportunities for whey fractionation, Int. Dairy J. 8 (1998) 243.

[10] R.H.C.M. van Einjdhoven, S. Saksena and A.L. Zydney, Protein fractionation using electrostatic interactions in membrane filtration, Biotechnol. Bioeng. 48 (1995) 406.

[11] E. Quenneville and M.D. Buschmann, A transport model of electrolyte convection through a charged membrane predicts generation of net charge at membrane/electrolyte interfaces, J. Membr. Sci. 265 (2005) 60.

[12] D.B. Rylatt, M. Napoli, D. Ogle, A Gilbert, S. Lim and C.H. Nair, Electrophoretic transfer of proteins across polyacrylamide membranes, J. Chromato. A. 865 (1999) 145.

[13] M. Bier, Recycling isoelectric focusing and isotachophoresis, Electrophoresis. 19 (1998) 1057.

[14] W. Pauli, Untersuchungen elektrolytfreien, wasserloeslichen proteinkoerper, Biochem. Z. 152 (1924) 355.

[15] A. Tiselius, A new appratus for electrophoretic analysis of colloidal mixture, Trans. Faraday Soc. 33 (1937) 524.

[16] A. Polson, Multi-membrane electrodecantation and its application to isolation and purification of proteins and viruses, Biochim. Biophy. Acta. 11 (1953) 315.

[17] M. Bier, (Edited) Electrophoresis, Academic Press, New York 1959, p263.

[18] P. Wenger and P. Javet, Isoelectric focusing using non-amphoteric buffers in free solution: I. determination of stable concentration profiles, J. Biochem. Bioph. Meth. 13 (1986) 259.

[19] P. Wenger and P. Javet, Isoelectric focusing using non-amphoteric buffers in free solution: II. apparatus and measures of pH stability, J. Biochem. Bioph. Meth. 13 (1986) 275.

[20] P. Wenger and P. Javet, Isoelectric focusing using non-amphoteric buffers in free solution: III. Separation of amino acid, J. Biochem. Bioph. Meth. 13 (1986) 289.

[21] C. Tragas and J. Pawliszyn, On-line coupling of high performance gel filtration chromatography with imaged capillary isoelectric focusing using a membrane interface, Electrophoresis. 21 (2000) 227.

[22] M.P. Bellini and K.L. Manchester, Synthesis of zwitterionic acrylic acid buffers for isoelectric focusing in immobilized pH gradients, Electrophoresis, 19 (1998)1590.

[23] P.G. Righetti and E. Giaffreda, Immobilized buffer for isoelectric focusing: from

gradient gels to membranes, Electrophoresis 15 (1994) 1040.

[24.] P.G. Righetti, E. Wenisch, and M. Faupel, Preparative protein purification in a multi-compartment electrolyzer with Immobiline membranes, J. Chromatogr. 475 (1989) 293.

[25.] P.G. Righetti, E. Wenisch, A. Jungbauer, H. Katinger and M. Faupel, Preparative purification of human monoclonal antibody isoforms in a multicompartment electrolyzer with Immobiline membranes, J. Chromatogr. 500 (1990) 681.

[26.] B. Herbert and P.G. Righetti, A turning point in proteome analysis: sample pre-fractionation via multicompartment electrolyzers with isoelectric membranes, Electrophoresis 21 (2000) 3639.

[27.] F. Fortis, P. Girot, O. Brieau, E. Boschetti, A. Castagna, and P.G. Righetti, Amphoteric, buffering chromatographic beads for proteome pre-fractionation. I: theoretical model. proteomics 5 (2005) 620.

[28.] F. Fortis, P. Girot, O. Brieau, A. Castagna, P.G. Righetti and E. Boschetti, Isoelectric beads for proteome pre-fractionation. II: Experimental evaluation in a multicompartment electrolyzer. Proteomics 5 (2005) 629.

[29.] S. Cherkaoui, P. Zell, and P. Javet, Characterization of immobiline membranes for application in a multicompartment electrolyzer, J. Biochem. Biophy. Meth. 25 (1992) 61.

[30.] A. Ayala, J. Parrado, and A. Marchado, Use of Rotofor preparative isoelectric focusing cell in protein purification procedure, Appl. Biochem. Biotech. 69 (1998) 11.

[31.] M. Bier, G.E. Twitty and J.E. Sloan, Recycling isoelectric focusing and isotachophoresis, J. Chromoto. 470 (1989) 369.

[32.] M. Bier, (Edited) Membrane processes in industry and biomedicine, Plenum Publishing, New York 1971, p233

[33.] M. Bier, N. Egen, N, in: H. Haglund, J.G. Westerfeld, J.T. Ball, (Eds.), Electrofocusing, Elsevier North Holland, New York 1979.

[34.] M. Bier, N.B. Egen, T.T. Allgyer, G. E. Twitty and R.A. Mosher, in: E. Gross, J. Meienhofer, Peptides: Structure and Biological Function, Pierce Chemical Co., Rockford, IL 1979, pp. 79-89.

[35.] J.H. Cheng, Y. Li, T.S. Chung, S.B. Chen and W.B. Krantz, High-performance protein separation by ion exchange membrane partitioned free-flow isoelectric focusing system, Chem. Eng. Sci. 63 (2008) 2241.

[36.] J.H. Cheng, Y.C. Xiao, C.M. Wu, T.S. Chung, Chemical modification of P84 polyimide as anion-exchange membranes in free-flow isoelectric focusing system for protein separation, submitted to J. Membr. Sci.

[37.] H.J. Keh and J.L. Anderson, Boundary effects on electrophoretic motion of colloidal spheres, J. Fluid. Mech. 153 (1985) 417.

[38.] J. Ennis and J.L Anderson, Boundary effects on electrophoretic motion of spherical particles for thick double layer and low zeta potential, J. Colloid Interf. Sci. 185 (1997) 497.

[39.] J. Ennis, H. Zhang, G. Steven, J. Perera and S. Carnie, Mobility of protein through a porous membrane, J. Membr. Sci. 119 (1996) 47.

[40.] H.J. Keh and J.Y. Chiou, Electrophoresis of colloidal sphere in a circular cylindrical pore, AIChE J. 42 (1996) 1397.

[41.] H.J. Keh and T.H. Hsieh, Electrophoresis of colloidal sphere in a spherical cavity with arbitrary zeta-potential distributions and arbitrary double layer thickness, Langmuir. 24 (2008) 390.

[42.] H. Svensson, Isoelectric focusing, analysis and characterization of ampholytes in natural pH gradient I, Acta. Chem. Scand. 15 (1961) 325.

[43.] R.A. Mosher and D.A. Saville, W. Thormann, The dynamics of electrophoresis, chapter 7, VCH publishers, New York, 1992. p172.

[44.] R.J. Hunter, Introduction to modern colloid science, Melbourne, 1993, p205~206.

[45.] J.P. Hsu, Z.S. Chen, M.H. Ku, L.H. Yeh, Effect of charged boundary on electrophoresis: sphere in spherical cavity at arbitrary potential and double-layer thickness, J. Colloid Interf. Sci. 314 (2007) 256.

[46.] J.P. Hsu and Z.S. Chen, Electrophoresis of a Sphere along the Axis of a Cylindrical Pore: Effects of Double-Layer Polarization and Electroosmotic Flow, Langmuir 23 (2007) 6198.

[47.] M. D. Afonso, Surface charge on loose nanofiltration membranes, Desalination. 191 (2006) 262.

[48.] J. Schaep and C. Vandecasteele, Evaluating the charge of nanofiltration membrane, J. Membr. Sci. 188 (2001) 129.

[49.] C.J. Chuang, W.Y. Tao and K.L. Tung, Determining zeta potential of membrane pores by electro-osmosis and streaming potential methods, 2001 Symposium on Transport Phenomena and Applications, Taipei, Taiwan, pp.249.

[50.] P.C. Hiemenz and R. Rajagopalan, Principles of colloid and surface chemistry, Marcel Dekker, 1997.

[51.] K.H. Youm and W.S. Kim, Prediction of intrinsic pore properties of ultra-filtration membrane by solute rejection curves: effects of operating conditions on pore properties, J. Chem. Eng. Jpn. 24 (1991) 1.

[52] J.K. Fang, H.C. Chiu, J.W. Wu, S.Y. Suen, Preparation of polysulfone base cation exchange membranes and their application in protein separation with a plate-and-frame module. Reactive & Functional Polymer 59 (2004) 171.

[53] H.H.P. Yiu, C. H. Botting, N.P. Botting and P.A. Wright, Size selective protein adsorption on thiol-functionalised SBA-15 mesoporous molecular sieve, Phys. Chem. Chem. Phys. 3 (2001) 2983.

[54] http://en.wikipedia.org/wiki/Myoglobin, 2007

[55] http://en.wikipedia.org/wiki/hemoglobin, 2007

4.7 Appendix

According to Ennis and Anderson's work [38], the numerous functions given in this paper can be defined as:

$$f(x) \approx \frac{2x^3 + 51x^2 + 242x + 208}{2x^3 + 57x^2 + 363x + 312}$$

where the rational approximant is within 0.2% for all ***x***.

$$L(x) \approx \frac{x^4 + 14x^3 + 58x^2 + 112x + 84}{x^4 + 14x^3 + 42x^2}$$

where the rational approximant is within 0.06% for all ***x***.

CHAPTER 5 SELF-SHARPENING PHENOMENON ARISEN BY ION-EXCHANGE MEMBRANES IN MULTI-COMPARTMENT FREE-FLOW ISOELECTRIC FOCUSING (IEM-FFIEF)

5.1. Introduction

The ever-increasing demands for biomolecular medicine have made the separation technology receiving significant attention from both academia and industry. Since 1970s, tremendous attentions have been given to protein separation worldwide and important progresses have been made, such as protein separation by membrane ultrafiltration [1, 2, 3], microfiltration, diafiltration [4]. Factors influencing membrane based protein separation processes have been studied [5, 6, 7, 8]. After 1980, multi-compartment electrophoresis has been proven as an effective tool for the separation of multi-component charged mixtures, thereafter it has gained worldwide acceptance [9, 10]. Meanwhile, multi-compartment electrophoresis in some literatures is referred as free-flow isoelectric focusing (FFIEF) [11, 12, 13]. This is due to the fact that most of these devices are operated without gel assistance, but with free solutions partitioned by a series of sieving, such as immobiline (a kind of pH imbed gel-like membrane) or solid phase porous polymer membranes. Under an applied electric field, with these partitions in between chambers, charged biomolecules can be transferred to different chambers according to their values of isoelectric points (pI). As a consequence, membrane based FFIEF instruments have been rapidly developed; for instance: Proteome Systems (Proteome Systems Inc., USA), BD™ free-flow electrophoresis (FFE) system (Becton-Dickinson Inc., USA), Gradiflow™ (Gradipore Ltd, Australia) and Bio-Rad® (Bio-Rad Inc., USA). The multi-compartment electrophoresis of the Proteome Systems is partitioned by pH immobilized membranes – immobiline has a

significant self-sharpening separation due to its imbedded pH. Nevertheless, many researchers have proven that the immobiline membranes are weak in terms of mechanical strength and the immobilized pH can be easily depleted after few hours operation [14,15,16].

The other example of free flow isoelectric focusing is the BD™ FFE system which performs the separation within a chamber between two parallel electrodes. The feed sample is introduced in this chamber with a laminar flow. After a period of operation under electric fields, the feed components will be separated following their natural pI values in the downstream [17,18]. However, the current design may have difficulties in scaling-up to meet the high through-put demand because of the laminar flow constraint. The Gradiflow ™ apparatus is another type of FFIEF. With the aid of three partitioned membranes and an adequate pH buffer in the electrode chambers and separation chambers, the proteins are separated into different chambers by size discrimination. However, the individual samples from different chambers need further separation by IEF strip or 2D-electrophoresis. The published data indicate that the Gradiflow's technology combines both size selective means and pI difference to distinguish various components, and the feed solution was split into few chambers according to their natural pI values [19,20].

So far Bio-Rad Rotofor has achieved greater success and is broadly applied in lab scale protein purification. It has 20 chambers separated by nylon screens between two electrode chambers. Through this design the convective flow between chambers is reduced and the protein production becomes convenient. Many studies have been conducted to discuss its advantages and disadvantages. The most important advantage of Rotofor is its multi-components which can be split simultaneously [21,22]. However, as pointed out by Ayala and his associates that the Rotofor can not focus proteins sharply [23]. Namely, a single

protein component will be distributed in a series of neighbored chambers, and in some chambers, different components maybe overlapped each other if there are no significant difference of pI values between two components.

After analyzing those advantages and disadvantages of the aforementioned instruments, we propose to use porous anion-exchange membranes to replace the immobiline membrane commonly used in FFIEF for protein purification in order to meet the industrial demands of: easier scaling-up, larger volume, enhanced flux, higher purity and self-sharpening separation. The self-sharpening phenomenon refers to the simultaneous purification occurring in individual chambers. The proposed scheme, if successful, is extremely attractive for the separation of multi-component broths because of its high resolution. Previous studies showed that both the pI values and ion-exchange capacity (IEC) of immobiline membranes are crucial for a self-sharpening IEF process [[14]]. Therefore, the solid phase ion-exchange membranes must have similar characteristics due to its high IEC value in a confined space, but with much stronger mechanical strengths. It has been proven that a pH gradient exists across the ion-exchange membranes used in FFIEF along the electric field [[24],[25]]. In other words, a series of flat pH values (in chambers) and positive pH gradients (cross the partitioned membranes) queue up along the electric field direction in an increasing order of pH. The existence of pH gradient facilitates mass transfer across the membrane and self-sharpens proteins in specific chambers.

Basically, the IEM-FFIEF technology was developed by manipulating the net charge of proteins and their migrations in different media under electric fields. A given protein molecule will be concentrated at its isoelectric point, and in electrophoresis scope, this is

termed as “focusing” .Our previous studies revealed that the IEC value dramatically influences the flux of mass transfer across the membranes [25], and the performance (i.e., protein purity and concentration of permeate) of ion-exchange membranes with high IEC values is significantly higher than those lower ones. However, the effects of IEC value on the self-sharpening phenomenon have not yet been clearly revealed. Therefore, the objective of this study is to investigate the function of ion-exchange membranes in FFIEF, particularly the phenomenon of self-sharpening by using a 3-component protein mixture consisting of bovine serum albumin, myoglobin and lysozyme. A series of anion-exchange membranes with different IEC values are prepared through the quaternary amination of brominated poly(2,6-dimethyl-1,4-phenylene oxide) (BPPO). The FFIEF performance tests are compared in a home-made ten-chamber FFIEF system.

5.2. Experimental

5.2.1 Materials

The dense cation-exchange membrane (CEM) and dense anion-exchange membrane (AHA) were purchased from Astom Corporation, Japan. Brominated poly(2,6-dimethyl-1,4-phenylene oxide) (BPPO) with 90% bromination rate was obtained from Shandong Tianyi Imp. & Exp. Co., Ltd. China. We selected the BPPO as the polymer to be modified, is due to the fact that benzyl type BPPO is easy to be modified by amines. Myoglobin (Mb), lysozyme (Lys) and bovine serum albumin (BSA) were procured from Sigma-Aldrich, Singapore. The electrophoresis grade ampholyte (pH 3-10) was obtained from Bio-Rad, Singapore. The molecular weight (Mw) and pI value of BSA are 66.5k Da and 4.8, respectively; Mw and pI value of Mb are 17k Da and 7.0, respectively; while Mw and pI value of Lys are 14.4 k Da and 11.0, respectively. Udel P3500NT polysulfone (PSf)

was provided by Solvay, German. Tetrahydrofurane (THF) and triethylamine (TEA) were from Fisher sientific, UK; *N*-methyl-2-pyrrolidon (NMP), was from Panreac E.U.; isopropanol (IPA) was from Schedelco Pte.Ltd. Singapore; methanol, phosphoric acid (H_3PO4), sodium hydroxide (NaOH) trifluoroacetic acid (TFA), and potassium chloride (KCl) were all in analytical grade (AR) and purchased from Merck Singapore. Acetonitrile (ACN) was from Tedia Compony Inc. USA. For high performance liquid chromatography (HPLC) analyses, GR (Guaranteed reagent) grade ACN and water were used, while for other occasions, deionized water (electrical resistance R > 18.2 MΩ) was used. The ultrapure water used for HPLC was produced by "Milli-Q plus 185" pure water system in our lab.

5.2.2 Preparation of membranes

Normally there are two routes for the bromination of PPO (10 w/w % in chlorobenzene). As shown in Fig.5-1, the aryl type bromination is dominant at a temperature below 110 °C, while the benzyl type bromination becomes dominant when temperature reaches 130 °C [[26]]. For the induction of quarternary amination in the PPO polymer, the later case would be an easy and effective methodology by substitution reactions. Thus BPPO used in this study is specified as a benzyl type brominated PPO.

To prepare positively charged membranes, the following procedures were applied to BPPO: 1) 10% of BPPO and 10% of PSf were dissolved in 99.9% THF and then filtered by a 300-mesh sieving. 2) For different amination rates, 20% of triethylamine (TEA in THF) solutions were added into the BPPO-THF solution according to the ratios of TEA: BPPO in 1.0, 1.4 and 1.8, individually. 3) After 20 min agitation under ambient

temperature, the solutions were quenched in 99% methanol and then the polymers were precipitated. 4) Finally the aminated PPO (APPO) polymers with different amination rates were fully washed by methanol four times followed by drying in a vacuum oven (NSV9090, OILTEX Pte. Ltd., Singapore) under ambient temperature. The purpose of adding PSf in BPPO solution is to enhance the mechanical strength of the membrane.

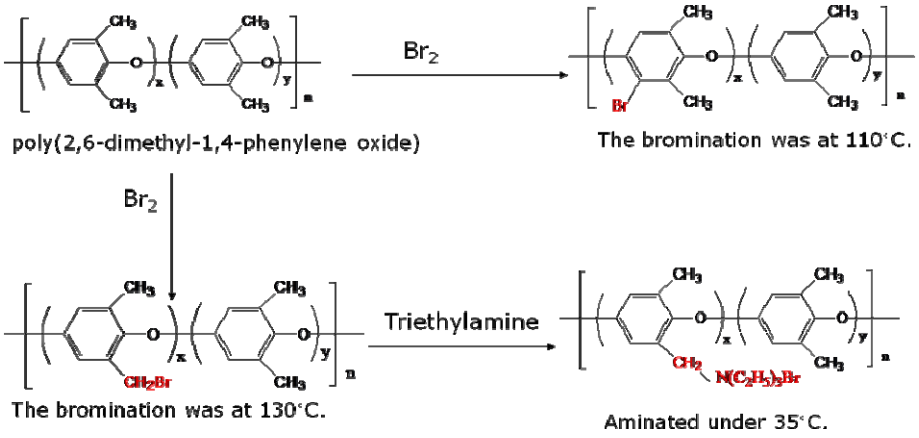

Fig. 5-1 The modification of brominated poly(2,6-dimethyl-1,4-phenylene oxide) (BPPO).

The three dried polymers with different amination rates were dissolved in 99% NMP with the same concentration of 20% w/w. The three polymer solutions were cast on non-woven clothes by a casting blade with a gap thickness of 250 μm. The cast non-woven clothes were dipped in an 99% IPA coagulant bath for 15 min and followed by a water bath. The temperatures of coagulant bathes and water bathes were all at room temperature of 23˚C. The APPO-PSf membranes obtained were named as: M-A, M-B, and M-C which corresponded to 1.0, 1.4 and 1.8 times of TEA additions, respectively. The membranes with different amination rates were then post-treated with the following procedures: 1) soaked in a 0.5M HCl solution overnight to remove unreacted TEA, followed by thorough rinsing, and 2) soaked in a 0.5M NaCl solution overnight, followed by

thoroughly rinsed by demonized water. After the post-treatments, the charging group became $CH_2N^+(C_2H_5)_3Cl^-$.

5.2.3 Polymer and membrane characterizations

To confirm the chemical modification, pure PPO, BPPO and APPO polymers without PSf blends were dissolved in GR grade THF and scanned by a Bio-Rad FTS 135 Fourier transform infrared - Attenuated Total Reflectance (FTIR-ATR with resolution of 4 cm^{-1} and the range of 400cm^{-1}-4000cm^{-1}) spectrometer in a wave-number range from 400 to 1800 cm^{-1}. An AXIS HSi spectrometer (Kratos Analytical Ltd. England) for X-ray photoelectron spectroscopy (XPS 15kV, 10mA, mono Al K_α with the resolution of 0.05 eV and the energy range of 1486.7 eV-0 eV) was applied to analyze the amination extent on pure APPO membrane surfaces without PSf blends. All core-level spectra were collected under 1486.71 eV photons and a photon electron take-off angle of 90°. The membrane morphologies were observed through a JSM-6700F FESEM (field emission scanning electron microscopy, with the resolution of 1.0 nm at 5.0 kV and range of x25-x650,000). Membrane samples for the FESEM study were dried in a freeze drier, fractured in liquid nitrogen, and coated with platinum before FESEM observation.

The IEC values (meq/m^2) of the newly developed membranes were determined by the Mohr method where a given membrane area was soaked in a 100 ml 0.1 M Na_2SO_4 solution for 48 hrs and the released Cl^- ions from each membrane was tested by an ion chromatography of Metrohm 792 basic IC. The pure water permeation (PWP) tests were performed with a constant membrane area of 10.46 cm^2 and a constant pressure of 3 kg/cm^2 as below:

$$PWP = \frac{Q}{A \times t} \qquad (m^3/m^2.\ sec) \qquad (5\text{-}1)$$

where A (m^2) is the constant membrane area, t (s) is the testing time, and Q (m^3) is the total permeate volume.

The pore size distribution was characterized by a capillary flow porometer CFP-1500AE (Porous Materials Inc. Dutch). A piece of isopropanol wetted membrane was sealed in the sample chamber. Nitrogen gas was then allowed to pass through the membrane. When the pressure reaches a point that can overcome the capillary effect within the largest pore of the given wetted membrane, the bubble point was then found. The pore size distribution was calculated through the bubble point and the measured flows.

The SurPASS electrokinetic analyzer (streaming potential or ζ-potential analyzer, Anton Paar GmbH, Australia) was applied for surface charge characterization. The apparent ζ-potentials can be measured by the Helmholtz–Smoluchowsky method:

$$\zeta_{apparent} = \frac{dU}{dP} \times \frac{\eta}{\varepsilon_r \times \varepsilon_0} \times \frac{L}{A \times R} \qquad (5\text{-}2)$$

where dU/dP (mV/mbar) is the slope of streaming potential versus pressure; η is the electrolyte viscosity (mbar.sec); ε_r is the relative dielectric constant of electrolyte; ε_0 is the vacuum permittivity ($\varepsilon_0 = 8.85\times10^{12}\ C^2\ J^{-1}\ m^{-1}$); L is the length of streaming channel (m); A is the cross-section area of the streaming channel (m^2); R is the resistance inside the measuring cell (kΩ). The membrane for the streaming potential test was titrated from pH 3.0 to pH 10 in a 0.1M KCl buffer and a series of ζ-potential data were obtained as a function of pH. This pH range covers all pH values appeared in the IEM-FFIEF process in this study.

5.2.4 Protein separation by APPO membrane partitioned FFIEF

Fig. 5-2 shows the experimental setup for the IEM-FFIEF system and Fig. 5-3 shows the design of FFIEF cell. As demonstrated in Fig. 5-2, three circulated flows were driven by a cartridge pump (MasterFlex® I/S model 7519-06) and the concentration in chamber 3, 7 and 9 are measured by a UV-Vis spectrometer. The kinetic function of UV-Vis can automatically measure the concentration variation for the analysis of the mass transfer across the whole system [[24,25]]. As demonstrated in Fig. 5-3, the IEM-FFIEF cell includes two electrode chambers and ten buffer chambers. The anode chamber was fed with 0.1M H_3PO_4 and the cathode chamber was fed with 0.2M NaOH. Self-made porous APPO membranes partitioned all buffer chambers, while the electrode dense ion-exchange membranes AHA and CEM partitioned electrode chambers and buffer chambers. The effective separation areas for all ion exchange membranes are 42.9 cm^2 and the chamber thicknesses of buffer chambers are 1.0 cm.

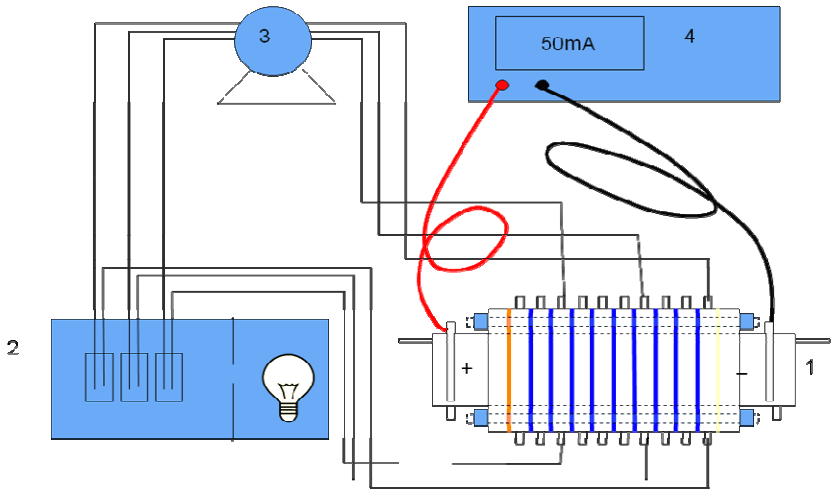

Fig. 5-2 Experimental set-up.

1. The IEM-FFIEF cell; 2. The UV-Vis spectrometer;
3. The cartridge pump; 4. The direct current electrophoresis power supply.

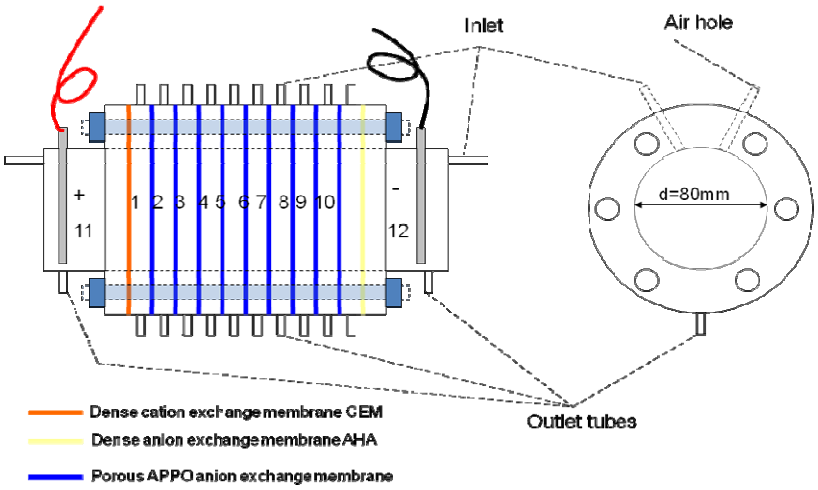

Fig. 5-3 The design of the IEM-FFIEF cell.

1~10 are the buffer chambers; 11 is the anode chamber; 12 is the cathode chamber;
All of the chambers are partitioned by membranes and fixed in series by six rods. The right hand side is the cross-section of one buffer chamber.

The buffer chambers were feed with ampholyte solutions (pH = 3-10) and a pH gradient will formed along the buffer chambers if an electric field is applied. Since protein molecules will move toward a pH that can reduce its surface charge to zero, the protein mass transfer across porous membranes takes place under an electric field. When the pH gradient is stable, the separated protein molecules will be concentrated in a specified chamber whose pH equals to proteins' individual pI values. After tests, protein samples were collected from every chamber for HPLC analyses and the pH values of every individual chamber were recorded. The HPLC used is Agilent technologies 1200 with VWD detector. The column applied is Grace Vydac C18 mass SPEC. The gradient elution included two mobile phases, A: 100% acetonitrile aqueous solution with 0.1% trifluoroacetic acid; B: 100% water with 0.1% trifluoroacetic acid. The HPLC was under a wavelength of 280 nm and a flow rate of 1.0 ml/min.

5.3. Results and discussion

5.3.1 Confirmation of the polymer modification

After reacted with triethylamine as shown in Fig. 5-1, the modified polymers are expected to exhibit characteristics of anion exchange resins. This chemical modification is confirms by FTIR spectra show in Fig. 5-4. The spectrum of bromine in the benzyl functional group is characterized by bands at 594 cm^{-1}, 1195 cm^{-1} and 1400 - 1450 cm^{-1}. The band at 594 cm^{-1} shows the existing of $–CHBr_2$ group; the band at 1195 cm^{-1} shows the C-Br stretching on $–CH_2Br$; and the bands at 1400 - 1450 cm^{-1} shows the C-H stretching on $-CH_2Br$ group. After the modification, the APPO spectrum shows obvious differences from the BPPO spectrum through significant intensities reduces at 594 cm^{-1}, 1195cm^{-1} and 1400-1450cm^{-1}, indicating chemical structure changes. Meanwhile, new peaks appear at 1172 cm^{-1} (C-N bond of tertiary or quoternary amines) and 1388 cm^{-1} ($-NCH_3$ groups on quaternary amine) [27], clearly confirm the amination reaction.

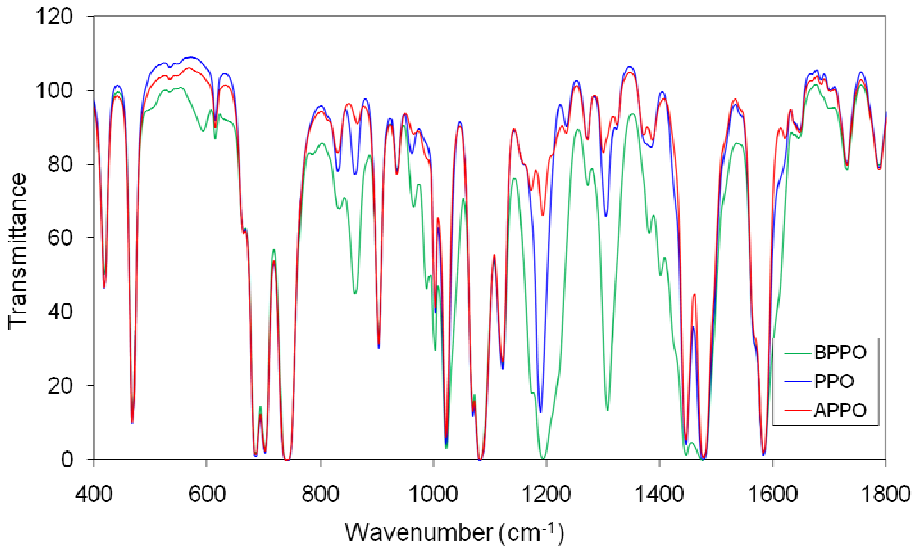

Fig. 5-4 FTIR scanning of PPO, BPPO and APPO

where 594,1195,1400~1450 cm^{-1} are due to Br substitution; 1172 cm^{-1} is due to the C-N of quaternary aliphatic amines; 1388 cm^{-1} is due to $–NCH_3$ of quaternary amine.

On the other hand, APPO membranes with different extent of modification were studied through the X-ray photoelectron spectroscopy (XPS). Fig. 5-5 shows the chemical states and their quantities of C 1s core-level of BPPO and APPO membrane surfaces. During the modification process, the oxygen content is supposed to be constant. Hence, the increased quantity of C-N species implies that triethylamine has been effectively grafted on the PPO polymer. As indicated in XPS Handbook [28], the C 1s core-level spectrum on the pure PPO can be curve-fitted to four peaks, accordingly. The peak group near by 285 eV includes at least four peak compounds: the first, at 284.3 eV is for C-H species on the benzene ring; the second, at 284.71 eV is for the carbon on the benzene ring which connected to the benzyl groups; the third, at 285.00 eV is for the carbon on the benzyl groups; the fourth peak at 285.84 eV is for C-O species. While compared with the original PPO [27], the BPPO membrane exhibits one more peak at 286.7 eV for C-Br species.

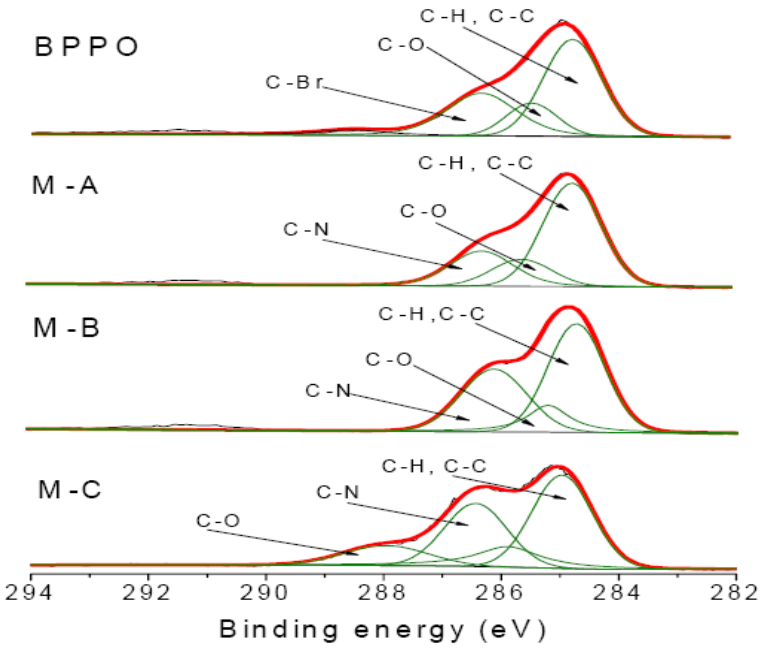

Fig. 5-5 XPS curve fitting of C 1s core-level on membrane surfaces with different amination rates.

Unlike the BPPO spectrum, APPO shows a shoulder at 286.2 eV and it increases with the TEA loading. The shoulder indicates a new peak resulting from the modification and this growing peak is due to the increase of C-N species. Therefore, the modification extent can be quantitatively measured by comparing the ratios of integration areas of A_{C-N} : A_{C-O} and A_{C-C} : A_{C-O}, as summarized in Table 5-1, where there is an obvious increase in C-N species as the TEA loading enhanced. Similarly, an increase in the ratio of A_{C-C}:A_{C-O} results in an enhancement in the C-C species.

Table 5-1. Comparison of XPS results of membrane surface with different extents of modification

Membrane ID	A_{C-N}:A_{C-O}	A_{C-C}:A_{C-O}
BPPO TEA:BPPO=0	0	1.83
M-A TEA:BPPO=1.0	1.69	2.97
M-B TEA:BPPO=1.4	2.45	3.46
M-C TEA:BPPO=1.8	3.41	3.88

Meanwhile, the same trend of the increase of C-N species was observed in a different fashion in XPS curve fittings of N 1s core-level in Fig. 5-6. It has been pointed out in ref. [29], the primary benzylic halide reagent, BPPO, is very reactive toward good nucleophile such as tertiary amines. As a consequence, the introducing of tertiary amine groups into BPPO leads to an increase in both integration area and binding energy of nitrogen element. As the TEA loading is enhanced, a red shift of bonding energy is observed in the nitrogen spectrum, from 402 eV to 400 eV, indicating the surfaces of modified membrane become easier to accept photoelectrons emitted by the X-ray source. Interestingly, the binding energy of nitrogen element in amine salt shifts to the same direction as in the previous work on polyimide aminations, both show an obvious red shift [30]. This may be

due to the fact that a quaternary amine salt has been formed after post-treatment and the ionic bond of quaternary amine exhibits the lowest bonding energy for accepting electrons than any other non-saturated amines. In addition, the two peaks displayed in Fig. 5-6 (M-A) and (M-B) may indicate that there exists an intermediate chemical state before the amine is fully saturated by TEA.

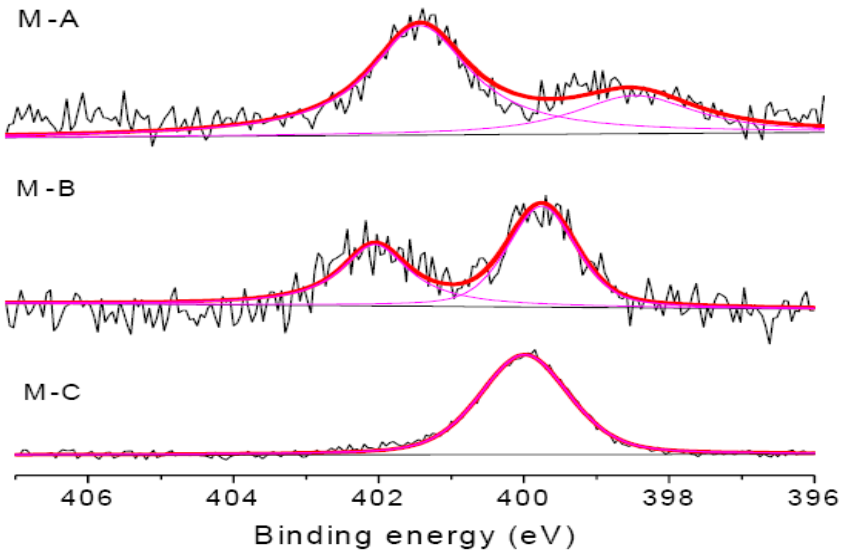

Fig. 5-6 XPS curve fitting of N 1s core-level on membrane surfaces with different amination rates,
where the integration areas are 1365, 1666 and 2924 individually for M-A, M-B and M-C.

5.3.2 Characterizations of membrane electric properties

Fig. 5-7 displays the streaming potential of APPO membranes with different degrees of modification. The surface streaming potential, called as ζ-potential, is the most important parameter for the ion-exchange membrane partitioned FFIEF. As demonstrated, the M-A membrane is slightly negatively charged in the range of pH 7 - 10 and positively charged in the range of 3 - 7. Compared to the M-A, the M-B and M-C demonstrate the same trends but higher absolute values of surface ζ-potentials. This result indicates that an

increase in TEA loading in the reaction does enhance the amination extent and the surface charge density. On the other hand, the surface ζ-potentials gradually decreases as the pH increases, leading to a negative ζ-potential of M-A in the range of pH 7-10. This trend will affect the performance in chambers 9 and 10 to some extent as showing later in this study.

Table 5-2 lists the ion-exchange capacities (IEC) and shows the IEC value increases with modification extent. This is consistent with the results from different characterization methods, such as XPS scanning, surface ζ-potentials and IEC values. In summary, a higher loading of TEA (in the rage of 1.0 to 1.8 times of BPPO mole numbers) results in a higher charge density on membrane surface.

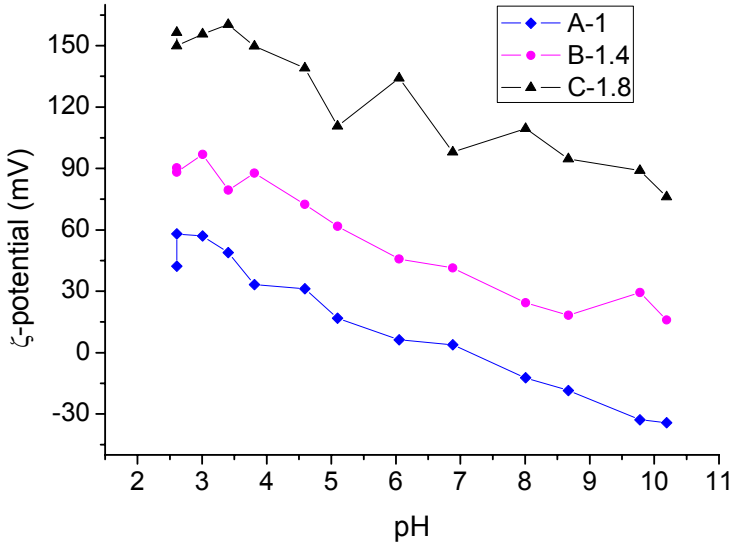

Fig. 5-7 Membranes' streaming potentials with different modification rates, where all the membranes were titrated in the range of pH 3~10 in 0.1M KCl buffer.

Table 5-2 Ion exchange capacity of the membranes with different modification rates

Membrane ID	Given area (cm^2)	Ion Chromatography (Cl^- ppm)	IEC (meq/m^2)
M-A (1.0)	110.44	5.40	1.375
M-B (1.4)	108.40	6.85	1.796
M-C (1.8)	93.94	6.94	2.086

5.3.3 Morphology and pore size distributions

Fig. 5-8 shows the morphology of the as–cast APPO membrane applied in the IEM-FFIEF process in this study. As can been seen in Fig. 5-8, the pore size decreases in the order of A > B > C. Because of using an active nucleophile reagent, triethylamine (TEA), the benzyl bromide can easily induce a substitutive reaction so that the triethyl group can be grafted to the PPO polymer chain. Therefore, the modification extent increases with the TEA loading amount. Fig. 5-9 and Table 5-3 show the pore size distribution measured by a capillary flow porometer. Consistent with the FESEM observation, the mean pore size and pure water permeation (PWP) decrease with an increase in TEA loading.

Table 5-3 Pore size characterization and pure water permeation (PWP)

Membrane ID	Mean flow d_p(nm)	PWP $m^3.m^{-2}.sec^{-1}$
M-A (1.0)	81.9 ± 26.5	0.301
M-B (1.4)	45.4 ± 22.3	0.171
M-C (1.8)	33.0 ±10.0	0.127

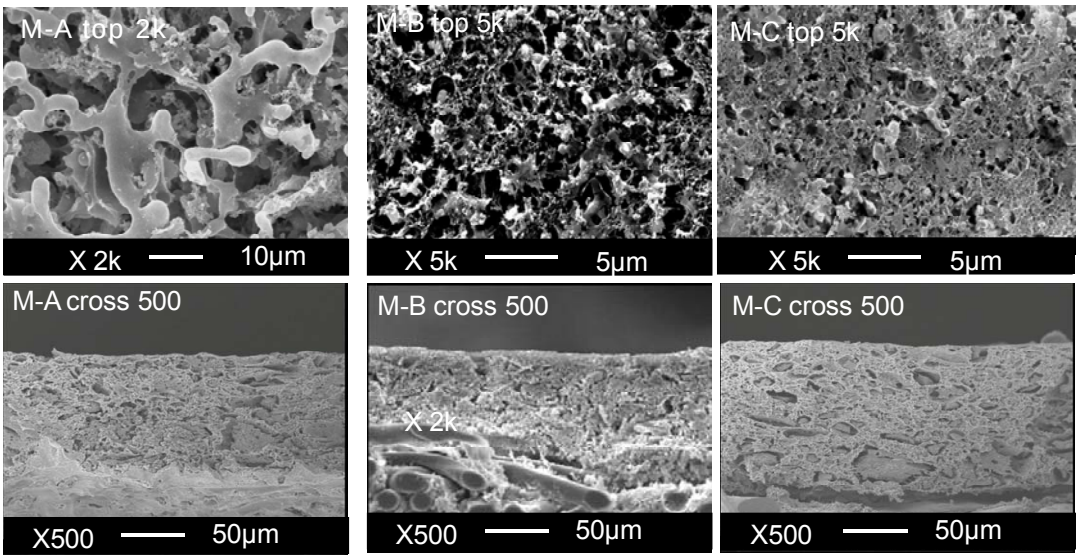

Fig. 5-8 The SEM image of membranes' surfaces and cross-sections

The JSM-6700F FESEM with the resolution of 1.0 nm at 5.0 kV and the magnification range of x25-x650,000.

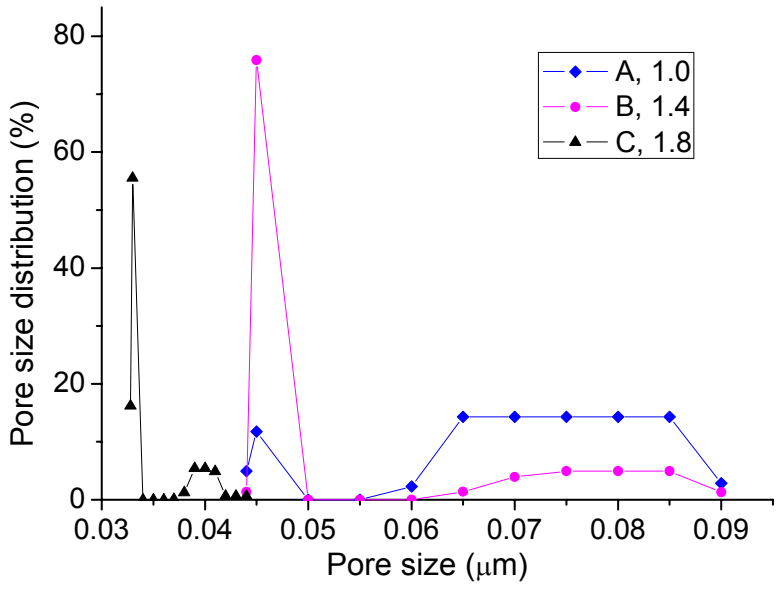

Fig. 5-9 Pore Size distributions of M- A, B and C measured by a porometer.

5.3.4 Protein separation through an IEM-FFIEF

The protein separation was monitored by an UV-Vis spectrometer and the protein components in every chamber were analyzed by HPLC. The UV-Vis reads the absorbance of compositions in chambers 3, 7 and 9 as a function of time individually circulated by a cartridge pump from each chamber. Fig. 5-10a is an example of the original data at the early stage of FFIEF separation, which is from chambers 3, 7 and 9 when the membrane M-C is employed. The absorption data from chambers 3, 7 and 9 correspond to BSA, Mb and Lys, respectively.

As can be seen in Fig. 5-10a, there is a peak appears in chamber 7 and plateaus appear in chamber 3 and 9. This may be due to the fact that the final focusing of a specific component depends on the formation of a linear pH gradient across the system. The formation and stabilization of a linear pH gradient needs a certain period of time. Consequently, the protein component will drift with the pH location which corresponding to its pI value. For instance, when the protein mixture was fed in chamber 6 and the electric field was applied, the Mb first transferred to chamber 7, then moved back to chamber 6. As the running time increased, the focusing chamber again shifted back to chamber 7, and finally focused in it. Similarly, the lysozyme first arrived in chamber 9; then it migrated to chamber 10 and focused in it, because the pH of chamber 10 will finally be around pH 10-11. However, no matter which chamber was the feed and from which chamber the UV-Vis data was collected, the final focusing location of a specific component would not be changed from batch to batch.

In order to compare mass transfer rates of different membranes, the original data of Mb (chamber 7) produced by three different membranes A, B and C are overlapped in Fig. 5-10b. While the BSA and Lys fluxes are compared in Fig. 5-10c and 5-10d, respectively. The membrane M-C has a higher flux for Mb as shown in Fig. 5-10b, but a lower flux for Lys as shown in Fig. 5-10d. This comparison implies that a higher opposite charge is favorable to the mass transfer of counter-ion particles across the membrane. In other words, the negatively charged Mb molecules can be easier than other species being transferred through the positively charged membrane under the electrical field. This phenomenon can be simply explained in terms of the Ohm law. In a typical membrane electrophoresis like this study, oppositely charged molecules are first attracted by the charged membrane pore surface and form a double layer. For the balance of local electrical charges, the higher membrane surface charge will lead to the higher concentration of counter-ions around it. After that, the diffusion layer nearby the double layer is mainly driven by the applied electric field and move toward the corresponding electrodes.

Our previous work has observation that a high IEC value will increase membrane conductivity, reduce electric resistance and increase mass transfer rates of counter-ions [25, 31] under an applied electric field. A comparison of Mb transfer rates from the slopes of these three membranes in Fig.5-10b reconfirms our previous conclusion. Therefore, enhancing membrane surface charge is an effective way to increase the flux of a counter-ion across the membrane. On the other hand, one must take into consideration the variation of charge signs in different pH. As shown in Fig.5-10d, the positively charged Lys has a much lower flux across the M-C membrane compared to that across M-A. This is due to the fact that these membrane exhibit different streaming potentials and polarities

in the range of pH 7-10. As shown in Fig. 5-7, the M-C surface is positive under pH 7-10, while Lys molecules are also positively charged under these pHs. In contrast, the M-A surface displays negative charge in this range. As a result, the Lys flux across M-A is higher than M-C. In summary, a higher surface charge improves the flux of a counter-ion, but reduces the flux of a co-ion. In addition, the proposed amination process can effectively enhance the productivity of protein separation in FFIEF.

However, the flux of BSA across M-C fails to maintain its high flux after 100 min. As shown in Fig. 5-10c, the flux across M-B becomes higher than that across M-C. This is due to the fact that the M-C membrane has the smallest pore size as illustrated in Fig. 5-9 and Table 5-3. Since the BSA molecule has a radius of 5.0 nm and the Mb of 2.1 nm [32]. The former may have higher stereo-hindrances than the latter, thus reduces the mass transfer flux.

The HPLC results of all chambers for FFIEF protein separation process are plotted in 3-dimensional graphs. Figs. 5-11a, b and c correspond to the performances of M-A, M-B, and M-C, individually. The retention times of Lys, BSA and Mb appear at 10.1 min, 10.7 min and 12.5-15.2 min, respectively. There exist different peaks appeared in each figure. Fig.5-11a looks furry in appearance and at least two protein peaks are shown in every chamber from chambers 2 to 6.

On the contrary, the Fig. 5-11c looks very neat in appearance and only one protein peak shows in every chamber except for the feed chamber; whereas as an intermediate status. Fig. 5-11b shows an appearance in between Fig. 5-11a and c. For Fig. 5-11c the pure BSA appears in chambers 4 and 5; the pure Mb only appears in chamber 7; and the pure

Lys only appears in chamber 10. In other words, the M-C membrane purifies proteins with higher concentration and higher purity than that of M-A and M-B membranes. This phenomenon reconfirms our previous hypothesis that the membrane with a higher charge density or higher IEC value can dramatically improve the self-sharpening phenomenon and be favorable to the performance of a multi-component protein separation.

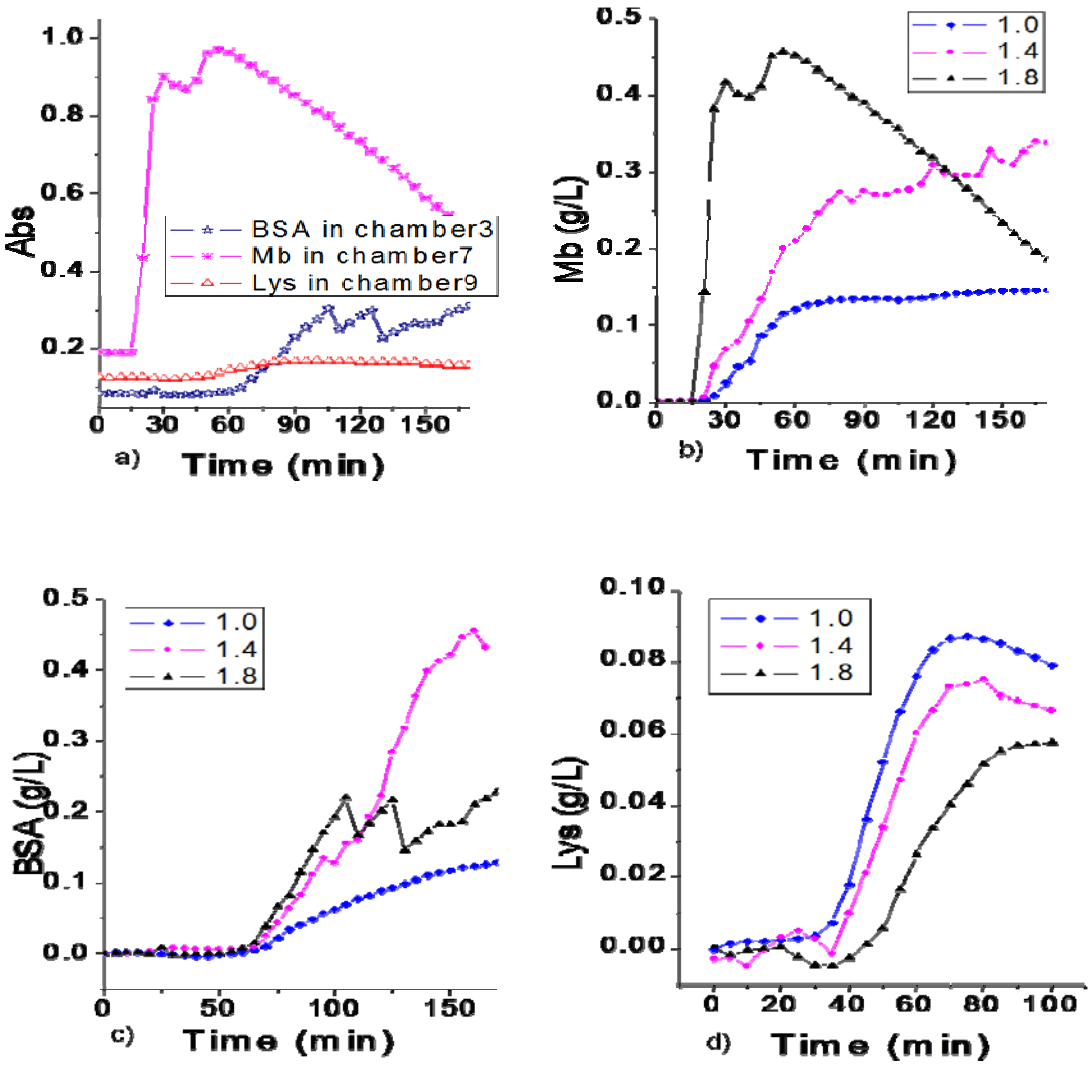

Fig. 5-10 The comparison of mass transfer rates through the slopes of concentration vs. time.

a) UV results in different chambers; b) Mb concentration vs. time in chamber 7;
c) BSA concentration vs. time in chamber 3; d) Lys concentration vs. time in chamber 9.

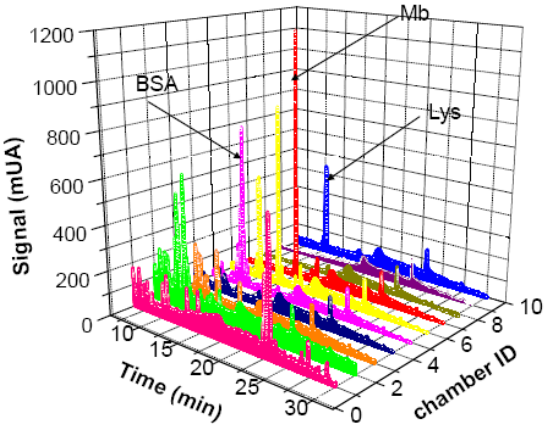

Fig. 5-11a M-A

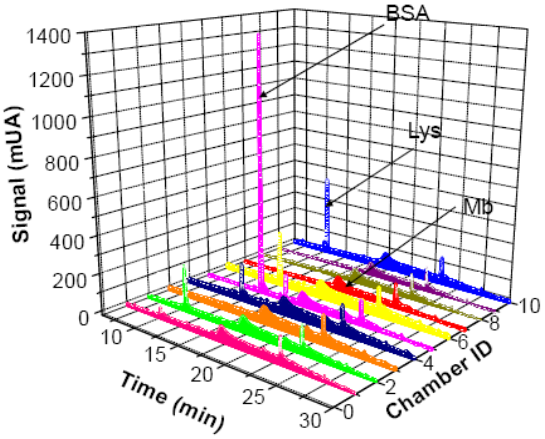

Fig. 5-11b M-B

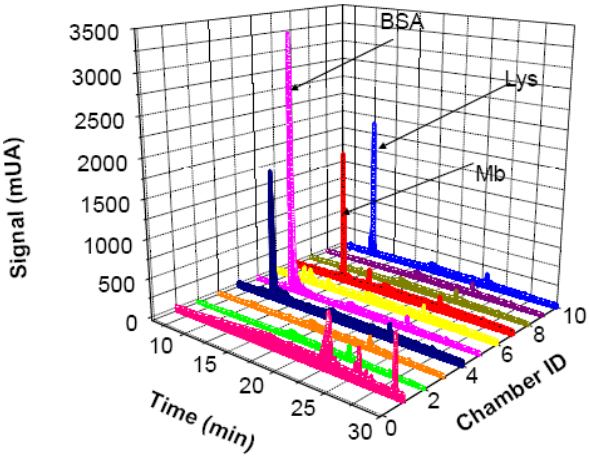

Fig. 5-11c M-C

Fig. 5-11 HPLC results of 3-component protein separation in IEM- FFIEF

where 9 pieces of identical M-A, M-B and M-C membranes were employed in separation chromatography of Fig.5-11a, Fig.5-11b and Fig.5-11c.

The self-sharpening phenomenon was directly influenced by five factors: 1) a stable pH gradient across the system for stable mass transfer; 2) reasonable differences in pI values among proteins; 3) a small pH difference between each chamber, 4) a reasonable number of chambers, and 5) high charged membranes with appropriate pore sizes.The charged membrane serves as a separation medium with a linear pH gradient along the electric field. Different from the nylon screening (about 5μm thick) used in Rotofor, the anion exchange membrane applied in this study has a much smaller pore size in the range of 33 nm - 82 nm and the grafted charge sites are confined in a membrane layer of 60 - 80 μm thick. A pH gradient will form in the membrane cross-section when the confined charged sites interact with pH buffer under an electric field. As a result, the pH inside the membrane will queue in an increasing order from the anode to the cathode because of the decreased proton concentration along the electric field. Actually, the individual charged membrane can be imagined as a piece of IEF gel with a pH gradient and this hypothesis has been proven in our previous study [25]. Furthermore, the stability of the pH gradient will be the decisive factor for the "focusing" function.

As revealed by the study on boundary effects [33], a higher charge density in membrane will result in stronger surface interactions between counter-ions, in turn a stronger buffer capacity and a more stable pH gradient will be present in membrane. Therefore, the 9-piece identical porous membranes applied in this study can form nine ionic selective barriers with different sub-ranges of pH gradients, and actively respond to different pI values of protein molecules. Accordingly, the protein molecules with different pI values will be simultaneously focused in different chambers with least undesired components. In other words, the solid porous membranes with highly charged surfaces can perform the

function of self-sharpening similar to the gel-like immobiline membranes, without ion depletion and structure failure in a long term operation.

To overcome the issue of many components appearing in one chamber, a reasonable number of chambers and an adequate range of natural pH gradient are the most effective factors to improve the resolution of "self-sharpening". Generally, the number of components appear in a single chamber can be manipulated. For instance, the resolution of single piece membrane in the current study is around 0.7 pH units, and the smallest ΔpI is 2.0 pH units (pI_{BSA}= 4.8, pI_{Mb} = 6.8 and pI_{Lys} = 11.0). The given ΔpI is much large than 0.7 pHs, hence the model protein mixture can be effectively separated. Nevertheless, the difference in pI values of the target components in real applications can not be manipulated. If they have very close pI values, increasing the number of chambers and reducing the range of pH gradient are the appropriate routes to improve the separation resolution.

5.5 Conclusions

The following conclusions can be drawn from this study:

1) We have grafted the triethylamine onto the BPPO polymer and the resultant anion-exchange membranes are applied in free-flow isoelectric focusing (FFIEF).
2) The membrane morphology and charge characteristics are highly affected by the degree of amination. For 1:1 BPPO: PSf blend membranes, a higher degree of amination results in a higher charge density and a smaller pore size.

3) Experimental results demonstrate that a 3-component protein mixture can be fully separated by the IEM-FFIEF process. In addition, membranes with a higher charge density produce a higher flux, and a higher purity protein.

4) HPLC results reconfirm that self-sharpening phenomenon can occur in a FFIEF system, and a higher membrane charge density will be favorable to the self-sharpening phenomenon.

5.6 References

[1] C.K. Colton, S. Friedman, D.E. Wilson and R.S. Lees, Ultrafiltration of lipoproteins through a synthetic membrane, implications for the filtration theory of atherogenesis. J. Clin. Invest., 51 (1972) 2472.

[2] C.K. Colton, Analysis of membrane processes for blood purification. Blood Purificat. 5 (1987) 202.

[3] Z.F. Cui and R. Ghosh, Protein fractionation using ultrafiltration: opportunities and challenges. J. Dalian University of Technology 33 (1998) Suppl.1, S26-S33.

[4] J. Shao and A.L. Zydney, Optimization of ultrafiltration / diafiltration processes for partially bound impurities. Biotechnol. & Bioeng., 87 (2004) 286.

[5] R. Chan and V. Chen, The effects of electrolyte concentration and pH on protein aggregation and deposition: critical flux and constant flux filtration. J. Membr. Sci. 185 (2001) 177.

[6] C.C. Ho and A.L. Zydney, Protein fouling of asymmetric and composite microfiltration membranes, Indu. & Eng. Chem. Res. 40 (2001) 1412.

[7] Hu, L; Xu, X. and Coleman, M. R., 2008. Impact of ion type on structure and transport property evolution of Matrimid®. Separation Science and Technology 43, 4030-4055.

[8] R.X. Zhuo and W. Li, Preparation and characterization of macroporous poly(*N*-isopropylacrylamide) hydrogels for the controlled release of proteins, J. Polymer Sci. A, 41 (2003) 152.

[9] C.F. Ivory, Several new electrofocusing techniques, Electrophoresis 28 (2007) 15-25.

[10] M. Aider, D. de Halleux and L. Bazinet, Potential of continuous electrophoresis without and with porous membranes (CEPM) in the bio-food industry: review, Trends Food Sci.Tech. 19 (2008) 351.

[11] S. Tam, Electrophoretic prefractionation: new commercial tools from an old concept.

Expert Review of Proteomics 3 (2006) 379.

[12] P. Wenger and P. Javet, Isoelectric focusing using non-amphoteric buffers in free solution: I. determination of stable concentration profiles, J. Biochem. Bioph. Meth. 13 (1986) 259.

[13] P. Wenger and P. Javet, Isoelectric focusing using non-amphoteric buffers in free solution: II. apparatus and measures of pH stability, J. Biochem. Bioph. Meth. 13 (1986) 275.

[14] P.G. Righetti, Preparative purification of human monoclonal antibody isoforms in a multi-compartment electrolyser with immobiline membranes. J.Chromato. A 500 (1990) 681.

[15] S. Cherkaoui, P. Zell, and P. Javet, Characterization of immobiline membranes for application in a multicompartment electrolyzer, J. Biochem. Biophy. Meth. 25 (1992) 61.

[16] M. Chiari, M. Nesi, P. Roncada and P.G. Righetti, Preparative isoelectric focusing in multi-compartment electrolyzers: novel, hydrolytically stable and hydrophilic isoelectric membranes, Electrophoresis 15 (1994) 953.

[17] R. Kuhn and H. Wagner, Application of free flow electrophoresis to the reparative purification of basic protein from an E.coli cell extract, J. Chromatog. A, 481 (1989) 343.

[18] Becton Dickinson Inc. 2009. www.bd.com/

[19] V.L. Locke, T.S. Gibson, T.M. Thomas, G.L. Corthals and D.B. Rylatt, Gradiflow as a prefractionation tool for two-dimensional electrophoresis, Proteomics, 2 (2002) 1254.

[20] D.L. Rothemund, V.L. Locke, A. Liew, T.M. Thomas, V. Wasinger and D.B. Rylatt, Depletion of the highly abundant protein albumin from human plasma using the Gradiflow, Proteomics, 3(2003) 279.

[21] P. Aran, Rapid automated differential protein expression profiling with IEF Rotofor and SDS-PAGE chip system, Molecular & Cellulose Proteomics 3.10, 2009, S277.

[22] J. Hey, A. Posch, A. Cohen, N. Liu and A. Harbers, Fractionation of Complex Protein Mixtures by Liquid-Phase Isoelectric Focusing, Method Mol. Cell. Biol., 424 (2008) 225.

[23] A. Ayala, J. Parrado and A. Marchado, Use of Rotofor preparative isoelectric focusing cell in protein purification procedure, Appl. Biochem. Biotechenol., 69 (1998) 11.

[24] J.H. Cheng, Y. Li, T.S. Chung, S.B. Chen and W.B. Krantz, High-performance protein separation by ion exchange membrane partitioned free-flow isoelectric focusing system. Chem. Eng. Sci. 63 (2008) 2241.

[25] J.H. Cheng, T.S. Chung and S.H. Neo, Investigation of mass transfer in the ion-exchange membrane partitioned free-flow isoelectric focusing system (IEM-FFIEF) for protein separation, Electrophoresis 30 (2009) 2600.

[26] W.H. Yang, T.W. Xu, Fundamental studies on a novel series of bipolar membranes

prepared from poly(2,6-dimethyl-1,4-phenylene oxide)(PPO), J. Membr. Sci. 238 (2004) 123.

[27] G. Socrates, Infrared and Raman characteristic group frequencies. John Wiley & Sons, New York, 2004, pg 38 or pg146.

[28] G. Beamson, D. Briggs, High resolution XPS of organic polymer: the Scienta ESCA300 database, Wiley, New York, 1992.

[29] F.A. Carey, Organic chemistry, 6th edition. McGraw Hill, New York, 2006.

[30] Y.C. Xiao, L. Shao, T.S. Chung, D.A. Schiraldi, Effects of thermal treatments and dendrimers chemical structures on the properties of highly surface cross-linked polyimide films, Ind. Eng. Chem. Res. 44 (2005) 3059.

[32] H.H.P. Yiu, C.H. Botting, N.P. Botting and P.A. Wright, Size selective protein adsorption on thiol-functionalised SBA-15 mesoporous molecular sieve. Phys. Chem. Chem. Phys. 3 (2001) 2983.

[33] J. Ennis, H. Zhang, G. Stevens, J. Perera and S. Carnie, 1996. Mobility of protein through a porous membrane, J. Membr. Sci., 119 (1996) 47.

CHAPTER 6 CHEMICAL MODIFICATION OF P84 POLYIMIDE AS ANION-EXCHANGE MEMBRANES IN A FREE-FLOW ISOELECTRIC FOCUSING SYSTEM FOR PROTEIN SEPARATION

6.1. Introduction

The demand of pure protein products has been increasing rapidly which triggers the research of more efficient technologies for protein separation. Many technologies for protein separation have been developed such as chromatography, crystallization, moving bed column, electrodialysis, electrophoresis, membrane ultrafiltration and membrane chromatography, etc. Among them, membrane based protein separation is believed possible to meet the industrial demands of high throughput and high selectivity [1]. However, the surface charge characteristics of proteins make protein separation through a membrane complicated because of the electrostatic interactions between solute molecules and membrane pore surfaces.

The basic theory of long-range colloidal interactions (electrostatic effect) between a protein solute and membrane pores has been developed by Smith and Deen [2, 3]. Taking the advantage of electrostatic interaction, Zydney and his co-workers have developed pioneering technologies for membrane based protein separation [4, 5]. Meanwhile, other scientists also reported enhanced protein separation with the aid of electric driving force applied across the membrane [6-9], e.g. the membrane based electrodialysis systems and the electrophoretic membrane contactors. Of all known electrophoretic methods, the isoelectric focusing (IEF) gains the highest resolution [10]. Recycling isoelectric focusing (RIEF) was therefore developed to concentrate charged macromolecules at specific

locations with pH equals to their pI values [10, 11]. The RIEF can be designed with or without porous screens as partition media between chambers. Beir and his coworkers were the pioneers developing the screened RIEF, e.g. Rotofor, which has been commercialized by Bio-Rad Laboratories, for lab-scale protein fractionation. However, the screens used in their design have big pores that can only reduce the convective flow between chambers but not confine specific protein molecules in a narrow range, for example in one chamber. Thus in the Rotofor device, separated proteins are distributed in a range of neighborhood chambers. On the other hand, since the turbulent flow is inevitable in a big scale process, the non-specific distribution of protein products is an issue and will increase production cost for further purification. Therefore, we propose using ion-exchange membranes with tailored pore sizes for FFIEF, because the permselectivity possessed by the membrane surface can simultaneously prevent the convective mixing and confine the separated protein in a specific chamber.

To obtain a high flux from FFIEF protein separation, the molecular design of ion exchange membranes with a suitable ion exchange capacity (IEC) and pore properties is essential [12, 13]. To design a positively charged polymer, various chemical modifications have been published. They are 1) chloromethylation through chloromethylmethyl ether (CME) or bis-chloromethyl ether (BCME), followed by amination [14, 15]; 2) bromination of benzyl group followed by amination [16, 17]; 3) acetylation followed by amination [18-19]; 4) Surface amination by ammonia plasma treatment [20]. However, the wet processes like the first three methods normally involve very toxic and carcinogenic reagents [21]. Bromination of PPO (poly(2,6-dimethyl-1,4-phenylene oxide)) needs boiling the bromine in a chlorobenzene solution at 131°C, and both bromine and chlorobenzene are in the

forbidden list of disposal in some countries [22]. For the fourth method, the high cost plasma-generator limits its extensive application.

An anion exchange membrane has been developed in this work under milder operation conditions using a commercially available co-polymer P84 polyimide. P84 is a high temperature polyimide (glass transmission temperature T_g 315°C, density 1.31 g/cm3) with superior thermal and membrane structural properties [23-28]. As a member of polyimide family, it can react with amine for further modifications [27, 28]. The modified membranes were then characterized by a series of analytic equipment and tested in the IEM-FFIEF system using a kinetic UV-vis spectrometer as an on-line process monitor. The purity of permeate products was measured by high performance liquid chromatography (HPLC).

6.2 Experimental

6.2.1 Experimental set-up

Combining the electrostatic effects between protein molecules and membrane pores, and the isoelectric focusing technology, we have designed an IEM-FFIEF (ion-exchange membrane partitioned isoelectric focusing) system for bovine serum albumin (BSA) and hemoglobin (Hb) separation [12] as shown in Fig.6-1. It consists of a FFIEF cell, power supply, circulation pumps, pH automation system and UV-vis spectrometer. Fig.6-2 shows the details of the IEM-FFIEF cell. The electrode chambers were set at two ends and buffer chambers were inserted in between two electrode chambers. All of chambers were partitioned by the newly developed ion-exchange membranes to prevent the convective flow between chambers and to confine the separated proteins in specific

chambers. Chambers 1, 2, 3 and 4 were fed in buffers with different pH values in a designed sequence as shown in Fig.6-2. A quasi-stable pH gradient in a protein separation membrane (between chambers 2 and 3) was realized by adjusting pH values in chambers 1 and 4 at a stable level.

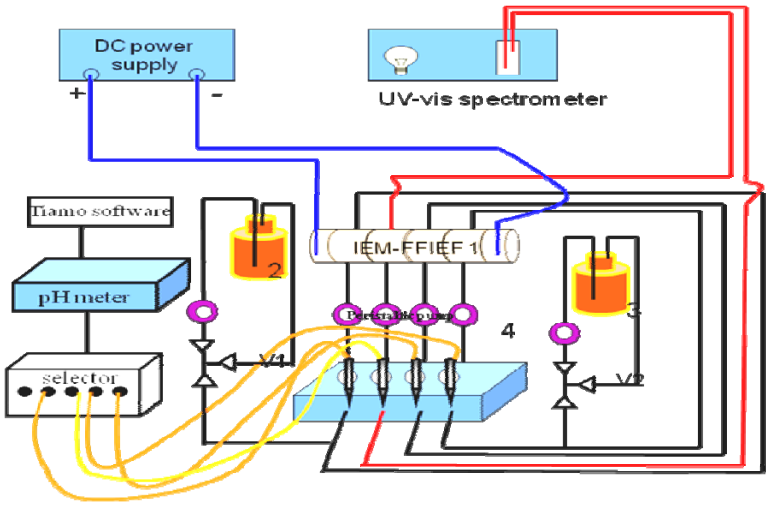

Fig. 6-1 Experimental set up of the IEM-FFIEF system

where 1 is ion-exchange membrane partitioned free-flow isoelectric focusing cell; 2 & 3 are base and acid storage for pH adjustment; 4 is peristaltic pump; V1 & V2 are the auto-valves controlled by Metrohm pH adjust system.

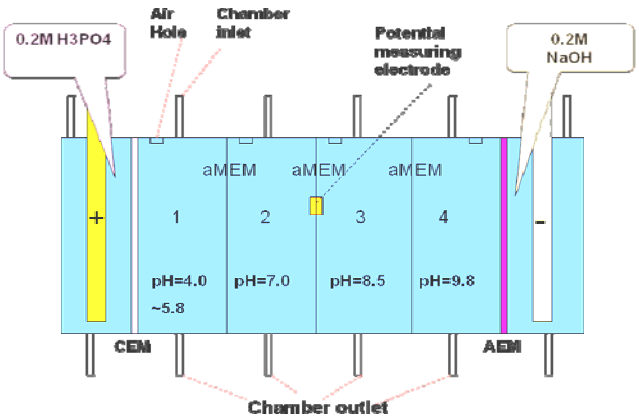

Fig. 6-2 Close-up of the membrane partitioned isoelectric focusing cell

where aMEMs are the home-made P84 anion-exchange membranes, chambers 1, 2, 3 & 4 are partitioned by aMEM; CEM is commercial dense cation-exchange membrane; AEM is commercial dense anion-exchange membrane.

It has been well known that most proteins can be ionized under various pH as shown in eqn. (6-1) and (6-2):

For pH < pI

$$R-NH_2+H^+ \rightarrow R-NH_3^+$$
$$R-COO^- + H^+ \rightarrow R-COOH \quad (6\text{-}1)$$

For pH > pI

$$R-NH_3^+ + OH^- \rightarrow R-NH_2 + H_2O$$
$$R-COOH + OH^- \rightarrow R-COO^- + H_2O \quad (6\text{-}2)$$

Therefore, the charged proteins show ionic characteristics under a wide range of pH. A protein can spontaneously move toward the location where the medium pH equals to its pI (isoelectric point) value and be stationary at that location. Thus the protein molecules can migrate across membranes and be relocated into different chambers according to their pI values. When a charged membrane is used, proteins would be rejected if the membrane surface has the same charge, while be adsorbed and/or migrate across the membrane under an electric field if the membrane surface has an opposite charge. It has been known that the interaction between protein molecules and membrane pore surface in electrophoresis is different from the phenomenon of electrostatic effects. In electrophoretic scope this interaction was called boundary effects which induced electro-osmotic flow, viscous retardation and the distorted electrostatic interaction between charged particles and pore surfaces arising from applied electric fields [13].

6.2.2 Materials

The P84 co-polyimide as shown in Fig.6-3 with a molecular weight (M_w) of 153k Da [29] was obtained from HP polymer GmbH, Austria. Myoglobin (Mb), lysozyme (Lys), ethylene diamine, diamine butane and polyethylene oxide (PEO), polyvinylpyrrolidone (PVP) were obtained from Sigma-Aldrich. The M_w and pI values of Mb are 17 kDa and 6.8, respectively; the M_w and pI values of Lysozyme are 14.4 kDa and 11.0, respectively.

N-methyl-2-pyrrolidone (NMP), phosphoric acid (H_3PO_4), phenolphthalein, trifluoroacetic acid, acetic acid, methyl iodide (CH_3I), sodium hydroxide (NaOH), methanol and acetonitrile (ACN) were all provided by Merck. Tris was from Bio-Rad, and isopropanol (IPA) was from TEDIA Inc. Hydrochloric acid was purchased from Fisher Scientific. All of reagents except ACN were of AR (analytical reagent) grade. For HPLC, GR (guaranteed reagent) grade water from Merck was used, while for other occasions, deionized water (DI water, electrical resistance $R < 18.2$ MΩ) was used. The dense cation exchange membrane and anion exchange membrane (commercial name CEM, AHA) were purchased from Astom Corporation

6.2.3 Preparation of P84 anion exchange flat membranes

The P84 polymer was used to prepare anion exchange membranes with the following procedures: (1) Phase inversion: P84 powder was dissolved in NMP with a concentration of 23% w/w. Then the solution was cast onto a piece of non-woven cloth by a casting blade with a gap thickness of 150μm. The non-woven cloth was immediately immersed in IPA. After 20 min, it was taken out and immersed in methanol for 2 hrs. The P84 porous membrane as obtained was named M-O. (2) Amination with diamine: the M-O membrane was directly soaked in a 5/5/90 (in V/V) ethylene diamine/ diamine butane/ methanol solution for 30 min. Capitalizing on the porous nature of the membrane surface and the short length of the diamine molecules, some diamine will react for the cross-linkage [30], while some free $–NH_2$ groups will remain which can be utilized for further methylation to form quaternary amine. Then the un-reacted diamine was removed by washing with methanol and the modified membrane was named M-1. (3) Methylation with methyl iodide: the M-1 membrane was subsequently dipped in a 20 wt% methyl iodide-methanol

solution for 12 hrs. Methyl iodide is chosen for the preparation of quaternary amine salt because of its high reactivity for nucleophilic substitution [30]. Two different reaction temperatures, 42°C or 48°C, were applied and the obtained membranes were named M-2 and M-3 individually. The above amination and methylation processes are schemed in Fig. 6-3. (4) All of the membranes M-O, M-1, M-2 and M-3 were post-treated as per routine: soaking in 0.5 M HCl for 12 hrs followed by fully washing with DI water; soaking in 1M NaCl solutions for 12 hrs followed by fully washing with DI water. As shown later, the membrane charging property increases with an increase in the degree of modification.

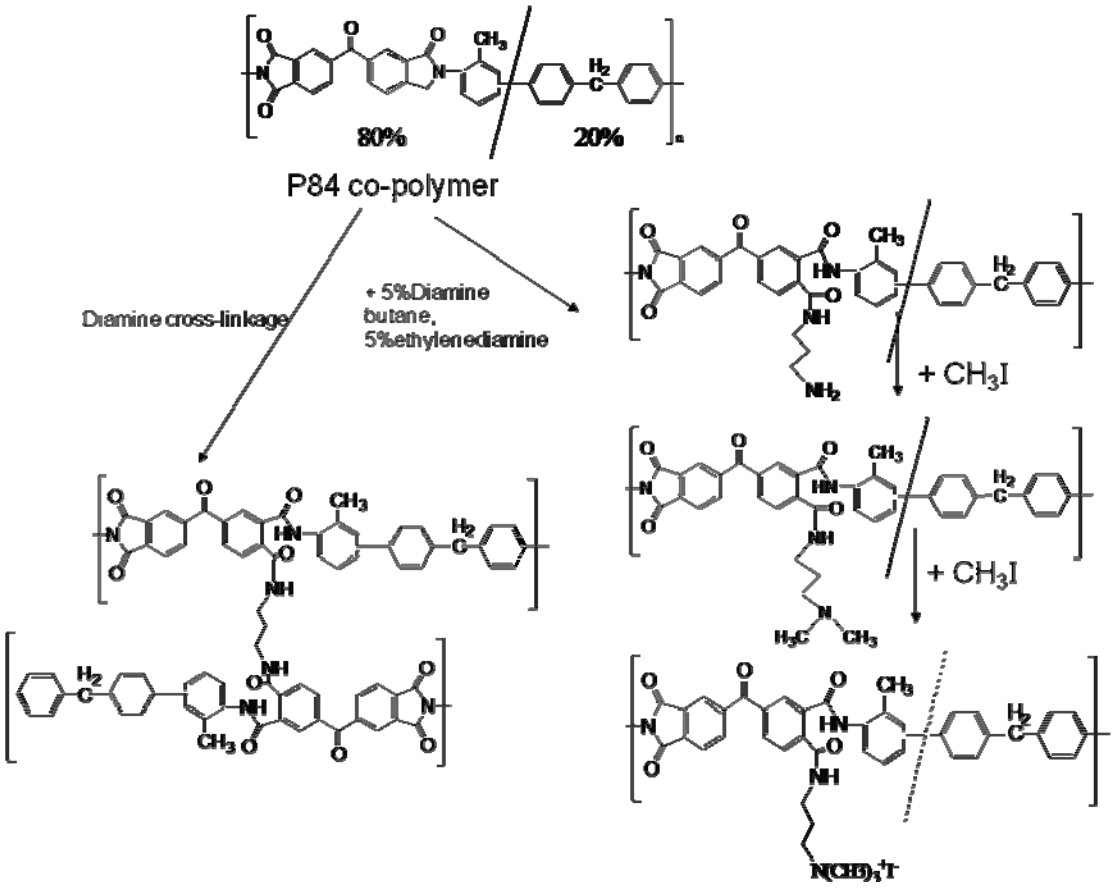

Fig. 6-3 Chemical structure and reactions of P84

6.2.4 Membrane characterization

Fourier transform infrared-attenuated total reflection (FTIR-ATR) measurements were carried out using a Bio-Rad FTS 135 FTIR spectrometer to identify the changes of chemical structure of membrane surface in a wave-number range from 700 to 3000 cm^{-1}. XPS (X-ray photoelectron spectroscopy) measurements were applied to analyze the membrane surface modification through AXIS HSi spectrometer (Kratos Analytical Ltd. England). All core-level spectra were collected under 1486.6eV photons and a photon electron takeoff angle of 90°. The morphologies of membranes were observed through a JSM-6700F FESEM (field emission scanning electron microscopy). Membrane samples were fractured in liquid nitrogen, dried under vacuum at room temperature and then coated with platinum before FESEM observation.

A streaming potential analyzer (Anton Paar GmbH) was used for surface charge characterization. As given by Helmholtz–Smoluchowsky method, the apparent ζ-potential can be measured through:

$$\zeta_{apparent} = \frac{dU}{dP} \times \frac{\eta}{\varepsilon_r \times \varepsilon_0} \times \frac{L}{A \times R} \qquad (6\text{-}3)$$

where dU/dP is the slope of streaming potential versus pressure; η is the electrolyte viscosity; ε_r is the relative dielectric constant of electrolyte; ε_0 is the vacuum permittivity; L is the length of streaming channel; A is the cross-section area of the streaming channel; R is the resistance inside the measuring cell. The sample for streaming potential measurements was titrated from pH 10 to pH 4.5 in a HCl -tris buffer. This pH range covered all related pH values in the IEM-FFIEF separation process. A series of ζ-potential data were obtained as a function of pH. It must be noticed that in order to mimic the real situations on membrane surface during the protein separation process, the buffer solution in a streaming potential analysis was 20 mM HCl-tris solution, which led to

much higher ζ-potential readings compared to the literature reports. The high apparent ζ-potential was due to the fact that in dilute solutions, such as 1 mM KCl or 20 mM HCl-tris buffers, the conductivity of charged surface was not negligible, thus the ζ-potential result needed to be corrected by 0.1M KCl through eqn. (6-4) [31]:

$$\zeta_{corrected} = \frac{dU}{dP} \times \frac{\eta}{\varepsilon_r \times \varepsilon_0} \times \frac{\kappa_{0.1MKCl} \times R_{0.1MKCl}}{R} \qquad (6\text{-}4)$$

where $\kappa_{0.1MKCl}$ is the conductivity of 0.1M KCl; $R_{0.1MKCl}$ is the cell resistance when running 0.1M KCl.

The ion-exchange capacities (IEC) were determined by the Mohr method [17, 18]. A given area of the membrane was soaked in a 100 ml 0.1 M Na_2SO_4 solution for 24 hrs and the Clconcentration as released was tested by a Cl^- ion selective electrode. The IEC value was expressed as meq/m^2. The pure water permeation (PWP) test was performed under 5 bar. The electric resistance (R) was measured in a special measuring cell as follows. Membranes M-O, M-1, M-2 and M-3 were immersed in 0.1M KCl for 24hrs, followed by placing each one of them in an electrical testing cell in which the membrane was mechanically sandwiched and tightened. Then electric resistance was individually measured at 25°C through a multi-meter.

The pore size distribution was measured by a real rejection method using a series of neutral molecules (PEG: 2k Da; PVP: 10 k, 55 k, 360 k, 1300k Da) with the aid of the following relationship between molecular weight and Stokes radius [32]:

$$\begin{aligned} &For \quad PEG \quad r = 16.73 \times 10^{-3} \times Mw^{0.557} \quad nm \\ &For \quad PVP \quad r = 8.40 \times 10^{-3} \times Mw^{0.593} \quad nm \end{aligned} \qquad (6\text{-}5)$$

The given standard neutral molecules were prepared into 100 ppm mixtures and filtered through the membrane which was mounted in a permeation cell under a 5 bar pressure. Then the permeate and feed compositions were analyzed with the aid of GPC (Gel Permeate Chromatography) using a 25 cm PL-aquagel-OH mixed 8 μm column (Agilent). The real rejection rate is obtained from the integration area of individual peaks as follows:

$$R_T = (1 - \frac{C_p}{C_f}) \times 100\% \qquad (6\text{-}6)$$

The real rejection rate as a function of molecular radius was further used to estimate the MWCO (molecular weight cut-off), mean pore size and pore size distribution according to the methods described elsewhere [32, 33]. An Agilent Technologies 1200 series high performance liquid chromatography (HPLC) instrument equipped with both a VWD and a RID detector was applied for PEG and PVP concentration tests through a GPC. The GPC was operated at the following conditions: pure water as solvent, 60 min running time, 0.5 ml/min flow-rate, and constant temperature at 30°C.

In order to investigate the mechanical strength and stability of the modified membranes, a tensile testing machine INSTRON 5542 was used to measure the tensile strength and Young's modulus. The mechanical strength and stability of one set of the M-3 samples were tested after one week of operation without protein feed under the conditions listed in Fig.6-2; while the other sets of M-3 samples were tested after immersing in 0.1M HCl and water for two weeks, individually. All samples were cut into 5mm widths, and the measuring lengths were all in 25 mm.

6.2.5 HPLC analyses of protein solution

High performance liquid chromatography (HPLC) was applied for the analysis of the concentration of individual protein. An Agilent Technologies 1200 HPLC with a VWD detector was used to determine the protein purity in the respective chambers. The C18 mass SPEC column was purchased from Grace Vydac Inc. The gradient elution was comprised by two mobile phases contained A: 100% acetonitrile with 0.1% trifluoroacetic acid; B: 100% water with 0.1% trifluoroacetic acid. The protein sample analyses were conducted with the parameters as showing in Table 6-1.

Table 6-1 Running conditions of HPLC

HPLC Parameters	Controlled values
VWD wavelength	214nm
Temperature	30°C
Flow speed	1.0ml/min
Running time	30min
Post time	5min
Injection	100μl

6.2.6 Protein separation by anion exchange membrane partitioned free flow isoelectric focusing (IEM-FFIEF)

Fig. 6-1 and 6-2 show the experimental setup for the IEM-FFIEF cell which includes two electrode chambers and four buffer chambers of different pHs: 4.0~5.8, 7.0, 8.5 and 9.8 individually. The effective separation areas for all ion exchange membranes were of 42.9 cm^2 and the chamber thicknesses were of 4.8 cm. The separation was running under a constant current of 100 mA. As shown in Fig. 6-2, dense cationic and anionic membranes

were used between an electrode chamber and chambers 1 or 4 to avoid the protein molecules from attaching to the electrodes. A 200ml protein mixture made of 500ppm Mb and 500ppm Lys was fed into chamber 3. Since chamber 3 had a pH value of 8.5 that was bigger than Mb's pI but smaller than Lys's pI, Lys molecules would carry positively charges and Mb molecules would carry negatively charges. Therefore, under an electric driving force, the negatively charged Mb would migrate through the positively charged anion exchange membrane and went into chamber 2 (pH 7.0) and be stationary in chamber 2, this is because the surface charge of protein would reduce to zero when pH = pI. The concentration of chamber 2 would increase and the increment can be on-line monitored by a UV-visible spectrometer at the wavelength of 408 nm [34]. The protein concentrations of all chambers were then measured by a HPLC to verify the separation performance.

6.3. Results and discussion

6.3.1 Confirmation of the modification

After amination with diamine and methylation with methyl iodide as shown in Fig.6-3, the as-cast P84 membranes were expected to exhibit characteristics of anion exchange membranes. The FTIR-ATR spectra shown in Fig.6-4 confirm the above reactions [35]. The strong and broad bands of imide groups of P84 at 1363cm^{-1}, 1732cm^{-1} and 1781cm^{-1} become significantly weakened after the diamine treatment, while a very weak new peak appears at 1650 cm^{-1}, which is due to the formation of –CO-NH- group [24-26, 36]. Similarly after methylation reaction, amine salt forms and new peaks in the range of 1500-1550cm^{-1} appear [36]. Moreover, -CH_3 groups absorption in the range of 2850~2921cm^{-1} appear, which is associated with characteristics of –CH_3 groups in

$-N(CH_3)_3^+ I^-$ [28, 36], thus confirming the methylation and quaternary amination on P84 membranes.

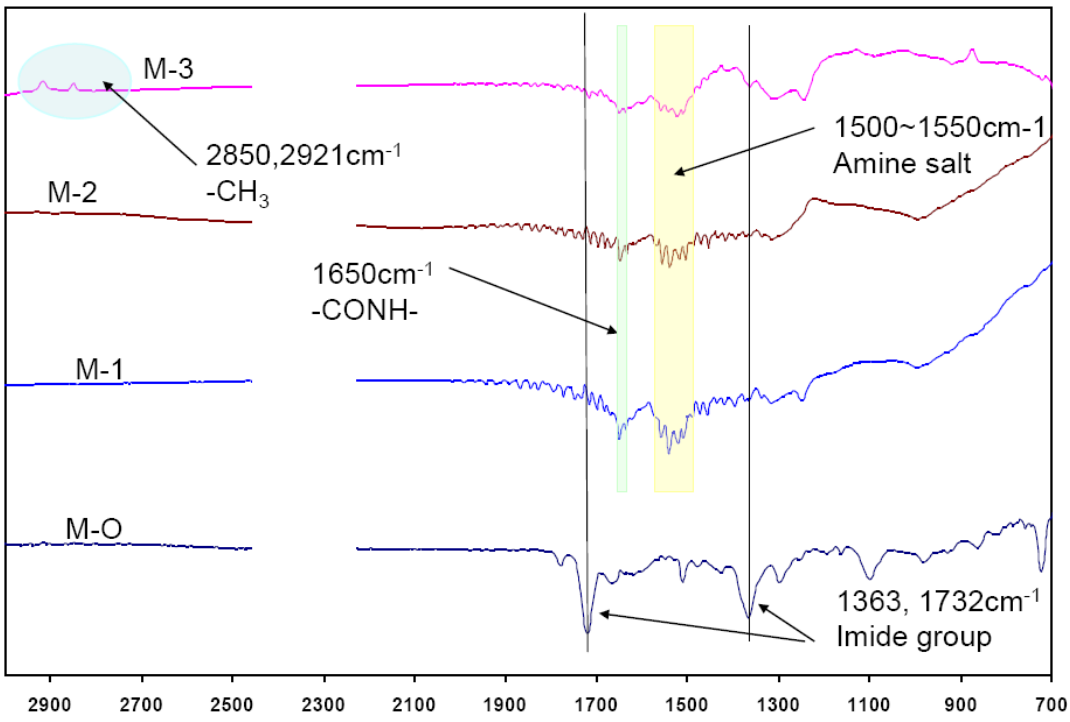

Fig.6-4. FTIR-ATR spectra of the original P84 membrane M-O, diamine modified membrane M-1, methylated amine membrane M-2 and M-3, where M-3 is quaternary amine membrane.

Fig.6-5 exhibits the element ratio of membranes M-0 and M-3 calculated from XPS spectra. Since the oxygen element remains the same chemical state and its amount is constant, while N and C elements change during the whole modification process, the changes in O:N:C ratio as shown in Fig.6-5 and Table 6-2 confirm the modification reactions. The increased content of carbon element in M-3 indicates the quaternary amination occurring on the P84 membrane surface.

Fig. 6-6 shows the quantity and chemical states of C 1s core-level of different membrane surfaces. As pointed by Xiao et al. [25], for the original P84 membrane, the bond at 284.6 eV is for C-H, at 285.8 eV is for C-N, at 288.4 is for $N(C=O)_2$ and at 291.1 eV is for

aromatic ring. After modifications, compared with the original P84 membrane, the intensity of imide group, $N(C=O)_2$, of M-1 and M-3 has a visible decrease. Clearly, the imide groups have been partially reacted, whereas a new peak appears at 286.8 eV which is attributed to –CO-NH- groups as a reaction product between primary amine and imide groups [36]. As the reaction going further, this amide group gradually shifted to the right hand side. When the M-3 is compared with the M-1, the ratio of the C-H peak to the $N(C=O)_2$ peak increases due to the methylation of free amino ends. Fig. 6-7 illustrates the quantity and chemical states of N 1s core-level of different membrane surfaces. The peak at 398 eV is due to –CO-NH-, whereas the peak at 400.7 eV is due to amine salts [36]. However, Fig. 6-7 seems to provide no help on distinguishing secondary, tertiary and quaternary amine salts, thus further characterization by streaming potential is needed to confirm the quaternary aminated surface. In addition, the functional peaks obviously shift to the right-hand side in both Fig. 6-6 and 6-7, which is the red-shift phenomenon [36], indicating the modified membrane surfaces have become easy to accept photonelectrons emitted by the X-ray source. As a result, the modified membrane surface tends to be positively charged.

Table 6-3 summarizes the IEC value, electric resistance and streaming (ζ) potential and PWP. Compared with the original P84 membrane, the IEC value increases from a negative value to a positive value as the modification proceeds: M-O < M-1 < M-2, M-3. Since a higher reaction temperature with CH_3I was utilized during the fabrication of M-3 membranes, M-3 has stronger anion exchangeable characteristics due to quaternary amine groups. Table 6-3 confirms this hypothesis because M-3 has a much higher IEC value than M-2. Correspondingly, the apparent ζ-potentials of these four membranes increase following the same trend, i.e. $\zeta_{M\text{-}O} < \zeta_{M\text{-}1} < \zeta_{M\text{-}2} < \zeta_{M\text{-}3}$ as shown in Fig.6-8.

Although streaming ζ-potential is a function of pH, the titration curves by the streaming potential analyzer shows that M-1, M2 and M-3 have positive apparent ζ- potentials in the range of pH 6.5~ 8.5, which means that M-1, M2 and M-3 are all positively charged under this pH range.

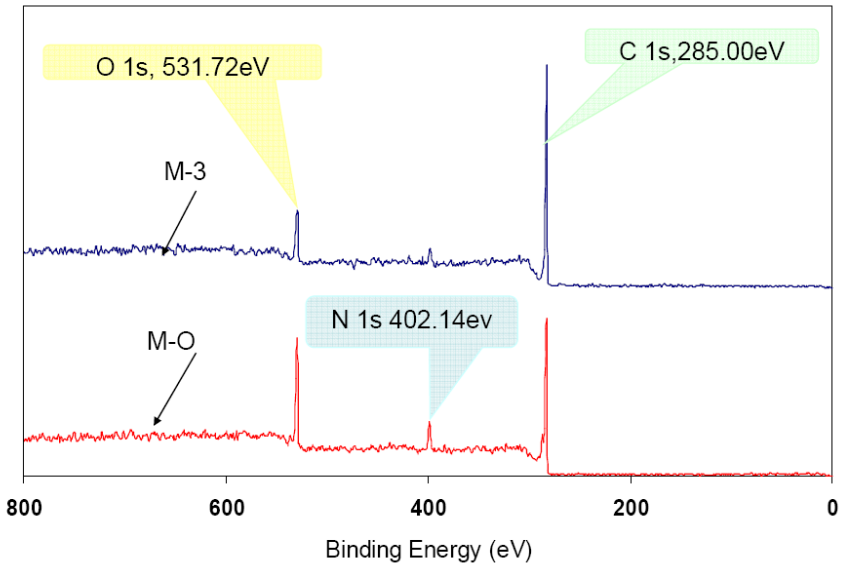

Fig.6-5 Comparison of element ratio from wide scans of the original P84 membrane (M-O) and quaternary amine membrane (M-3), where M-3 is quaternary amine membrane.

Table 6-2 The XPS element analyses of the original P84 membrane and methylated amine membranes

Element	Binding	M-O	M-2	M-3
O 1s	531.72	729	234	415.4
N 1s	402.14	294	117	213
C 1s	285.0	828	314	1172
O:N:C	-	1:0.4:1.14	1:0.5:1.34	1:0.5:2.82

Table 6-3 Membrane characterization data and protein separation fluxes of different types of membranes

Mem ID	M-O	M - 1	M- 2	M - 3
IEC value [a] (meq/m^2)	0	0.37	4.70	12.10
Electric resistance (MΩ)	9.65	7.78	6.52	5.36
Corrected ζ-potential (mV)[b] at pH 6.5	-30	+5	+12	+25
PWP [c] ($m^3/m^2.sec$) at 5bar	1.55E-5	1.05E-5	5.94E-6	4.71E-6
Pore size above r_p=3.9 nm [d]	63.3%	39.9%	35.5%	28.8%
Flux of (Mb)[e] ($g/hr.m^2$)	0.447	1.790	2.238	5.818

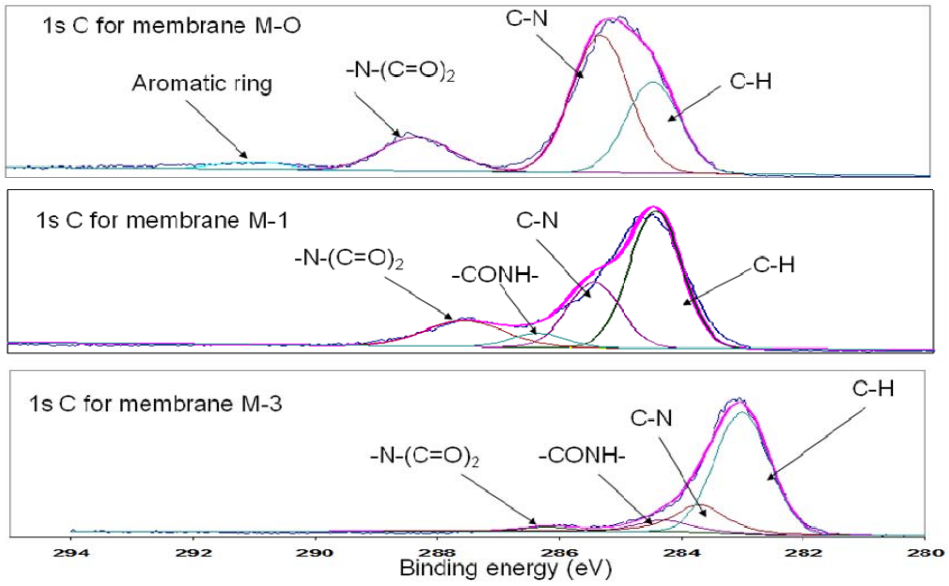

Fig. 6-6 XPS analysis of 1s C of the original P84 membrane M-O, diamine modified membrane M-1 and quaternary amine membrane M-3

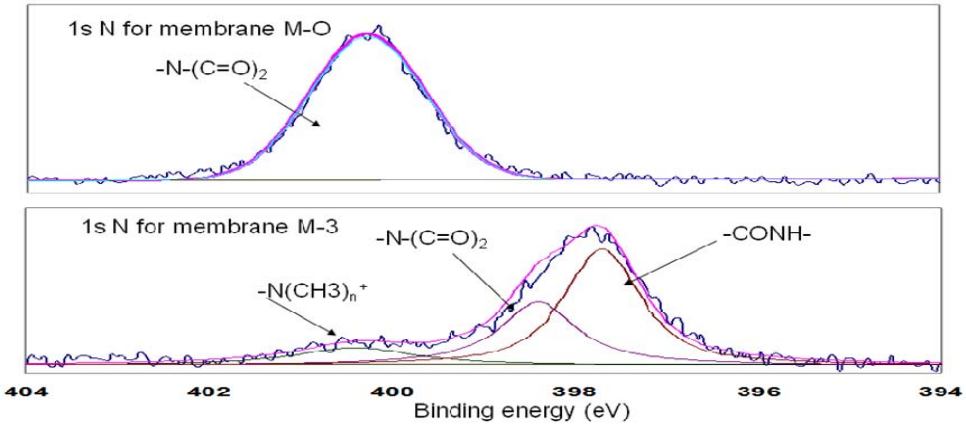

Fig.6-7 XPS analysis of 1s N of the original P84 membrane M-O and quaternary amine membrane M-3

As displayed in Fig. 6-8, the apparent ζ-potential of the original P84 membrane (M-O) is negative in the range of pH 4~10. This indicates that the unmodified P84 polymer is slightly negatively charged in the observed range, which is due to the unshared electron pair in imide group. Its high absolute value is mainly due to the surface conductivity on the membrane surface [31]. Similarly, the apparent ζ-potential values of M-1, M-2 and M3 shown in Fig. 6-8 (a) are also enlarged due to the same reason. As mentioned in the experimental section, when a rather dilute buffer solution is used, the surface conductivity has to be considered and the corrected ζ-potential should be calculated through eqn.(6-4). After the correction of surface conductivity, the corrected ζ-potentials of 1mM KCl buffers were also given in Fig. 6-8 (b). Different absolute values were displayed in (a) and (b). However, the same trend can be observed from them: compared with M-O, the ζ-potentials of M-1 and M-2 were more positive, and that of M-3 was extremely stable at a higher positive level with various pH. This is probably due to the formation of quaternary amine, thereby induces a higher density of positive charge at the M-3 surface. Since a higher density of surface charge will suppress the pH influence on streaming potentials [37], M-3 has quite stable ζ-potential values. On the other hand, because the number of

charged sites in per membrane volume increases with the proposed chemical modifications, a decrease in electric resistances (R) was observed in the order of resistance: $R_{M\text{-}O} > R_{M\text{-}1} > R_{M\text{-}2} > R_{M\text{-}3}$. As a result of the lower electric resistance, the higher membrane conductivity, solute mobility and protein mass transfer should be observed in a highly charged membrane. Therefore, according to this prediction, M-3 might have a superior performance among these membranes.

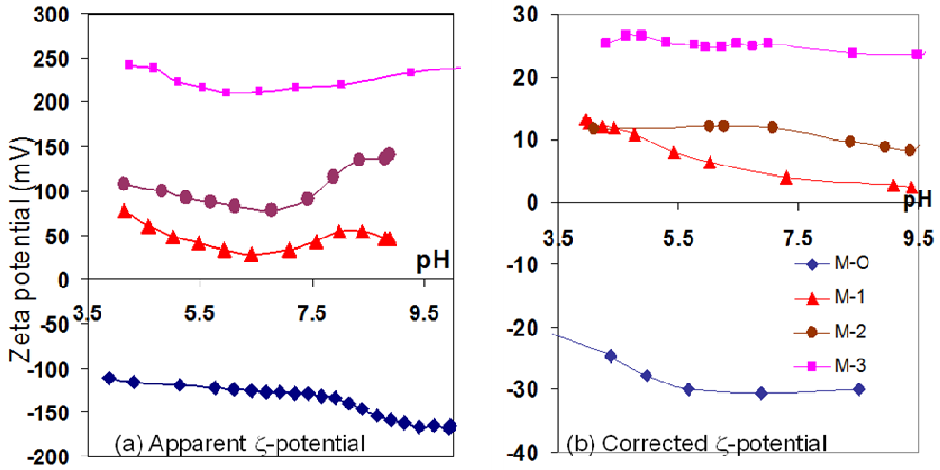

Fig.6-8. ζ-potential of four types of membranes from different modification steps

where all curves in (a) were obtained from auto titration results of 20mM HCl-tris buffer (pH=10); all curves in (b) were obtained from auto titration results of 1mM KCl (pH=10) and corrected by 0.1M KCl

6.3.2 Pure water permeation (PWP) and morphological changes during modifications

Table 6-3 shows the PWP values of these four membranes. Their PWP decreases with chemical modifications, and M-3 has the lowest PWP**.** The decreased PWP indicates that their pore sizes become smaller with modifications. Since the PWP value is strongly related to membrane structure such as pore size, porosity and intra-pore connections [38],

the PWP value may indirectly provide the information about porous flow channels within a membrane. The low PWP values of M-3 may be resulted from the effects of the insertion of diamine molecules and bulk groups $-N(CH_3)_4^+$ in a confined pore space.

Fig. 6-9 shows the mean pore sizes and pore sizes corresponding to MWCOs of the four membranes. It can be seen that the mean pore size follows the sequence of: M-O > M-1 > M-2 > M-3, whereas the MWCOs follows: M-O > M-1, M-2 > M-3. These tendency indicates that the pore size decreases when the modification proceeds, which is consistent with the PWP results. Fig. 6-10 displays the probability density functions. It can be seen clearly that there is a huge amount of small pores produced from the modification process and this leads to the density function moving closer to the y-axis as the modification proceeds. This phenomenon arises from the fact that the proposed chemical modifications reduce pore radius and change membrane morphology.

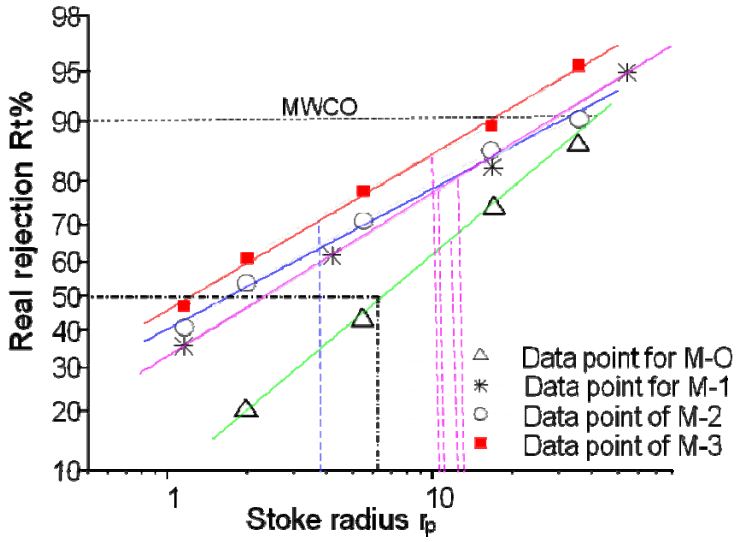

Fig. 6-9 Real rejection rates of four types of membranes

where the neutral standard molecules used in this experiment including:
PEG 2k and PVP10k, 55k, 360k, 1300k. The average pore sizes above 3.9nm are 12.56nm, 13.19nm, 11.68nm,10.2nm for M-O, M-1, M-2 and M-3, respectively.

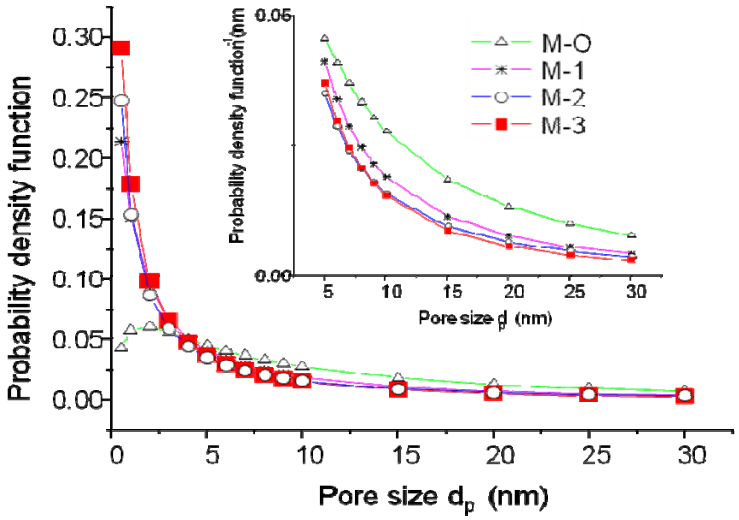

Fig. 6-10. Probability density functions of pore size distributions

where the neutral standard molecules used in this experiment including: PEG 2k and PVP10k, 55k, 360k, 1300k.

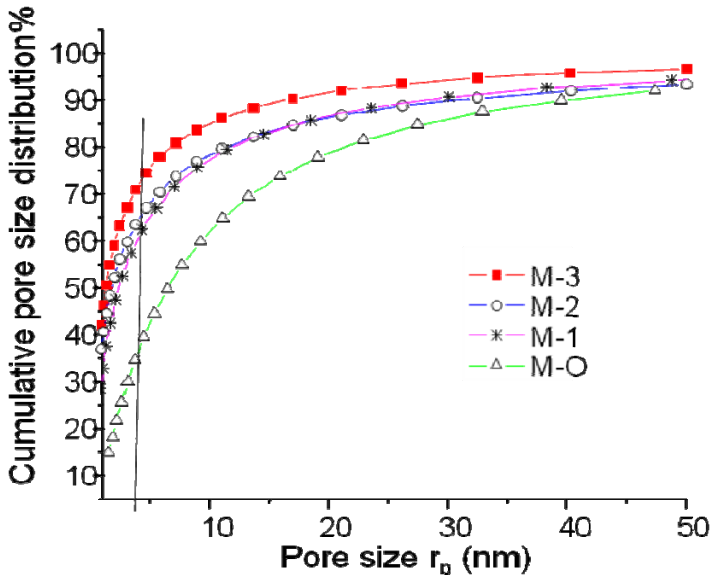

Fig. 6-11 Cumulative pore size distributions

where the neutral standard molecules used in this experiment including: PEG 2k and PVP10k, 55k, 360k, 1300k. The pores percentage above 3.9nm are 63.3%, 39.9%, 35.5% and 28.8% for M-O, M-1, M-2 and M-3, respectively.

As has been discussed in our previous work [13], protein molecules should not be regarded as infinitesimal in their dimensions. In order to offset the influence of small pores in membrane characterizations, a term called the "effective pore size" was proposed, concerning the minimum pore size allows protein molecules passing through. For Mb, this effective pore size is r = 3.9 nm [13]. Hence, the pore size which is smaller than the effective pore size will be removed from the calculation of the mean pore size, and the percentage of effective pores above this value will be counted. Fig. 6-11 shows the cumulative pore size distributions and demonstrates again that the amount of small pores increases after the modification process. It can be found that the percentage of pores (Fp) which is bigger than 3.9 nm (the minimal pore radius for Mb to pass through) [13] occupies 63.5%, 40.0%, 35.5% and 28.8% of the pores of the membranes M-O, M-1, M-2 and M-3, respectively.

Fig. 6-12 shows the FESEM images of the original and the as-modified flat membranes in dry conditions. The pore sizes of top surfaces display an obvious trend as follows: M-0 > M-1 > M-2 > M-3, which is consistent with the trends observed in PWP and pore size distribution. Interestingly, the chemically modified membranes become thicker as follows: M-0 < M-1 < M-2 < M-3 as shown in the cross-section images. This may be due to the swelling of the aminated polymer when the post-treatment was conducted in acidic or alkaline water solutions or may be due to self repulsion of charged molecules. The other possible factor might be due to the insertion of methyl groups of quaternary amine into the top surface during the methylation. From the 10 k magnification images of the top layer of the cross-section, it can be clearly seen that the modification process densifies the top layer. In addition to the FESEM observation, it is noticed that "gelation" apparently occurs at the membrane top surface after methylation. Under FESEM the gelation layer

has a similar image as a dense membrane but it is transparent under naked eyes. It is known that a dense membrane has no pores; it does not allow macro-molecules to pass through. On the contrary, a gel does not hinder the mass transfer of proteins and other macromolecules [39, 40]. Thus, the "denser" layer observed in Fig.6-12 for M-3 is a dried gel. It looks denser because of the contraction of a swelled structure during freeze drying to prepare samples for SEM.

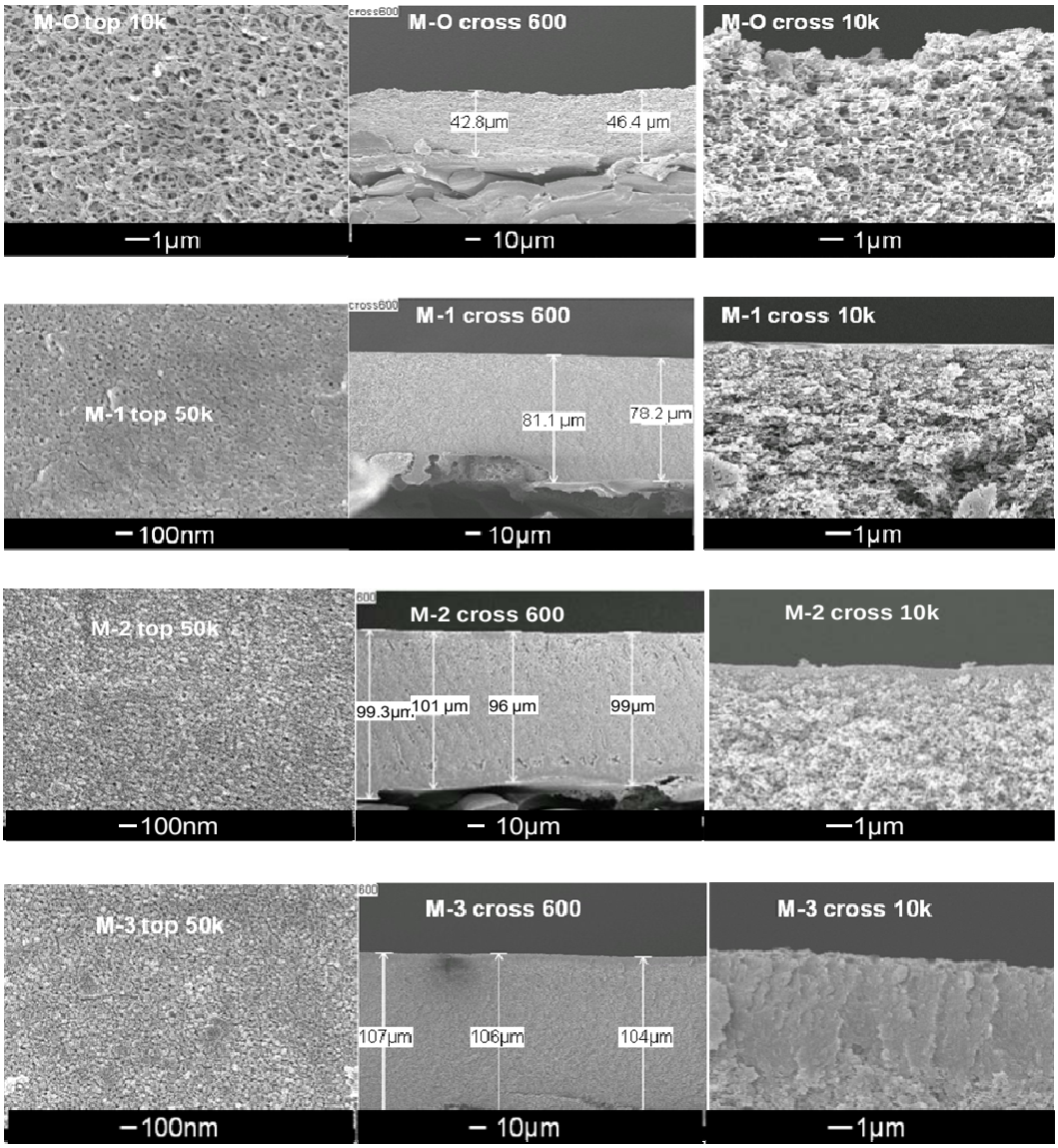

Fig. 6-12 Comparison of FESEM images of four types of membranes from different modification steps: M-O, M-1, M-2 and M-3.

6.3.3 Mechanical strength and stability of modified membrane

Generally, the P84 polymer is suggested to be used under pH 2~10, because the imide group can be hydrolyzed by some extreme acidic and caustic solution. The mechanical strength of the membrane becomes questionable, particularly after opening the imide ring. Hence the mechanical strength and stability of the membrane M-3 were tested by the method given in section 2.4. Newly prepared M-3, M-3 between chamber 1 & 2, M-3 between 3 & 4 and M-3 immersed in acid were compared by tensile strength and Young's modulus. As shown in Table 6-4, the M-3 membranes facing chamber 1 and chamber 4 did not show a significant reduce in tensile strength and in Young's modulus after operating under an electric field for one week. However, comparing to the newly prepared M-3, the M-3 immersed in acid displayed a 13% drop in tensile strength. This obvious effect of HCl verifies the suggested pH range of applying P84 polymer is reasonable. Therefore, the modified M-3 membrane operated under conditions given in Fig.6-2 possesses a reasonable mechanical strength and acceptable stability for daily operations.

Table 6-4. Mechanical strength and stability of membrane M-3

Membrane ID	Tensile strength (MPa)	Young's Modulus (Mpa)
M-3 immersed in water one week	15.18	475.53
M-3 immersed in 0.1M HCl two weeks	13.00	420.56
M-3 under pH=4 electric field one week	14.24	443.39
M-3 under pH=10 electric field one week	15.06	397.01

6.3.4 Protein separation performance

Fig.6-13 shows the myoglobin (Mb) concentrations in the 2nd chamber tested by an on-line UV-Vis spectrometer for these four membranes, and Table 6-3 summarizes their Mb fluxes. The membrane M-3 has the highest flux, the membranes M-2 and the M-1 have intermediate fluxes, while the original P84 membrane M-O has the lowest flux. Quantitatively, the M-3 (which was methylated at 48°C) has a flux 2.5 times of the M-2 (which methylated at 42°C) and 13 times of M-O. This implies that the flux is strongly related to membrane surface ζ-potential. This phenomenon corroborates well with our previous experiments that membrane surface ζ-potential facilitates protein flux [[12, 13]] as well as the theoretical predictions by Keh, Anderson and Ennis [[41]]. As can be seen from both experimental results and theoretical derivations, a charged cylindrical pore exerts positive effects to protein mass transfer in electrophoresis. Hence, membranes with a higher ζ_w will dramatically increase the mobility of counter-ion proteins in an IEM-FFIEF process [[42]]. This is particularly true when protein particles has a much smaller surface zeta-potential ζ_s than the pore wall potential ζ_w, ($\zeta_s << \zeta_w$). As a consequence, ζ_w will be the dominant factor that affects the mobility μ, thus the flux.

Normally, pore size is a dominant factor influencing the flux in a UF process. A larger pore will result in a higher flux in most hydraulic pressure driven UF processes. However, in this study, the protein separation flux behaves oppositely from the above common sense: an increase in flux is observed as the pore size decreases. This is due to the fact that the boundary effects of charged membrane have exceeded the steric hindrance of pores and the higher flux of M-3 is a result of the competition between boundary effects and steric hindrance. The flux results shown in Fig. 6-13 indicate that the increased

surface charge of a membrane is another important factor to improve the mass transfer of charged macromolecules across the membrane.

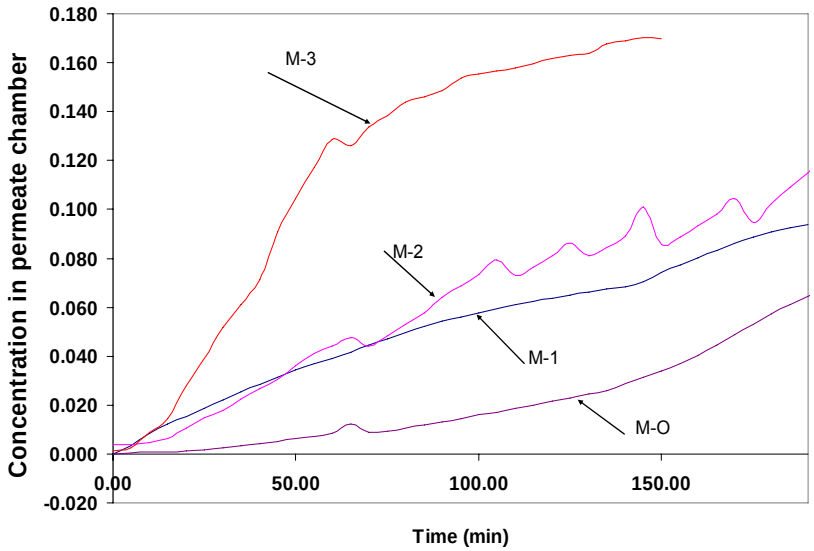

Fig. 6-13 Protein separation fluxes monitored by a UV-vis spectrometer where M-O, M-1, M-2 and M-3 were applied for protein separation individually.

Fig. 6-14 shows the protein compositions analyzed by HPLC in different chambers when applying M-3 in the IEM-FFIEF system. Only two peaks for myoglobin appear at the permeate side and no lysozyme peak can be found in the chamber 2, and only a trivial amount of myoglobin appears in the chamber 1. Meanwhile, most of lysozyme appears in the chamber 4, and a very small amount of myoglobin can be observed. The positively charged Lys molecules might be rejected by the anion exchange membrane or might migrate to the chamber 4. As a result of boundary effect, the rejection or migration of lysozyme takes place depending on pore size, pore surface charge and charge carried on lysozyme molecules. When pore size is small enough, the lysozyme should be rejected by the positively charged membrane. However in this study, there are 20% pores in the M-3

and 30% pores in the M-2 bigger than the molecular size of lysozyme, therefore the migration of lysozyme to the chamber 4 is inevitable. Compared to the M-3, the performance test for the M-2 has a similar HPLC results. The selectivity of the membranes M-2 between chambers 2 & 3 was infinitely large, but the flux was much smaller. This performance results imply that the purity and concentration of individual chamber (2 & 4) can reach to an extremely high level if a suitable anion charged membrane is used.

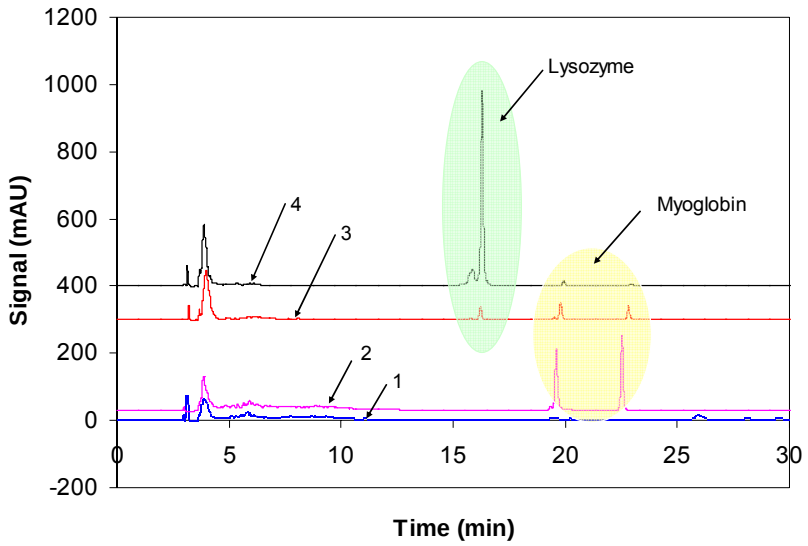

Fig. 6-14 HPLC results of protein separation of (Mb+Lys) in the IEM-FFIEF system, where numbers 1,2,3 and 4 correspond to chambers 1, 2, 3, and 4, respectively.

6.4 Conclusions

The objectives of this research are to (1) conduct a fundamental study on anion-exchange membrane formation and (2) develop a suitable anion-exchange membrane which can be integrated with IEM-FFIEF for enhanced protein separation. Experimental results show that amination by diamine and then methylation by methyl iodide is an effective route to produce a highly charged anion-exchange membranes based on P84 polyimide. The

membrane M-3 which was methylated at 48°C exhibits the highest and most stable separation because it possesses the highest IEC value, hence allowing anion type Mb molecules to migrate across the membrane faster. It is also found that the proposed chemical modifications reduce pore sizes and methylation by methyl iodide produces a gel-like structure with smaller pore sizes on the P84 membrane surface. This work also demonstrates that the determinant factor for the flux of IEFFFIEF includes both surface charge and pore structure of membrane, rather than pore size only. This conclusion means that ion-exchanged membrane is rather an advantage than an impediment for the purpose of increasing protein separation fluxes in the IEM-FFIEF system.

Acknowledgement

The authors would like to thank A-star and National University of Singapore (NUS) for funding this research with the grant numbers of R-279-000-164-305 and R-279-000-249-646. Special thanks are given to Dr. L.Y. Jiang and Y. Wang, for their valuable assistance.

References

[1.] R. van Reis and A.L Zydney, Membrane separations in biotechnology, Curr. Opin. Biotech. 12 (2001) 208.

[2.] F.G. Smith III and W.M. Deen, Electrostatic double layer interactions for spherical colloids in cylindrical pores, J. Colloid Interface Sci., 78 (1980). 444.

[3.] F.G. Smith III and W.M. Deen, Electrostatic effects on the partitioning of spherical colloids between dilute bulk solution and cylindrical pores, J. Colloid Interface Sci. 91 (1993) 571.

[4.] A.L Zydney, Protein separations using membrane filtration: new opportunities for whey fractionation, Int. Dairy J. 8 (1998) 243.

[5.] A.L Zydney and N.S. Pujar, Protein transport through porous membranes: effects of

colloidal interactions, Colloid Surface A, 138 (1998) 133.

6. S. Galier and H.R. Balmann, Study of the mass transfer phenomena involved in an electrophoretic membrane contactor, J. Membr. Sci. 194 (2001) 117.

7. J. Watson, Continuous, free-flow electrophoresis: a modified approach, Sep. Technol. 4 (1994) 239.

8. P. Wenger and P. Javet, Isoelectric focusing using non-amphoteric buffers in free solution: I. determination of stable concentration profiles, J. Biochem. Bioph. Methods, 13 (1986) 259.

9. van Nunen, C.A.P.M., Design of Large Scale Membrane, Electrophoresis Module for Separation of Proteins, PhD. thesis, University of Eindhoven, (1997).

10. M. Bier and T. Long, Recycling isoelectric focusing: use of simple buffer, J. Chromatogr. 604 (1992) 73.

11. M. Bier, Recycling isoelectric focusing and isotachophoresis, Electrophoresis, 19 (1998) 1057.

12. J.H. Cheng, Y. Li, T.S. Chung, S.B. Chen and W.B. Krantz, High performance protein separation by ion exchange membrane partitioned free flow isoelectric focusing system, Chem. Eng. Sci. 63 (2008) 2241.

13. J.H. Cheng, T.S. Chung, S.H. Neo, Investigation of mass transfer in the ion-exchange membrane partitioned free-flow isoelectric focusing system (IEM-FFIEF) for protein separation, Electrophoresis, 30, (2009) 2600.

14. H. Kawabe, Amination of chloromethylated polystyrene with amino alcohols, Bull. Chem. Soc. Jpn. 54 (1981) 2886.

15. A. Warshawsky and O. Kedem, Polysulfone-based interpolymer anion exchange membrane, J. Membr. Sci. 53 (1990) 37.

16. T. Gullinkala and I. Escobar, Controlled graft polymerization as a tool for membrane surface modification, Environmental Progress, 27 (008) 210.

17. H. Xu and X.Z. Hu, Preparation of anion exchangers by reductive amination of acetylated crosslinked polystyrene, React. Funct. Polym. 42 (1999) 235.

18. L. Wu, T.W. Xu and W.H. Yang, Fundamental studies of a new series of anion exchange membranes: membrane prepared through chloroacetylation of PPO followed by quaternary amination, J. Membr. Sci. 286 (2006) 185.

19. H. Xu and X.Z. Hu, A novel way to prepare anion exchangers based on crosslinked polystyrene, Polym. Bull. 40 (1998) 47.

20. A. Hartwig, M. Mulder and C.A. Smolders, Surface amination of poly(acrylonitrile), Adv. Colloid Interface sci. 52 (1994) 65.

[21.] The carcinogenic substance regulations, No. 879 HMSO London.

[22.] List of controlled toxic industrial waste, Singapore.

[23.] P.S. Tin, Y.C. Xiao and T.S. Chung, Polyimide-carbonized membranes for gas separation: structural, composition, and morphological control of precursors, Sep. Purif. Rev. 35 (2006) 285.

[24.] X. Li and M.R. Coleman, Functionalization of carbon nanofibers with diamine and polyimide oligmer, Carbon, 46 (2008)1115.

[25.] X.Y. Qiao and T.S. Chung, Diamine modification of P84 polyimide membranes for pervaporation dehydration of isopropanol, AIChE J. 52 (2006) 3462**.**

[26.] E. Baer, An Introduction to high performance polymer, High Perform. Polym. 11 (1990) 395.

[27.] B.T. Low, Y.C. Xiao, T.S. Chung and Y. Liu, Simultaneous occurrence of chemical grafting, cross-linking, and etching on the surface of polyimide membranes and their impact on H2/CO2 separation, Macromolecules 41*(*2008), 1297.

[28.] L. Shao, L. Liu, S.X. Cheng, Y.D. Huang and J. Ma, Comparison of diamino cross-linking in different polyimide solutions and membranes by precipitation observation and gas transport, J. Membr. Sci. 312 (2008) 174.

[29.] N. Peng, T.S. Chung, K.Y. Wang, Macrovoid evolution and critical factors to form macrovoid-free hollow fiber membranes, J. Membr. Sci. 318 (2008) 363.

[30.] F.A. Carey, Organic chemistry, 6th edition, Mc GRAW HILL, New York, 2006, pg967.

[31.] M. D. Afonso, Surface charge on loose nanofiltration membranes, Desalination 191 (2006) 262.

[32.] K.Y. Wang and T.S. Chung, The characterization of flat composite nanofiltration membranes and their applications in the separation of cephalexin, J. Membr. Sci., 247 (2005) 37.

[33.] K.Y. Wang, T. Matsuura, T.S. Chung and W. F. Guo, The effects of flow angle and shear rate within the spinneret on the separation performance of poly(ethersulfone) (PES) ultrafiltration hollow fiber membranes, J. Membr. Sci. 240 (2004) 67.

[34.] R. J. Simpson, Purifying proteins for proteomics: a laboratory manual, Gold Spring Harbor, New York, 2004, pg659.

[35.] G. Socrates, Infrared and Raman characteristic group frequencies, John Wiley & Sons, New York, 2004. pg 38 or pg146.

[36.] G. Beamson and D. Briggs, High resolution XPS of organic polymer: the Scienta ESCA300 database, Wiley, New York, 1992.

[37.] C.M. Wu, T.W. Xu and W.H. Yang, A new inorganic–organic negatively charged membrane: membrane preparation and characterizations, J. Membr. Sci. 224 (2003) 117.

[38.] Y. Li and T.S. Chung, Exploration of high sulfonated polyethersulfone as a membrane material with the aid of dual layer hollow fiber fabrication technology for protein separation, J. Membr. Sci. 309 (2008) 45.

[39.] D. Garfin and S. Ahuja, Handbook of isoelectric focusing and proteomics, Academic Press, 2005, pg127.

[40.] R.A. Mosher, D.A. Saville and W. Thormann, The dynamics of electrophoresis, VCH publishers, New York, 1992, Chapter 7.

[41.] J. Ennis and J.L Anderson, Boundery effects on electrophoretic motion of spherical particles for thick double layer and low zeta potential, J. Colloid Interface Sci. 185 (1997) 497.

[42.] Y.H. Su, Y.L. Liu, D.M. Wang, J.Y. Lai, M.D. Guiver, B. Liu, Increases in the proton conductivity and selectivity of proton exchange membranes for direct methanol fuel cells by formation of nano-composites having proton conducting channels, J. Power Sources, 194 (2009) 206.

CHAPTER 7 CONCLUSIONS AND RECOMMENDATIONS

The primary motive of this research dissertation was to address the problem of low selectivity and low efficiency of commonly used protein separation methods and to design a novel process that could achieve the twin objectives of improving both the selectivity and separation flux. In order to enhance our understanding on the membrane based IEF electrophoresis, the boundary effects based on the theoretical work of Ennis *et al.* were also investigated. The effect of membrane IEC values on the self-sharpening phenomenon was also explored through protein separation performances.

7.1 The conclusions drawn from this dissertation

7.1.1 The feasibility of IEM-FFIEF

Capitalizing on the electric properties of protein molecules and membranes, individual protein components within a mixture can be reallocated into different chambers by an applied electric field. Our experiments show that the IEM-FFIEF system is capable of separating proteins at high selectivity and high flux. Moreover, the strong mechanical strength of the SPSf polymeric cation-exchange membrane allowed for operations to be carried out over long periods of time before a membrane change was necessary for regeneration. The flexibility of the process and the reproducibility of the process data suggests a good prospect of industrial applications. IEM-FFIEF also experiences a very low fouling rate as compared to conventional protein filtration processes over similar operating time spans. This might be due to the fact that the highly hydrophilic SPSf material hinders hydrophobic interactions between the protein molecules and polymer chains, which were regarded as the main culprits behind membrane fouling. The IEM-

FFIEF process shows much higher separation efficiency than a conventional membrane filtration process; hence the application of IEM-FFIEF process in industry should be a feasible and economical option.

7.1.2 Mass transfer in IEM-FFIEF

In this dissertation, an attempt was also made to understand the membrane-partitioned FFIEF phenomenon and represent it analytically. The comprehension of membrane based free-flow electrophoresis stems from the understanding of boundary effects in electrophoresis. In order to integrate the boundary effects theory of Ennis *et al.* in the complicated conditions of FFIEF, two new terms were introduced and expressed in measurable parameters, which have never been reported before: 1) the disturbed electric field strength, $E_\infty' = E_\infty - E_0$; 2) the minimal electrical consumption E_0 for particles to overcome the electrostatic effect and to produce a flux breakthrough. From the theoretical studies that we have conducted thus far, we have experimentally proven that the theoretical prediction for protein velocity and mobility through a porous membrane as formulated by Ennis and Zhang *et al.* is applicable in the ion-exchange membrane partitioned free-flow isoelectric focusing system (IEM-FFIEF) after taking into consideration the effects of membrane pore size distribution and as well as the effects of a disturbed electric field. The experimental results indicate that the membrane properties dramatically affect the mass transfer rates; therefore, the mass transfer and separation can be manipulated by varying the membrane properties.

7.1.3 Self-sharpening phenomenon in IEM-FFIEF system

Our experiments also proved that IEM-FFIEF, with the inheritance of the advantage of isoelectric focusing (IEF), is adaptable to a sample with multi-component and similar molecular weights differing in pI values. Findings show that aminated PPO membranes are capable of self-sharpening under high charging rate; the higher charging rate results in sharper separation and higher flux. A triple component mixture of bovine serum albumin (BSA), myoglobin (Mb) and lysozyme (Lys) can be isolated from each other at high purities exceeding 99%. This self-sharpening phenomenon of membranes might arise from the local electrostatic interaction between charged surfaces and charged colloidal particles near the membrane surface. The stronger local electrostatic interaction can produce a stronger buffer capacity and in turn a high selectivity. This result indicates that a membrane with an appropriate pore size and charge density are beneficial rather than problematic for the free-flow isoelectric focusing of protein. From the view point of process designing, both the membrane pore size and charge density can be tailored in the membrane fabrication process. From the viewpoint of operation efficiency, the multi-component process is more productive and economical than a single permeate system. Therefore, the self-sharpening phenomenon can energize mass transfer in the IEM-FFIEF process and retains stability and robustness of the multi-component protein separation system.

7.1.4 Amination of P84 membrane surface

In this dissertation we also explored the influence of a different membrane structure on mass transfer- charge was only grafted on the outer layers of the membrane (without modification inside the membrane cross-section) through amination of the P84 co-polyimide membrane surface. Experimental results show that amination by diamine and

then methylation by methyl iodide is an effective route to produce a highly charged anion-exchange membranes based on P84 polyimide. The membrane M-3 which was methylated at 48 °C exhibits the highest and most stable separation because it possesses the highest IEC value, hence allowing anion type Mb molecules to migrate across the membrane faster. It is also found that the proposed chemical modifications reduce pore sizes and methylation by methyl iodide produces a gel-like structure with smaller pore sizes on the P84 membrane surface. This work also demonstrates that the determinant factor for the flux of IEF-FFIEF includes both surface charge and pore structure of membrane, rather than pore size only. This conclusion means that ion-exchanged membrane is rather an advantage than an impediment for the purpose of increasing protein separation fluxes in the IEM-FFIEF system. Moreover, the sandwich structure of the charged membrane appears to have no net negative effects on protein mass transfer; instead, a much higher transfer rate was achieved by M-3. This phenomenon implies that a thinner charged outer layer might be favorable in increasing flux. Therefore, sandwich-like anion exchange membranes with highly charged surface and well defined pore size will be a good option for the long term operation of a scaled-up IEM-FFIEF process.

7.2 Recommendations for future work

Based on the experimental results obtained, analytical expressions derived and conclusions drawn from this research, some recommendations are provided for future investigations related to process optimizations, other potential applications and membrane fabrication technologies.

7.2.1 Process optimizations

Our experimental results indicate that a thinner chamber thickness will result in a more rapid mass transfer across the membrane as well as a shorter operation time. By reducing the chamber thickness to a few millimeters, which is sufficient for forced flow through the chamber, the separation time and harvest period will be significantly shortened and the power consumption will be reduced correspondingly. However, there is a lower boundary limit to the chamber thickness, because a thinner chamber demands a pressure increase in the circulations of each individual chamber, and a higher driving pressure will increase the operation cost through increased energy demands. Therefore, a good chamber spacer with high porosity (> 95%), high mechanical strength, sufficient elasticity and highly smooth surface are required. On the other hand, the connectors in the circulating system need to be revised to very fine scales to match the thickness of the chambers.

7.2.2 Other potential applications

Theoretically, IEM-FFIEF is not only suitable for separations based on the difference of pI values, but also suitable for the separations based on difference of MW or difference of stereochemical structure. One example for MW-base separation is that the purification of hormones from the plasma of living subjects, while the purification of individual drug enantiomers from their racemic mixture is the best example for separations based on stereochemical structural differences. All these separations rely on the structure of separation membranes, hence the innovation of membrane fabrication technology is key to broadening the application of the IEM-FFIEF process. Membranes with homogeneous pores are required to separate molecules based on difference of MW, while,

enantioseparations require the use of homogeneous nano-membranes with chiral selectivity.

7.2.3 Membrane fabrication technologies

As mentioned previously, understanding the membrane structure is of key importance for the application of IEM-FFIEF process in different aspects. In our experiments, membrane structures with sponge-like cross-section, sandwich cross-section and gel-like top layer have been studied. Due to the time limitations, charged membrane with homogeneous pore structure and the chiral selective NF membrane have not been tried. They are highly recommended for future research.

Publications

[1] J.H. Cheng, Y. Li, T.S. Chung, S.B. Chen and W.B. Krantz, High performance protein separation by ion exchange membrane partitioned free flow isoelectric focusing system, Chem. Eng. Sci. 63 (2008) 2241.

[2] J.H. Cheng, T.S. Chung and S.H. Neo, Investigation of mass transfer in the ion-exchange membrane partitioned free-flow isoelectric focusing system (IEM-FFIEF) for protein separation, Electrophoresis, 30, (2009) 2600.

[3] J. H. Cheng and T.S. Chung, Self-sharpening Phenomenon Arisen by Ion-exchange Membranes in Multi-compartment Free-flow, Chem. Eng. Sci. 64 (2009) 5222.

[4] J.H. Cheng, Y.C. Xiao, C.M. Wu and T.S. Chung, Chemical modification of P84 polyimide as anion-exchange membranes in a free-flow isoelectric focusing system for protein separation, Accepted by Chem. Eng. J. 160 (2010) 340.

Appendix

A-1 The translation velocity (thin double layer) driven by electric force [Keh and Anderson, 1985, ref.1-42]

$$\upsilon = [1 - 1.28987\lambda^3 + 1.89632\lambda^5 - 1.02780\lambda^6 + O(\lambda^8)] * \frac{\varepsilon}{4\pi\eta}(\zeta_s - \zeta_w)E_\infty e_z$$

where U is the translation velocity; $\lambda = a / b << 1$ is the ratio of particle radius *a* and pore radius *b*; ε is the dielectric constant; η is the viscosity; $E_\infty e_z$ is the undisturbed electric field; e_z is the direction vector; ζ_s is the ζ-potential of solute; ζ_w is the ζ-potential of the pore wall.

A-2 The Stokes' translation velocity [Happel and Brenner 1983, ref.1-43]

$$\upsilon = [1 - 2.10443\lambda + 2.08877\lambda^3 - 0.94813\lambda 5 - 1.372\lambda^6 + 3.87\lambda^8 - 4.19\lambda^{10} + O(\lambda^{12})]\frac{1}{6\pi\eta a}Fe_z$$

A-3 The translation velocity (thick double layer) driven by electric force [Ennis and Anderson, 1997, ref.1-46]

$$\upsilon = \frac{\varepsilon\zeta_s}{4\pi\eta}E_\infty e_z\{f(\kappa a) - \gamma + \lambda^3(0.79683\times[f(\kappa a) - L(\kappa a)] - 1.28987\times[L(\kappa a) - \gamma]) + 1.89632\lambda^5[L(\kappa a) - \gamma] + \lambda^6(0.63494\times[f(\kappa a) - L(\kappa a)] - 1.02781\times[L(\kappa a) - \gamma])\}$$

$$\kappa \approx 3.288\sqrt{I} \quad in \quad (nm^{-1})$$

$$I = \frac{1}{2}\left(n_i^z C_i^f z_P^2 + \sum C_{bi} z_{bi}^{\ 2}\right)^{1/2}$$

where κ^{-1} is the Debye's length in nm; *I* is the ionic strength in mol L^{-1}, which is calculated from both the concentration of colloidal particle and the concentration of buffer solution; $\lambda = a / b < 1$ is the ratio of particle size and pore size; and $\gamma = \zeta_w/\zeta_s$, is the

ratio between the ζ-potential of pore wall ζ_w and the ζ-potential of solute particle ζ_s. The functions *L(κa) and f(κa)* are given in appendix A. The term $4\pi\eta\upsilon/(\varepsilon E_\infty \zeta_s)$ is defined as relative mobility.

A-4 The electrophoretic translation velocity of protein across a membrane [Ennis, Zhang, et al. 1996, ref.1-47]

$$\upsilon = \frac{\varepsilon\zeta_s}{4\pi\eta} E_\infty e_z \{ f(\kappa a) + \gamma \left(g(0,\kappa b) \frac{1 + 3.867\lambda - 1.907\lambda^2 - 0.834\lambda^3}{1 + 1.867\lambda - 0.741\lambda^2} - g(\lambda,\kappa b) \right) + \lambda^3 (0.79683 \times [f(\kappa a) - L(\kappa a)] - 1.28987 \times [L(\kappa a) - \gamma]) + 1.89632\lambda^5 [L(\kappa a) - \gamma] + \lambda^6 (0.63494 \times [f(\kappa a) - L(\kappa a)] - 1.02781 \times [L(\kappa a) - \gamma]) \}$$

$$g(\lambda,\kappa b) = 1 - \frac{2I_1(\kappa b(1-\lambda))}{\kappa b(1-\lambda) I_0(\kappa b)} - \frac{\lambda^2}{3(1-\lambda)^2 I_0(\kappa b)} \{ I_0[\kappa b(1-\lambda)] - 1 + \kappa b(1-\lambda) I_1[\kappa b(1-\lambda)] \}$$

where I_0 and I_1 are the zero and first order terms of the first kind of modified Bessel functions. The function *g(λ,κb)* represents the effects derived from the charged pore surface. When *λ = 0, g(0,κb)* represents this effect at the centre of the pore. Correspondingly, the function *γg(λ,κb)* represents the contribution of electro-osmosis to the average particle velocity (at the particle surface enclosed in the pore); and the *γg(0,κb)* term represents the contribution of Poiseuille flow (at the centre of the pore) to the average velocity.